# Clustering of Stars in Nearby Galaxies:

# Probing the Range of Stellar Structures

by

Catherine Kaleida

A Dissertation Presented in Partial Fulfillment
of the Requirements for the Degree
Doctor of Philosophy

Approved August 2011 by the
Graduate Supervisory Committee:

Paul Scowen, Co-Chair
Rogier Windhorst, Co-Chair
Rolf Jansen
Francis Timmes
Evan Scannapieco

ARIZONA STATE UNIVERSITY

December 2011

ABSTRACT

Most stars form in groups, and these clusters are themselves nestled within larger associations and stellar complexes. It is not yet clear, however, whether stars cluster on preferred size scales within galaxies, or if stellar groupings have a continuous size distribution. I have developed two methods to select stellar groupings across a wide range of size-scales in order to assess trends in the size distribution and other basic properties of stellar groupings. The first method uses visual inspection of color-magnitude and color-color diagrams of clustered stars to assess whether the compact sources within the potential association are coeval, and thus likely to be born from the same parent molecular cloud. This method was developed using the stellar associations in the M51/NGC 5195 interacting galaxy system. This process is highly effective at selecting single-aged stellar associations, but in order to assess properties of stellar clustering in a larger sample of nearby galaxies, an automated method for selecting stellar groupings is needed.

I have developed an automated stellar grouping selection method that is sensitive to stellar clustering on all size scales. Using the Source Extractor software package on Gaussian-blurred images of NGC 4214, and the annular surface brightness to determine the characteristic size of each cluster/association, I eliminate much of the size and density biases intrinsic to other methods. This automated method was tested in the nearby dwarf irregular galaxy NGC 4214, and can detect stellar groupings with sizes ranging from compact clusters to stellar complexes.

In future work, the automatic selection method developed in this dissertation will be used to identify stellar groupings in a set of nearby galaxies to determine if the size scales for stellar clustering are uniform in the nearby universe or if it is dependent on local galactic environment. Once the stellar clusters and associations have been identified and age-dated, this information can be used to deduce disruption times from the age distribution as a function of the position of the stellar

grouping within the galaxy, the size of the cluster or association, and the morphological type of the galaxy. The implications of these results for galaxy formation and evolution are discussed.

*To my family, who encouraged me*

*to reach for the stars...*

ACKNOWLEDGMENTS

This dissertation would never have come to fruition without the encouragement and shared knowledge of many teachers, friends, and colleagues. My undergraduate astronomy professor, Dr. Loris Magnani, once said that anyone can get a Ph.D, if they are willing to put themselves through the pain. I can now fully appreciate the level of commitment he was speaking of, the extreme dedication that every doctoral student must have for their work. I would like to thank Dr. Magnani, and the many teachers who made me believe that I could be one of those people, and for imparting the knowledge necessary to accomplish this task.

I would like to express my gratitude to my thesis advisors for their continued advice, insight, and enlightening discussions: Dr. Paul Scowen, for being incredibly supportive and patient at the times that I most needed it and least deserved it, and Dr. Rogier Windhorst, for opening new doors for me, and for always going to bat for his students. I would also like to thank Dr. Rolf Jansen for advising me on my secondary project, and teaching me to how to observe at a research-class telescope. Furthermore, I would like to express my gratitude to Drs. Bradley Whitmore and Rupali Chandar for many invaluable scientific discussions, for their patience, for providing guidance, and for teaching me how to ask the interesting questions. I also thank my whole dissertation committee for their feedback throughout this process. They are Drs. Paul Scowen, Rogier Windhorst, Rolf Jansen, Francis Timmes, and Evan Scannapieco. I am also indebted to Dr. Seth Cohen, for teaching me many, many practical and useful skills that I use every day in my research.

Furthermore, I am grateful to my fellow ASU graduate students who have enriched my life, including but not limited to: Hwihyun Kim, for being my friend, collaborator, and mentor, without whom I would be lost; my roommates over the

years: Angel Fuentes, Dr. Rosa Diaz, Emily McLinden, Matt Metchley, and Dr. Pascale Hibon, for keeping me company and providing an understanding ear; my office-mate and friend, Todd Veach, for his computer expertise and witty sense of humor; and also Dr. Russell Ryan, Dr. Nimish Hathi, Dr. Amber Straughn, Dr. Cynthia D'Angelo,Dr. Michael Lesniak, Brian Gleim, Michael Rutkowski, Dr. Carola Ellinger, and Dr. Vithal Shet-Tilvi.

In addition to those already mentioned, I would like to express my thanks to Dr. Bruce Balick for improving my knowledge of the interplay between gas and stars and teaching me how to look at the "big picture", Zolt Levay for producing the color image of NGC 4214 for Figure 3.1, and Dr. Max Mutchler for drizzling the *HST* WFC3 Early Release Science images of NGC 4214. Special thanks to the people in the SESE and Physics Department administration who have helped me immensely throughout my graduate school career, including: Sunny Thompson, Scott Smas, Teresa Robinette, Becca Dial, and Becky Polley.

This work has been supported by programs HST-AR 1068401A, HST-AR 12137, and HST-AR 11360, provided by NASA through a grant from the Space Telescope Science Institute, which is operated by the Association of Universities for Research in Astronomy, Inc., under NASA contract NAS5-26555. Analysis of NGC 4214, M83, and NGC 2841 was based on Early Release Science observations made by the WFC3 Scientific Oversight Committee. I am grateful to the Director of the Space Telescope Science Institute for awarding Director's Discretionary time for this program.

Last but not least, thank you to my family: Mom, Dad, Beth, and David, and to my dear friends Ariela Friedman and Natalie Beckman. Your unending patience and support have carried me along the way! Final thanks to everyone who has helped me to this point. With the proper encouragement, support, and stubbornness, ordinary people can accomplish extraordinary things.

TABLE OF CONTENTS

Page

TABLE OF CONTENTS . . . . . vi

LIST OF TABLES . . . . . vii

LIST OF FIGURES . . . . . viii

CHAPTER . . . . . 1

1 INTRODUCTION . . . . . 1

2 SINGLE-AGED STELLAR ASSOCIATION SELECTION IN THE M51/NGC 5195 SYSTEM . . . . . 7

2.1 Galaxy Overview . . . . . 7

2.1.1 M51 Dynamics . . . . . 7

2.1.2 Star Clusters and Associations in M51 . . . . . 8

2.2 Observations . . . . . 10

2.2.1 Pointings . . . . . 11

2.3 Data Reduction . . . . . 11

2.3.1 Processing . . . . . 11

2.3.2 Photometry and Initial Stellar Association Selection . . . . . 12

2.3.3 Extinction/Reddening and Redshift Corrections . . . . . 13

2.3.4 Stellar Association Selection and Age Determination . . . . . 15

2.3.5 Other Parameters (Stellar Association Size, Position) . . . . . 20

2.4 Results . . . . . 20

2.4.1 Properties of Isolated Stellar Associations in M51 . . . . . 20

2.5 Discussion . . . . . 21

2.5.1 Age, Size, Mass, and Dust Distribution with Position . . . . . 21

2.5.2 The Recent Star Formation History of M51 . . . . . 24

2.5.3 Next Steps in the Analysis of the System . . . . . 25

2.6 Conclusions . . . . . 26

Chapter Page
3 AUTOMATED STAR CLUSTER/ASSOCIATION SELECTION IN NGC 4214 39
3.1 Overview . . . . . 39
3.2 Observations and Data Processing . . . . . 41
3.3 Selection and Catalogs of Stellar Groupings . . . . . 42
3.3.1 Manual Catalog . . . . . 43
3.3.2 Automatic Catalog . . . . . 44
3.3.2.1 Construction of Compact Cluster Catalog using DAOphot 44
3.3.2.2 Construction of Diffuse Association Catalog using Source Extractor . . . . . 45
3.3.3 Comparison Between Manual and Automated Catalogs . . . . 47
3.4 Size Measurements and Stellar Groupings . . . . . 47
3.5 Photometry and Age Estimates of Stellar Groupings . . . . . 50
3.6 Results and Discussion . . . . . 53
3.6.1 The Size Distribution of Stellar Groupings . . . . . 53
3.6.2 The Age Distribution of Stellar Groupings in NGC 4214 . . . . 54
3.7 Conclusions . . . . . 56
4 FINAL CONCLUSIONS . . . . . 80
4.1 Summary . . . . . 80
4.2 Future Work . . . . . 83
REFERENCES . . . . . 87

LIST OF TABLES

Table Page

2.1 Stellar Association Parameters for 120 Single-Aged Associations in the M51/NGC 5195 System . . . . . 32

3.1 SExtractor Parameter Values Used for each Gaussian Blur Size . . . . . 72

3.2 Master Table of Stellar Groupings in NGC 4214 . . . . . 73

LIST OF FIGURES

Figure Page

2.1 CM and CC diagrams, and $V$-band images for three example stellar associations from our set. The blue-purple dotted lines are Padova stellar isochrones for stellar masses from 0.15 to 66.56 $M_{\odot}$ , metallicity Z=0.019, and ages are 1 Myr (lightest blue), 6 Myr, 10 Myr, 20 Myr, and 50 Myr (purple) (Girardi 2002, and 2006, unpublished: http://pleiadi.pd.astro.it/isoc_photsys.02/isoc_acs_wfc/). The red line in the left hand panel is a BC03 model evolutionary track for an instantaneous burst stellar population of metallicity Z=0.02. Datapoints have been corrected for Milky Way dust, and $A_{V_{M51}}$=0.3 mags has been added to all models plotted. The two large dots represent the total association flux from summing the sources (open circle), and the total flux from within a large circular aperture centered on the association(closed circle). Ages for these three associations are, from top to bottom, 4 Myr, 160 Myr, and 610 Myr. . . . . 29

2.2 Top: A map of M51 indicating the age, size and location of each of the associations in our 120-association sample. For each association the relative size is represented by the size of the circle used, the age is represented by the color of the circle, and the location is presented as an overlay on the full field ACS V-band image itself. Bottom: A histogram of number of associations per size bin. . . . . 30

2.3 A map of M51 indicating the age, mass and location of the 120 associations in our sample. For each association the mass is represented by the size of the circle used, the age is represented by the color of the circle, and the location is presented as an overlay on the ACS V-band image. . . . . 31

Figure Page

3.1 *HST* WFC3/UVIS image of NGC 4214. The $F225W$ and $F336W$ filters are shown in blue, $F547M$ in green, and $F814W$ and $F657N$ in red. North is up and East is right. *Image Credit: Z. Levay, NASA, R. O'Connell (University of Virginia), the WFC3 Science Oversight Committee.* . . . . . 58

3.2 Manual (green) and automatically selected (blue) stellar groupings from this study, and seven massive young clusters (MYCs) from Maíz-Apellániz (2001) (red), overlaid on the $F336W$ *HST* WFC3/UVIS image of NGC 4214. Of the seven MYCs from the Maíz-Apellániz (2001) study, six are scaled OB associations (SOBAs), and only one (cluster I-A) is a compact super star cluster (SSC). . . . . 59

3.3 Zoom-ins of previous figure: Manual (green) and automatically selected (blue) stellar groupings from this study, and seven massive young clusters (MYCs) from Maíz-Apellániz (2001) (red), overlaid on the $F336W$ *HST* WFC3/UVIS image of NGC 4214. . . . . 60

3.4 *HST* WFC3/UVIS $F336W$ image of NGC 4214 convolved with Gaussians of $\sigma = 10, 20, 40$ and $80$ pc (from left to right). North has been rotated $11$ degrees counter-clockwise from vertical on these images and all subsequent images of NGC 4214, unless otherwise noted. . . . . 61

3.5 Sources detected using SExtractor on Gaussian-blurred *HST* WFC3/UVIS $F336W$ images of NGC 4214. The top image shows all detections overlaid on the original $F336W$ image, while the four images below show the detections found for individually blurred images with Gaussians of $\sigma = 10, 20, 40,$ and $80$ pc, from left to right. Detections are color-coded according to the standard deviation of the blurring Gaussian used on the image in which they were found: $\sigma = 10$ pc (magenta), $20$ pc (blue), $40$ pc (cyan), $80$ pc (green). Black ellipses demark highly elongated detections ($a/b < 1.9$), which are usually spurious and are rejected from the potential source list. . . . . 62

3.6 Automatically selected stellar groupings with the radius which encloses the total flux ($r_{tot}$) shown for three different thresholds above the background value: 1.9 (magenta), 1.5 (blue), 1.1 (cyan). The threshold of 1.5 (blue) provides the best $r_{tot}$ for the majority of objects in NGC 4214. 63

3.7 Size histograms for three different thresholds above the background for determining $r_{tot}$: 1.1 times the background (left), 1.5 (middle), and 1.9 (right). The dashed vertical lines represent the respective radii of a star as determined by the automated method for this data. . . . . 64

3.8 LEFT: Annular flux per until area versus the central radii of the annulus. The labeled "background" level is determined by taking the mean of the flux/pixel of the $10$ largest annuli. The radius which encloses the total flux, $r_{tot}$, is indicated in red. See § **??** for more details. RIGHT: A $250 \times 250$ pixel cutout of the *HST* WFC3/UVIS $F547M$ image of NGC 4214, centered at the candidate stellar grouping position. North is up and East is right on the thumbnail images. . . . . 65

3.9 Color-color diagrams for manually selected stellar groupings in NGC 4214 (LEFT), and automatically selected stellar groupings (RIGHT). The y-axis color is $F336W-F438W$, whereas the x-axis color is $F336W-F438W$. The overlaid models are GALAXEV (Bruzual & Charlot, 2003, unpublished updated 2010 models, personal correspondance) evolutionary tracks for star clusters of twice-solar metallicity (solid line) and half-solar metallicity (dashed line). *Figure credit: R. Chandar.* . . . . . 66

3.10 Age histograms for all automatically selected regions (TOP) and manually selected regions (BOTTOM) in NGC 4214. The dashed vertical lines represent the respective radii of a star as determined by the automated method for this data. . . . . 67

3.11 Three alternative age classification schemes versus SED-fitted age for the manually selected stellar groupings in NGC 4214: Morphological classification (TOP), RMS (MIDDLE) and total radius from the automated size determination method (BOTTOM). *Figure credit: B. Whitmore.* 68

3.12 Linear-linear size histograms for $r_{tot}, r_{3/4}, r_{1/2},$ and $r_{1/4}$ (top to bottom) for stellar groupings selected by the automated method (left column) and the manual method (right column). The dashed vertical lines represent the respective radii of a star as determined by the automated method for this data. . . . . 69

3.13 Log-log size histograms for $r_{tot}, r_{3/4}, r_{1/2},$ and $r_{1/4}$ (top to bottom) for stellar groupings selected by the automated method (left column) and the manual method (right column). The dashed vertical lines represent the respective radii of a star as determined by the automated method for this data. . . . . 70

3.14 Lograrithmic size histograms of $r_{tot}$ for stellar groupings binned by age: $< 6.8$ Myr (top), $6.8-7.8$ Myr (middle), and $> 7.8$ Myr (bottom) for stellar groupings selected by the automated method (left), the manual method (right). The dashed vertical lines represent the respective radii of a star as determined by the automated method for this data. . . . . 71

4.1 *HST* WFC3/UVIS image of NGC 2841. $F336W$ is shown in blue, $F547M$ in green, $F814W$ in red, and $F657N$ (H$\alpha$) in red-orange. *Image Credit: Credit: NASA, ESA, and the Hubble Heritage (STScI/AURA)-ESA/Hubble Collaboration, M. Crockett and S. Kaviraj (Oxford University, UK), R. O'Connell (University of Virginia), B. Whitmore (STScI), and the WFC3 Scientific Oversight Committee.* . . . . . 85

4.2 *HST* WFC3/UVIS $F336W$ image of NGC 2841, with initial SExtractor-selected sources overlaid, as in Figure **??**. This is the first step in the automated stellar grouping selection method. The next steps in the automated method clean the initial source list of spurious detections, edge effects, and double-counting, and determines the characteristic size of each grouping. . . . . 86

# Chapter 1

## INTRODUCTION

The clustering of stars is one of the most visually stunning astronomical phenomena in the universe. From the groups of stars we see in our own Milky Way Galaxy to the large-scale star-forming clumps we see in galaxies in the earlier universe, these structures are both spectacular and informative. They reveal the current state of a galaxy, as well as telling the story of its history and providing clues to its future. We observe that the largest galaxies are dominated by old stars and reside in dense clusters, whereas star-forming irregular and spiral galaxies have younger stellar populations and are found in field and in the outskirts of galaxy clusters. One explanation for this difference in stellar populations is that large elliptical galaxies form from the merger of smaller spiral and irregular galaxies in galaxy clusters. If this hypothesis is true, then the collision of smaller, actively star-forming galaxies must lead to gas expulsion, disruption of existing stellar groupings, and repression of the formation of new stellar groupings. For the elliptical galaxies we see to form from colliding galaxies, interacting systems and galaxies that inhabit areas of high galactic density must form stellar groupings at a slower pace than the disruption rate. A detailed study of the stellar groupings in a statistically significant sample of galaxies, spanning the range of morphologies from isolated spirals and irregulars to actively colliding systems, will provide the insight necessary to verify and quantify the effect of local galactic environment on stellar clustering.

Stars are born out of the collapse and fragmentation of molecular hydrogen ($H_2$) clouds. The initial mass of these clouds, and their differentiation into few or many fragments, determines the nature of the group of stars that result from this collapse. Many of these initial stellar groupings subsequently dissolve or are disrupted, modifying the distribution of sizes still further. In the Milky Way, as well as

in external galaxies, stars are found in groups ranging in size from binary or multiple star systems to large complexes ($\sim$100+ pc), in mass from tenths of a solar mass to $\sim 10^8 M_\odot$, and in stellar mass density from $\lesssim 0.1\ M_\odot/\mathrm{pc}^3$ in OB associations (Preibisch & Mamajek, 2008) to $\lesssim 10^5\ M_\odot/\mathrm{pc}^3$ (assuming an average star to be of solar mass) in the core of a massive globular cluster (Lightman & Shapiro, 1978).

A star cluster is generally defined as a self-gravity dominated group of stars that was born out of a single parent cloud of $H_2$. Initially, young stellar clusters are embedded within this $H_2$ cloud, where their light is absorbed by the surrounding gas and dust and re-emitted at the infrared (IR) wavelengths. Thus, these embedded young clusters are not visible at optical wavelengths. Relatively few clusters survive beyond this embedded stage: as winds from the young stars drive out gas, the infant clusters become gravitationally unbound and dissolve into the surrounding interstellar medium (ISM). Even those star clusters that do survive past the embedded phase are likely to become unbound as the high-mass stars explode as supernova. Thus, this so-called "infant mortality" plays a very important role in the population of star clusters that remain to contribute to the overall structures we see and the light we detect from galaxies. Many researchers are currently working to quantify the rate of infant mortality in star clusters, and its dependence on properties such as the cluster's initial mass, local density of the ISM, and the presence of tidal forces (i.e. from galaxy mergers, spiral arms, bars, and other giant molecular clouds within the galaxy).

In the literature, the terminology used to define different types of star clusters can vary greatly depending on the author and galaxy being studied. This confusion stems from historical nomenclature, as Milky Way star clusters were categorized and named first, while star clusters in other galaxies were not found until much later as telescope aperture size increased and galaxy image resolution improved. In the

Milky Way, we observe two main populations of star clusters: open clusters and globular clusters. Open clusters are found in the disk of the Galaxy, are younger, more diffuse, contain more gas and heavy elements (high metallicity), are asymmetrical, and contain fewer stars. Globular clusters occupy the spherical halo component of the Milky Way galaxy, are older, larger, more dense, spherically symmetric in shape, and contain many more stars than open clusters. In general, they are found to have lower metallicities than open clusters. This low metallicity and their distribution throughout the halo, instead of being confined to the galactic disk, has led to the conclusion that globular clusters may be the remnants of infalling dwarf galaxies (e.g., Omega Centauri), or may even have formed in the proto-galactic components that coalesced to form our Galaxy (e.g,. NGC 7078; (Fe/H)$= -2.37$; Harris, 1996).

The Milky Way is a biased laboratory in which to study star clusters, both because our position within it makes assessing the big picture difficult and because we do not know if the Galaxy has a typical stellar population or a unique one. As more studies of star clusters in other galaxies were completed, populations of clusters emerged that differed significantly from what was seen in the Milky Way. In external galaxies we find Super-Star Clusters (SSCs) that are more massive than any found in the Milky Way, as well as populations of clusters that cannot distinctly categorized as "globular" or "open." Thus, in external galaxies, it is more appropriate to divide stellar groupings into compact or diffuse categories. So-called "compact clusters" are highly centrally concentrated, small ($< 5$ pc) and usually only partially resolved, even in the nearest galaxies. More diffuse objects are called "stellar associations," and have much lower densities than their compact brethren. An important difference to note is that while compact clusters have Gaussian radial light profiles, stellar associations are often asymmetrical, need not have a central concentration, and may have multiple clumps of stars within them.

One of the most useful properties of star clusters is the effectively identical ages of their member stars. It is believed, both from observations and simulations, that the $H_2$ clouds that from stars fragment and collapse relatively quickly, forming stars with ages within $5$ Myrs of one another. Compared to the timescales of galaxy formation and evolution, this $5$ Myr difference can be considered as nearly instantaneous. An important consequence of the coeval nature of stars in a star cluster is that one can determine the likelihood that the stars within an area were born from the same gas cloud by measuring the color and magnitude of the stars in that region. The position of stars on the color-magnitude diagram gives an approximate age for the star cluster, a fact which we utilize heavily in Chapter 2.

Though much progress has been made over the years in our understanding of stellar clustering, there are still many fundamental aspects of this process that have not been fully explained. At least 50% of stars are thought to form in groups and clusters (Lada & Lada, 2003). The exact proportion of field stars that come from dissolving star clusters or that are born isolated *in situ*, and how this proportion varies from galaxy to galaxy, is still an area of active investigation. In the Milky Way, stellar agglomerations are generally broken into compact (globular) and diffuse categories (open clusters and associations). But do these represent separate physical modes of clustered star formation or are they actually a part of a continuous distribution? Similar questions are relevant for external galaxies. For example, Maíz-Apellániz (2001) argues that young star cluster formation is bimodal, with compact clusters and scaled O and B associations (SOBAs) being preferentially formed. Other authors emphasize the continuous, or fractal-like nature of the clustering (e.g., Elmegreen et al., 2006). Also, evidence has shown that young star clusters do not form in isolation, but are themselves clustered into larger cluster complexes (Larsen, 2004). The interplay between smaller clusters, the larger associations they are embedded in, and the disruption time of star clusters and

associations is poorly understood, but is integral to our understanding of how the stellar populations of galaxies evolve with time. I will investigate these questions by uniformly selecting stellar groupings across the range of size scales in nearby galaxies. By tabulating and analyzing the properties of these groupings, I can assess the likelihood of a variety of cluster evolution schemes.

Historically, the study of compact star clusters and of larger scale stellar associations in external galaxies have relied on different selection techniques, with a result that most authors have studied one or the other, but not both of these classes of stellar groupings. For example, searches for compact clusters in nearby galaxies typically use software that is designed to detects individual stars (e.g., DAOPHOT, Stetson, 1987), since the clusters are point-like and only partially resolved. When the individual components or groups of stars can be resolved, as is the case with larger stellar associations, detection algorithms such as friends-of-friends (e.g., Garcia et al., 2009; Bresolin et al., 1998; Regan & Wilson, 1993), minimum spanning tree (e.g., Cartwright & Whitworth, 2004; Sánchez & Alfaro, 2009), two-point-correlation functions (e.g., Simon, 1997), and Gaussian-smoothing (Elmegreen et al., 2006) are commonly employed. Because they are tuned towards finding a particular type of stellar groupings these studies are intrinsically biased to find objects of a certain size and light profile. The main work of this dissertation is to develop a uniform way to select stellar agglomerations spanning a range of size scales, so that we can study the size distribution of stellar groupings without the predetermined discretization of the groupings. We produce two different methods for the selection of stellar groupings. The first method assesses whether or not a group of stars is likely to be coeval based on the color-magnitude (CM) and color-color (CC) diagrams. This method is highly manual and user-intensive, and is only valid for stellar groupings whose stars are resolved. The second method uses Gaussian-blurring of images to aid automatic selection and a curve-of-growth type analysis to

determine the size of the stellar groupings. This process has the advantage of automation, which reduces personal bias and makes selection of stellar groupings in a statistically significant sample of galaxies feasible. The major disadvantage of this approach is that chance superpositions of unrelated stars are unchecked, since the stellar groupings are selected solely based on their projected surface brightness profile with respect to the background. Both selection methods have their advantages and drawbacks, and their respective results are compared and contrasted.

This dissertation is outlined as follows: Chapter 2 explains a manual method for selecting single-aged stellar associations in M51, which has already been published in *The Astronomical Journal* (Kaleida & Scowen, 2010). Chapter 3 presents an automated method for selecting star clusters and stellar associations in NGC 4214 and shows the results of the automated selection method in this galaxy, which is in preparation for submission to a peer-reviewed journal, with expected submission in September 2011. Chapter 4 summarizes the main results. This work sets the stage for study of stellar groupings in a statistically significant set of nearby galaxies which span the range of galaxy morphologies, luminosities, and local galactic environment (cluster or field galaxies).

# Chapter 2

# SINGLE-AGED STELLAR ASSOCIATION SELECTION IN THE M51/NGC 5195 SYSTEM

## 2.1 Galaxy Overview

M51(also known as NGC 5194) is one of the nearest and largest grand design spiral galaxies. The galaxy is known to be undergoing an interaction with its companion NGC 5195 (Toomre & Toomre, 1972), and shows an active system of star formation (SF), largely confined to two spiral arms. The morphology of NGC 5194 is listed by de Vaucouleurs et al. (1976) as a SA(s)bc(pec)III galaxy. The companion has been determined to be type SB0 by Sandage & Tammann (1987), and as an I0(pec) by de Vaucouleurs et al. (1976), and its nucleus hosts a nonthermal source (Ford et al., 1985). Physical parameters adopted in this chapter include a distance of $8.4 \pm 0.6$ Mpc (Feldmeier et al., 1997), a tilt angle of $20°$and a positional angle of the major axis of $170°$(Tully, 1974). M51 is consistent with super-solar metallicity ($Z \sim 2 - 3\, Z_{\odot}$) and shows a weak metallicity gradient as a function of distance from the nucleus (Zaritsky et al., 1994).

### 2.1.1 M51 Dynamics

M51 is a very complicated and dynamic system. Most of the unique properties exhibited by the system appear, not surprisingly, to be directly related to the interaction the disk is experiencing with the companion. This interaction has been modelled extensively throughout the years, with increasing success in matching the present state of the M51/NGC 5195 system. Early models fit optical data well, but were unable to explain M51's extended unionized hydrogen (HI) gas tail (Toomre & Toomre, 1972; Hernquist, 1990; Rots et al., 1990). More recent attempts fit HI maps well, but differ in the histories they paint for the M51 system. Salo & Laurikainen's (2000) N-body model suggests elliptical orbits and multiple passages of NGC 5195 through

the disk of M51. In contrast, Wahde & Donner's (2001) model utilizing a genetic algorithm favors a hyperbolic and thus single-passage encounter, but fails to match the observed velocities in the HI tail. Theis & Spinneker (2003) combines N-body methods with a genetic algorithm, and achieve a good fit to both the HI intensity and velocity maps. Their results suggest a highly elliptic orbit with two recent disk passages at $400-500$ Myr and $50-100$ Myr ago, in agreement with Salo & Laurikainen (2000).

### 2.1.2 Star Clusters and Associations in M51

In addition to its intrinsic properties, the uniqueness of the M51 system as a test bed for understanding the effects of galaxy interaction on star formation has led to many systematic studies of its stellar populations. Previous Hubble Space Telescope (*HST*) studies of the compact star clusters in M51 include Bik et al. (2003) and Bastian et al. (2005a,b), who investigated clusters near the center of M51, Lee et al. (2005), who utilized a morphological cluster selection criteria across the whole of the galaxy, and Hwang & Lee (2008), who detected over 2,000 clusters in the M51/NGC 5195 system.

Observations have shown that M51 exhibits a much bluer color than its companion overall, and the blue and yellow-red stellar populations within M51 are spatially separate structures (Zwicky, 1955). The bluer star cluster colors seen in late-type galaxies such as M51 indicate recent star formation, as the O and B stars that produce this light are short-lived. In addition, interacting galaxies tend to contain very luminous and massive young star clusters, as compared to solitary galaxies (Whitmore, 1999, and references therein). In this chapter I use the data from the *HST* Advanced Camera for Surveys/Wide Field Channel (ACS/WFC) imaging survey program $\#10452$ of M51 to study in detail the structure, dynamics, stellar populations and ongoing star formation in this system.

The high spatial resolution and broad wavelength coverage of the ACS/WFC provide unique data on the stellar populations in and around singly-ionized hydrogen (HII) gas regions in M51. Our initial objective is to observe colors and magnitudes of stellar associations covering a range in luminosity and galactocentric radius within M51. These data can be used to build CM and CC diagrams for the youngest stars, and thereby assess the fundamental parameters of the young stellar populations. At the distance of M51, we calculate that the limiting magnitude of the ACS/WFC ($M_V = -3.12$) will restrict detection of CM turnoffs to only the youngest and brightest stellar populations, corresponding to an age of $\sim 12$ million years in the $V$-band. Thus, the stellar groupings which we will explore here are generally OB associations ($\sim 100$ pc in size) or subgroups within OB associations ($\sim 50$ pc) (Brown et al., 1999; Elmegreen et al., 2006). The stellar data can also be used to assess possible systematic variations in the stellar content of these complexes as a function of position within the galaxy.

The timescale between local compression and the peak in star formation (SF) can be made based on the apparent separation of the arms delineated by the dust and HII regions respectively (Shu et al., 1972). This timescale is found to be a constant at $4.6$ Myr for the southern arm (Elmegreen et al., 1992), and increasing as a function of radius for the northern arm, although the actual value for the northern arm timescale is less than that exhibited by the southern arm. By looking at the stellar components across the divide and their apparent ages we can learn how long the youngest stars reside where they were born, and thus track the position of the stars over time and when and where the SF event actually happened. In addition, we can use this stellar association sample to gauge the SF history as a function of position and determine the role the local environment plays in the rate and efficiency of the process. We already know that environment plays a key role in determining the stability of the local ISM to triggers or compressions that may

induce gravitational collapse, and ultimately cause star formation. What is less obvious is how that characteristic is set by the presence of a generation of stars from an earlier SF event. Clearly, if a massive stellar cluster is formed, that cluster imparts not only strong ultraviolet (UV) radiation to the local ISM (as the resulting HII region is not typically radiation bounded), but also leaks strong continuum photons into the surrounding gas. The cluster can also contribute strong mechanical energy from its intense stellar winds that can sweep up and collect material into dense sheets or interfaces. These interfaces are ripe for the second generation of SF to ignite upon the incidence of a supernova blast wave (from the same short-lived massive stars), or from the nearby compression of material due to a variety of other possible triggers, such as cloud-cloud collisions, spiral density waves, etc..

## 2.2 Observations

The datasets used in this study were obtained with the *HST* ACS/WFC as part of program $\#10452$, which was completed in January 2005 and became publicly available in April 2005 (Mutchler et al., 2005). The datasets provide a six-tile image mosaic, with four dithered exposures taken for each of four filters. The four different imaging bands are $B$, $V$, and $I$ broadbands ($F435W$, $F555W$ and $F814W$ respectively), and the narrowband redshifted $H\alpha$ filter $F658N$. The standard archival data was retrieved "on-the-fly" from the archive with standard ACS pipeline (CALACS) processing, including bias, dark, and flat-field corrections. The $H\alpha$ exposures are of sufficient depth to reach surface brightnesses of at least $10^{-16}$ ergs/cm$^2$/s/arcsec$^2$ to allow us to probe the faintest HII regions.

An ACS/WFC pixel subtends $2.0$ pc at the distance of M51 and its companion NGC 5195. This means that a single pixel in the image could contain one or multiple stars, and thus there is the possibility of more than one star being sampled by each pixel. If two or more stars fall on the same pixel, this will still yield

a non-symmetric wing in the point-spread function (PSF) that may be detected in the surrounding pixels. Also, the total luminosity of a pixel is a good determinant of the number of stars in a single pixel or source. If the intrinsic brightness of a pixel or source is greater than the maximum luminosity expected for a single star then it can be assumed that the pixel contains multiple stars. On our CM diagrams, luminosities at or above $M_V{=}{\sim}{-}9$ are assumed to be multiple stars or compact clusters.

#### 2.2.1 Pointings

Using the *HST* ACS/WFC, a $2{\times}3$ mosaic ($6$ pointings, $4$ orbits per pointing) was obtained in $4$ filters (Johnson $B$,$V$,$I$, and $H\alpha$) at a telescope orient of $\sim 270^{\circ}$. Details of these exposures along with the central coordinates of the $6$ pointings or “tiles" in the $2{\times}3$ mosaic are available in Mutchler et al. (2005). Each pointing provides $4$ orbits of integration providing the limiting magnitudes listed in Mutchler et al. (2005). The $4$ exposures within each tile were dithered: a small sub-pixel dither ($2.5{\times}1.5$ pixels), and a larger dither which spans the interchip gap ($5{\times}60$ pixels).

### 2.3 Data Reduction

#### 2.3.1 Processing

The initial raw data was processed using the standard Hubble pipeline, through the Image Reduction and Analysis Facility (IRAF)[1] task CALACS (Mutchler et al., 2005). CALACS performs the corrections for bias, dark, and flat fielding. The resulting images were then cosmic-ray rejected by combining two images of the same exposure time and gain, discarding the saturated cosmic ray pixels from one image, and replacing the “bad" pixel with the good signal from the second image. Distortion effects from the camera’s off-axis position within the observatory are smaller than

[1] IRAF is distributed by the National Optical Astronomy Observatories, which are operated by the Association of Universities for Research in Astronomy, Inc. (AURA), under cooperative agreement with the National Science Foundation.

the photometry aperture used, and thus are inconsequential for this application (but would be relevant if exact astrometry of individual stars was needed).

### 2.3.2 Photometry and Initial Stellar Association Selection

The associations included in this catalog were chosen to be relatively isolated from neighboring groups of stars in order to produce a single-aged CM diagram. After processing with CALACS and cosmic-ray rejection, the V-band image was inspected by eye for isolated stellar groups from which CM and CC diagrams could be derived. Initial sample selection was performed by visually scanning each image for groupings of stars/sources that could be associated with one another. A total of $969$ stellar associations were selected in this way for subsequent analysis. For each association, a CM diagram was produced to assist in determining if the group of stars in question was indeed coeval. A more detailed description of this method of analysis is described in following sections. Photometry was performed on these groupings of stars using the Interactive Data Language (IDL)[2] Goddard Space Flight Center (GSFC)'s Astronomy User's Library (ASTROLIB[3]) package IDLPHOT. This package selects the individual stars and outputs the flux from each star, as measured within an aperture with a two pixel radius, in the $B$, $V$, and $I$ broadband filters and the $H\alpha$ narrowband filter. Two pixels is the approximate full-width-at-half-maximum (FWHM) of point sources in these images, and this aperture size was chosen to help exclude unresolved compact clusters from our source selection, although selection of the most compact clusters along with the stars is unavoidable. Thus the "sources" plotted include stars, unresolved multiple star systems, and some compact clusters. Background maps for each tile, chip and imaging band were produced by iteratively replacing any pixel greater than $1.3$ times the median of the surrounding $12\times12$-pixel box with the median value, until

[2] http://www.ittvis.com/language/en-us/productsservices/idl.aspx
[3] http://idlastro.gsfc.nasa.gov/

all stellar sources were masked out by the median value. These background maps were then subtracted from the images to properly correct for the local sky level. The fluxes derived from our initial methods were then converted to absolute Vega magnitudes by dividing by the exposure time, multiplying by the spectral flux density per unit wavelength that would generate $1$ count/sec (header value PHOTFLAM), and then translated to an $ST$ magnitude via the equation m$=-2.5\,log_{10}(F)+$ PHOTZPT (where PHOTZPT$=-21.10$ for the $ST$ magnitude scale). These magnitudes were converted to Vega magnitudes and compared to magnitudes calculated via the method detailed in Sirianni et al. (2005). The magnitudes calculated in these two methods were identical to within a thousandth of a magnitude. Finally, a CM diagram of absolute magnitude in the $V$-band versus ($B-V$) and a CC diagram of ($B-V$) versus ($V-I$) were produced for each stellar association.

### 2.3.3 Extinction/Reddening and Redshift Corrections

Photons collected from the M51/NGC 5195 system experience reddening and extinction due to dust internal to M51 and Milky Way dust, as well as redshift from the radial component of the galaxy's proper motion. All of these factors must be carefully corrected to insure accurate photometry. The redshift of M51 is z$=0.00154$, which corresponds to shifts of $6.62$, $8.23$, $12.8$, and $10.1$, for the central wavelengths of the $B$, $V$, $I$, and $H\alpha$ filters, respectively (Scoville et al., 2001). These corrections were applied to all wavelengths. Extinction due to dust poses a more complex problem, as decomposing internal and Galactic dust is extremely difficult without data across the whole spectral range. Also, most authors utilize the Galactic extinction corrections from Table 6 of Schlegel et al. (1998), but these values are not ideal for our purposes since they were acquired by convolving the SED of an elliptical galaxy with the specified filter throughput curves. Assuming the SED of an elliptical galaxy neglects the blue continuum from young stars present in a spiral

galaxy, and would introduce an $\sim$5$\%$ error in our reddening corrections (Schlegel 2008, personal correspondence). For the present analysis, we treat the internal and Galactic extinction separately, and follow the precedent of other authors (Lee et al., 2005; Mora et al., 2009; Úbeda et al., 2007) and use the Schlegel et al. (1998) values to correct for extinction due to dust in the Milky Way, in spite of the $5\%$ error. Future work is planned to explore the possibility of avoiding this error by producing de-reddened Simple Stellar Population (SSP) Spectral Energy Distributions (SEDs) from the GALAXEV (Bruzual & Charlot, 2003) models and fitting the reddening values to the data available from *HST* (optical), GALEX (UV), and Spitzer (IR) observatories for each stellar association. This method would bypass the necessity of decomposing internal and Galactic reddening, and avoid the error imposed by assuming the SED of an elliptical galaxy. For the present study, we correct for Galactic extinction using equations 1, 3a, and 3b in Cardelli et al. (1989), with $R_V$=3.1 and $A_{V_{MW}}$=0.117 for the direction of M51 (Cardelli et al., 1989; Schlegel et al., 1998).

The intrinsically dusty environment of M51 is known to hamper studies of both the ionized gas and the HII regions themselves. The overall apparent structure and excitation state of gas around massive ionizing stars is strongly affected by the presence of the dust and may modify the continuum of photons that escape to ionize and energize the surrounding ISM. The effect these modifications have on the dynamics and susceptibility of the ISM to subsequent second-generation triggering or propagation of star formation make this galaxy an interesting candidate for the study of star formation as a global mechanism for distributing and regulating the formation of the next generations of stars. To account for the effects of dust internal to M51, we assume a global extinction correction of $A_{V_{M51}}$=0.3 mags, corresponding to an reddening correction of E($B-V$)=0.097, using $R_V$=3.1 (Cardelli et al., 1989). This value was found to be an average of the best fit for the majority of the associations studied, if $A_{V_{M51}}$ is allowed to vary between $0-1$ mags, in incre-

ments of $0.1$ mags. This value is in good agreement with with Hwang & Lee (2008), who use E($B-V$)=$0.1$ (A$_{V_{M51}}$=$0.31$ mags), and is less than the maximum value in the bulge, which is E($B-V$)=$0.25$ (A$_{V_{M51}}$=$0.775$) (Lamers et al., 2002). Ideally, it would be best to leave the extinction correction as a free parameter in the SED fitting, since dust content varies noticeably over the disk of M51, and thus a single correction value for the entire galaxy can only be an approximate correction. Unfortunately, with only $BVI$ fluxes, we are unable to discern fluctuations in the local dust environment and stellar association ages simultaneously. Visual inspection of the CM and CC diagrams of the $120$ associations in our set show that A$_{V_{M51}}$ lies between $0$ and $1$ magnitudes for most of the associations. We choose an intermediate value of $0.3$ magnitudes, knowing that some associations will be slightly over- or under-corrected.

### 2.3.4 Stellar Association Selection and Age Determination

The use of a CM diagram of M$_V$ versus ($B-V$) was originally chosen to allow direct comparison with the Sandage age estimation model (Sandage, 1957), in order to test the viability of determining stellar association ages via their main sequence (MS) turnoff magnitude, given the distance of M51 and depth of *HST* ACS/WFC images. These colors were chosen over other available bands to maximize the depth of the sample, as $B$ and $V$ have fainter limiting magnitudes than $I$ or $H\alpha$. The Sandage model is based on MS turnoff ages of 10 galactic clusters and one globular cluster. These clusters provide an age-MS turnoff magnitude relation, which we derived via a simple empirical interpolation of Sandage's Figure 1. For each association in our sample, a selection box of the appropriate size was chosen to produce the narrowest sequence and thus the tightest fit to the Sandage model when it was overlaid on the resulting CM diagram. Dense stellar regions which did not closely

fit the model were not included in the list of potential associations, as they are most likely blends of multiple cluster. These groups may be spatially related, but are not necessarily coeval, making determination of a single age impossible.

More modern treatments of this approach involve the use of model isochrones to accurately predict the apparent locus of stellar points on such a CM diagram for known differences in metallicity, age, and cluster size. However the underlying treatment is still sound—to use the distribution of member stars in an association to determine an estimate for the apparent age of the grouping based on the turnoff exhibited. Complications arise in the application of the method due to blends of multiple stars and/or compact clusters being detected as a single source. Plotting sources in both CM and CC space helps to separate stars from compact clusters, and to weed out groups of stars that are not massive enough to be accurately fit with the SSP models of Bruzual & Charlot (2003, hereafter BC03). The M51/NGC 5195 system is at the very limit of the *HST* ACS/WFC's ability to resolve individual stars, and the corresponding brightness limit due to the exposure times used narrows the ages we could detect via this method to only the most recent of SF events. Consequently, this study is only sensitive to the bluest of associations containing the most massive, and therefore the shortest-lived, stars.

Even if blending or resolution limits were not an issue, the fact that we are working at the blue end of the MS also constrains the resolution in magnitude space that can be used to resolve turnoffs on CM diagrams. At the top end of the MS, the sequence is almost vertical, meaning that the locus of turnoff points is also almost vertical. The degree to which we can measure small changes in brightness therefore limits the degree to which we can pull out departures from the MS due to evolutionary turnoff, as opposed to a simple intrinsic spread in brightness due to population and possibly internal reddening etc. There is an intrinsic scatter in apparent brightness for any collection of stars in a cluster or association, and it is

the art of distinguishing intrinsic scatter from changes due to stellar evolution that is at the heart of this approach, and is also the most difficult part of the technique. The limiting magnitude of the ACS observations translates into an inability to detect main sequence turnoff ages any older than $\sim 12$ Myrs. This is a flaw in the approach, but given the distance to the galaxy, this is at the boundary of what we can do observationally at this time (Rey et al., 2007).

To help make the final selection of single-aged associations to be included in the sample, Padova stellar isochrones (Girardi et al., 2002)[4], and a BC03 stellar population evolutionary track were overlaid on the CM and CC diagrams. Figure 2.1 shows these plots for three example associations from our set that span the range of ages found ($4 - 610$ Myr). One must carefully assess the distributions of sources for each association on these two plots to be certain that the stars/compact clusters in it are in fact coeval. Groups of stars that did not lie along a single isochrone (within the scatter of the data), whose total magnitude did not align with the BC03 model SED, or whose CM and CC diagrams indicated discrepant ages were excluded from the set. This second iteration of the selection process yielded a final list of $120$ associations. Figure 2.1 shows the CM and CC diagrams for three representative stellar associations from this set, alongside the image subraster that generated it.

Since M51 is at the limits of our ability to resolve individual stars and measure MS turnoff ages, we decided to employ a modern refinement - the use of stellar population models in tandem with SED fitting to allow the prediction and subsequent measurement of stellar association age. In order to fit model SEDs to the selected stellar associations, we have written a series of IDL scripts that calculate the flux from each of the associations, produce model stellar population SEDs from the GALAXEV library, calibrate these models for comparison to the data, and perform a $\chi^2$ fit between the observations and the model SEDs. The SED with the

[4]Most recent isochrones (2006), unpublished: http://pleiadi.pd.astro.it/isoc_photsys.02/isoc_acs_wfc/

minimum $\chi^2$ value when compared to the data is the best-fit model.

The GALAXEV library allows for tuning of the input parameters in order to best match the stellar population of interest, in our case stellar associations in the M51/NGC 5195 system. For associations in M51 we choose the Padova 1994 stellar evolutionary tracks (BC03, and references therein), a Salpeter initial mass function of $\xi(log_{10}(M)) \propto M^{-1.35}$ (Salpeter, 1955), and an instantaneous burst star formation rate (SFR) of $\psi(t) = 1M_{\odot} \cdot \delta(t)$ (BC03), which best replicates the scenario of triggered star formation. We allow for a range of models between the ages of $0.1$ Myr$-1$ Gyr (this range should include the two most recent perigalacticon passages of the two galaxies) (Salo & Laurikainen, 2000), extinction due to dust in M51 of $A_V$=$0.3$ mags, and a metallicity of $2.5Z_{\odot}$ (Zaritsky et al., 1994). The mass of each association is quantitatively calculated during the $\chi^2$ fitting process, details of which are described below.

To perform model SED fitting, a library of BC03 SSP models was produced, and the model stellar association SEDs were created by converting the GALAXEV output into fluxes that can be compared directly to fluxes calculated from the *HST* data. The library of BC03 SSP models are created by running two scripts available in the GALAXEV package: CSP_GALAXEV and GALAXEVPL. CSP_GALAXEV evolves the composite stellar populations spectrally for a constant metallicity using Equation (1) of BC03, and outputs a binary file of the evolved spectral evolutionary model. The program GALAXEVPL then reads in the binary file from CSP_GALAXEV, and outputs ASCII files of SEDs at the ages requested by the user. This ASCII file contains wavelength (column 1) and specific luminosity density in ($\ell_{\lambda}$ in Papovich et al., 2001), or luminosity per unit wavelength, in units of $L_{\odot}$·Å$^{-1}$ (column 2). In order to convert from this number to flux ($F_{\nu}$), we followed

the procedure outlined in Section 4.2 of Papovich et al. (2001), using

$$L_\nu = \frac{10^8 \lambda_0^2 \ell_\lambda L_\odot}{c M_{tot}} 10^{-0.4(A_{\lambda,MW}+A_{\lambda,M51})} \tag{2.1}$$

to calculate the luminosity per unit frequency, and

$$F_\nu = (1+z) L_\nu \frac{1}{4\pi d^2} \tag{2.2}$$

to calculate the flux per unit frequency, where $\lambda_0$ is the redshifted wavelength, $\ell_\lambda$ is the specific luminosity density, $M_{tot}$ is the total mass of the stellar population at a particular timestep, $A_{\lambda,MW}$ is the extinction due to dust in the Milky Way (Cardelli et al., 1989; Schlegel et al., 1998), $A_{\lambda,M51}$ is the extinction due to dust internal to M51, d is the distance to the galaxy, and all units are in the CGS system. $F_\nu$ calculated from Equations (1) and (2) is for a $1\,M_\odot$ stellar population, and has units of erg $\cdot$ cm$^{-2}$ $\cdot$ s$^{-1}$ $\cdot$ Hz$^{-1}$. The quantity $M_{tot}$ is obtained by extracting the value of Mgalaxy in column 9 of the $*.4color$ ASCII file output from GALAXEVPL which corresponds to the desired age to be modelled, and is the same quantity as $m^*(t)$ in Papovich et al. (2001).

We then convolved each model SED with the $B$, $V$, $I$, and $H\alpha$ filter throughput curves to get the flux per unit frequency in each filter, $f_\nu$, using

$$f_\nu = \frac{\int \frac{F_\nu \tau_\nu}{\nu} d\nu}{\int \frac{\tau_\nu}{\nu} d\nu} \tag{2.3}$$

where $\tau_\nu$ is the total system throughput curve, including all transmission and detection effects of the telescope, camera, filter, and CCD chip (Fukugita et al., 1996).

The mass of each stellar association is calculated using the fact that the BC03 model SEDs are normalized to a $1\,M_\odot$ stellar population. The mass which produces the smallest $\chi^2$ value between the data and each model SED is calculated by minimizing the following equation with respect to $M$ and then solving for $M$, then plugging this mass back into the equation to calculate the minimum $\chi^2$ for each

model.

$$\chi^2 = \sum_i \left[ \frac{f_{\nu,i}^{obs} - M f_{\nu,i}}{\sigma_i} \right]^2 \tag{2.4}$$

where the summation is over $i$ filters, $f_{\nu,i}^{obs}$ is the observed flux in filter $i$, $M$ is the best-fit mass for a particular stellar association, $f_{\nu,i}$ is the model SED flux in the filter $i$, and $\sigma_i$ is the error in the observed flux for filter $i$. The best-fit model stellar association SED was then chosen from the array of model SEDS by finding the minimum $\chi^2$ value between model and data in the $B$, $V$, and $I$ bands. It should be noted that it is not valid to use $H\alpha$ flux directly as a fitting parameter for a stellar population, since $H\alpha$ is emitted and absorbed both from the stellar photosphere and the surrounding gas.

### 2.3.5 Other Parameters (Stellar Association Size, Position)

The size of each association was estimated by determining the spatial extent of the FWHM of the flux density profile of stars. Specifically, stars/sources were counted in radial bins from the association center, the flux from sources in each bin were totaled, and the standard deviation of the spatial flux density distribution was computed. The full width at half maximum was then computed assuming that the distribution was Gaussian.

The position of each stellar association in equatorial sky coordinates was calculated using the WCSTools package (Mink, 1997, 1999), which allows for the non-linear conversion from pixel coordinates in the undrizzled images output from CALACS to right ascension and declination in the appropriate epoch. Associations were named according to the tile of the mosaic they reside in, and the lower left and upper right corners of the bounding box for that association, in pixels.

## 2.4 Results

### 2.4.1 Properties of Isolated Stellar Associations in M51

Results presented here are from SED fitting of the ages, masses, metallicities, and internal extinctions for each stellar association. Ages were also assessed by attempting to pin down the location of the main sequence turnoff point on the color-magnitude diagram, but we found that turnoffs were not apparent for the vast majority of associations (see Section 2.5). Table 2.1 lists the derived properties for the $120$ associations selected from our sample using the criteria and methods laid out above. The identifier for each association is based on a $4-$digit number indicating which image in the mosaic the association is located in, and the x,y pixel coordinates of the lower left and upper right corners of the selection box used for selection of that association. The location of the central pixel in Epoch 2000.0 coordinates and $BVI$ magnitudes in the Vega system are listed for each association.

It should be emphasized that this is the subset of associations from the full sample whose CM diagrams indicated that they were likely to be single-aged, allowing indisputable measurement of the properties listed, within the limitations of the method.

Figure 2.2 shows a map of the galaxy with various annotations derived from the measurement exercise described above, and a number density histogram of the stellar association sizes. On this diagram each of the associations has been pictorially represented by a colored circle. The size of the circle reflects the relative size of the association in physical extent. The color of the circle depicts the best-fit age of the association in question - with red associations being the oldest at $\sim 600$ Myrs, ranging down through the rainbow to the youngest ages found at $4$ Myrs, in blue. Figure 2.3 shows a similar map of the galaxy, where the size of the circle corresponds to the best-fit mass calculated quantitatively from the SED model, in-

stead of the association size. Masses found range from $\sim 1.1 \times 10^3 - 7.4 \times 10^6\ M_\odot$. The contents of Table 2.1 are therefore pictorially represented in these two galaxy maps.

## 2.5 Discussion

### 2.5.1 Age, Size, Mass, and Dust Distribution with Position

Examination of Figure 2.2 (top) shows that the majority of our association sample is resident on one or the other of the two primary spiral arms in the galaxy, or on spurs coming off the spiral arms, with few found in the interarm region. This is not a surprising result, but considering that associations in our set are defined to be single-aged groupings, this makes a statement about the dominant outcome of SF in these regions due to the recent SF episodes active in the disk. The lack of single-aged groupings in the inter-arm region may indicate that stellar associations disperse relatively quickly after formation. There is also a noticeable concentration of associations along the northern arm, the arm closest to NGC 5195, indicating an enhancement in the most recent SF activity in that area. The distribution of stellar association ages along this arm, coupled with the relative spatial positions of M51 and NGC 5195 indicates that gas is actively streaming along the arm and forming stars in its wake. Clearly, our association selection criteria limits the sample to the most dominant SF regions, since we require the associations to be well defined and well isolated from neighboring associations or dense collections of field stars. Figure 2 shows no noticeable trend between global position and association age, but does show some local trends indicating the possibility of secondary and tertiary SF events. There is also no apparent correlation between association age and distance from the galactic nucleus measured along each spiral arm. The sequencing of stellar associations spatially with age, which one would expect from SF propagating from a trigger, are apparent in some instances, particularly on the bend of the Northern spiral arm closest to the companion, but is not widespread across the

whole of the galaxy. The cycling time necessary to go from one generation of stars to the next is $\sim 5$ Myr, meaning that many cycles of triggered star formation could have occurred in this time range ($4 - 610$ Myr). It could be the case that while we see the sequential propagation of triggered star formation on star cluster scales ($1 - 5$ pc), this propagation may not occur on the larger stellar association and star complex scales ($\sim 50 - 200$ pc) investigated in this study. Another interesting result is that we see no apparent surge in the local SFR at either of the two "breaks" in the spiral arms, where the gravitational effects of the interaction has warped the spiral structure. One might expect an increased SFR in these regions, but the lack of associations found here indicates that conditions are not conducive to the condensation of gas into stars. It is likely that the dynamical shear at these two "breaks" disrupts the collapse of $H_2$ and HI clouds into stars. The size histogram shows a peak at $\sim 25$ pc, which may be due to the mixing or collapse length in the ISM dictating the dominant size of the fragment of the molecular gas cloud that will collapse into a stellar association.

In Figure 2.3, we see that there is a tendency towards more massive stellar associations in the northeastern side of the galaxy, particularly near the nucleus and on the northern spiral arm. This trend hints at the fact that stellar association mass may be more sensitive to triggers such as galaxy interactions and spiral density waves than age or size of the association.

The main sequence turnoff age determination method proved to have several major limitations. The vertical and horizontal location of any apparent MS turnoff is limited by the vertical slope of the MS at this location in the CM diagram, and the horizontal scatter of member stars in the association. Since our limiting magnitude of $M_V = -3.12$ defines that we are only seeing the very upper end of the MS, the OB stellar population. Typical lifetimes of the members of this population are really quite short, and indeed are much shorter than the $12$ Myr age cutoff that

the $M_v$=$-3.12$ should represent. As such many members of the associations we are studying never achieved turnoff, but instead probably went supernova. Older associations would, as a direct extension of this principle, be composed of much fainter stars and would therefore fall below both our limiting magnitude and selection criteria for analysis as part of our sample, and not be resolved into individual populations. Analysis of turnoff tracks based on stellar evolution theory also indicates that those B stars that do survive this long follow much smaller turnoff tracks than we expect to see from lower mass stars further down the MS. All of these factors combine to diminish the size of the effect we are trying to measure and therefore act to reduce the final sample of associations from which we could draw conclusions that could withstand scrutiny. Technically, the main sequence turnoff method should allow detection of association MS turnoffs up to $12$ Myrs of age, but no associations with a turnoff at this brightness were found, because of the confusion limit encountered when trying to verify the integrity of a turnoff right at the vertical magnitude limit of the observations on diagrams like the one depicted in Figure 2.1.

### 2.5.2 The Recent Star Formation History of M51

Using all the results presented in this chapter, we can make several rather broad statements about the recent SF history of M51. It is clear from Figure 2.2 that the interaction with NGC 5195 has generated many large, well-isolated young stellar associations across the northern arm of M51, many more than are apparent along the southern arm. This implies an enhancement in the SF on that side of the galaxy, but does not represent a system-wide elevation in the SFR. Within the limitations of the measurements we have been able to make as part of this study, we cannot see any systematic age sequencing of SF as a function of location.

This is somewhat disappointing since one would expect to see evidence of age sequencing with location as a direct result of SF propagation in the disk.

Why do we not see such evidence? Aside from the limits of the data, it is very possible that the ISM in the galaxy is sufficiently well-mixed and in an increased dynamic state that it is possible to trigger SF in any given location far easier than it might be with a more quiescent ISM. We are encouraged that our sample reflects our original expectations concerning enhanced SF on the northern arm, it would however appear that that SF locations are much more random in nature.

Indeed, the quiescent SF state reflected by the southern arm of the galaxy seems to represent a very low level of active SF over the last $5$ Myrs, when compared to the northern arm. As noted in the Introduction, the expected timescale between the passage of the compression wave in the spiral arm and the formation of stars is just less than $5$ Myrs, and so this would suggest that these results are commensurate with this view, but that the size of the compression apparent in the northern arm, and therefore the SFR this represents, is dramatically elevated, and would result in a different Schmidt law. These results explicitly depict a large variation in the SFR active in the disk of M51 from one side to the other apparently as a direct result of the passage of NGC 5195.

### 2.5.3 Next Steps in the Analysis of the System

While the human eye is an ideal detector for picking up patterns, the human brain is prone to bias. Thus our method of visual inspection for association selection and turnoff magnitude is prone to the bias of the observer. In order to reduce this effect, we plan to supplement our visual inspection methods by using an automated selection algorithm in Chapter 3, to produce an initial set of candidate associations and ages, and then using visual inspection of each candidate to eliminate false positives and assure accurate age fits.

Also, it has been shown that fitting model SEDs to optical broadband colors alone can be inaccurate, in that it is difficult to differentiate between the reddening

effects of age, dust, and metallicity (Cerviño & Luridiana, 2006; Anders et al., 2004; Piskunov et al., 2009). In future work on M51, we will incorporate UV data from GALEX and IR data from Spitzer in order to better differentiate the reddening effects of stellar population age, dust content, and metallicity.

In Chapters 3 and 4, we apply similar SED-fitting techniques to stellar associations in NGC 4214, M83, and NGC 2841, using the multiwavelength images of this galaxy taken with the new *HST* Wide Field Camera 3 (WFC3). The wide range of wavelength sensitivity available with WFC3 will allow for better differentiation between the reddening effects of age, dust, and metallicity, and thus more accurate dating of stellar groupings. Findings from this chapter's study of stellar associations in M51 will be compared and contrasted with those from using the automated stellar grouping selection method in Chapter 4.

## 2.6 Conclusions

We have taken the first high-resolution, multiwavelength, system-wide imaging dataset of the interacting spiral system M51/NGC 5195 and conducted a photometric study of the stellar associations in the system in an effort to measure and characterize the SF in the system, using the associations as age tracers. We identified $969$ stellar groupings of interest, and from this set drew a smaller sample of $120$ associations that were deemed potential candidates for further analysis. Those associations which were isolated enough to be unequivocally regarded as coeval and largely unpolluted by field stars were included in a final sample explored in this chapter. This subset was extracted and presented as the best representatives the properties of the stellar association population resident in M51.

To summarize, from the selection, photometry and SED fitting of $120$ single-aged stellar associations in the M51/NGC 5195 system, we conclude the following main points:

1. Visual inspection of the CM and CC diagrams for each potential stellar association is an effective way to weed out groups of star that are not coeval. We find that the vast majority of the single-aged stellar associations selected in this manner lie along one of the spiral arms on M51, or on spurs coming off the spiral arms.

2. Very few single-aged associations are found in the interarm regions, suggesting that either the conditions in these inter-arm regions are not ripe for the formation of stellar associations, or that stellar associations formed here disperse quickly after their birth.

3. There is an enhancement in the number of single-aged stellar associations in the northern arm spiral arm closest to the companion, most likely triggered by the interaction of M51 and NGC 5195.

4. No correlation between position within the galaxy and age of the association was found. There is also not an apparent relationship between the physical size of the association and position.

5. We see few instances of sequential formation of stellar associations, which suggests that this type of triggering may only occur on scales smaller than investigated in this study (i.e. smaller $\sim 5$ pc, on the scale of compact clusters).

6. Single-aged associations in this system range in size from $5-90$ pc, with the peak in the size-number density histogram occurring at an average radius of $\sim 25$ pc, hinting that this may be the dominant size of the scale length for collapse within the molecular clouds that stellar associations form from.

7. There is a slight trend for more massive associations to to exist preferentially in the region of M51 closest to NGC 5195. This indicates that the galaxy interaction facilitates the collapse of larger segments of molecular hydrogen

clouds than would occur without this interaction, resulting in higher-mass stellar associations.

8. Even with the resolution of *HST* ACS/WFC, main sequence turnoffs are not evident for the vast majority of stellar associations in M51, due to the limiting magnitude of our images, and the vertical nature of the turnoff at the bright end of the main sequence.

This type of study has not been possible before because no other face-on spiral has been completely imaged in the photometric bands necessary to sufficient depth and resolution to conduct such an investigation on an entire external galaxy. In recognition of this fact, the study itself has been very challenging and while we have had some success in measuring the ages of associations in our sample, there have been many fundamental limits to what we can achieve and access because of the distance to the galaxy, the limiting magnitude of the datasets, and the available bandwidths, even when done with the exquisite optics of the *HST* from space. Despite these limitations, we do believe the dataset provides an unprecedented view of the very recent SF process across the entire disk of the galaxy and reflects a definitive change in the SFR from one side of the galaxy to the other probably as a direct result of the interaction with NGC 5195. In the next chapter we use what was learned in the course of this analysis of the M51/NGC 5195 system to develop an automated method of selecting stellar groupings in nearby galaxies.

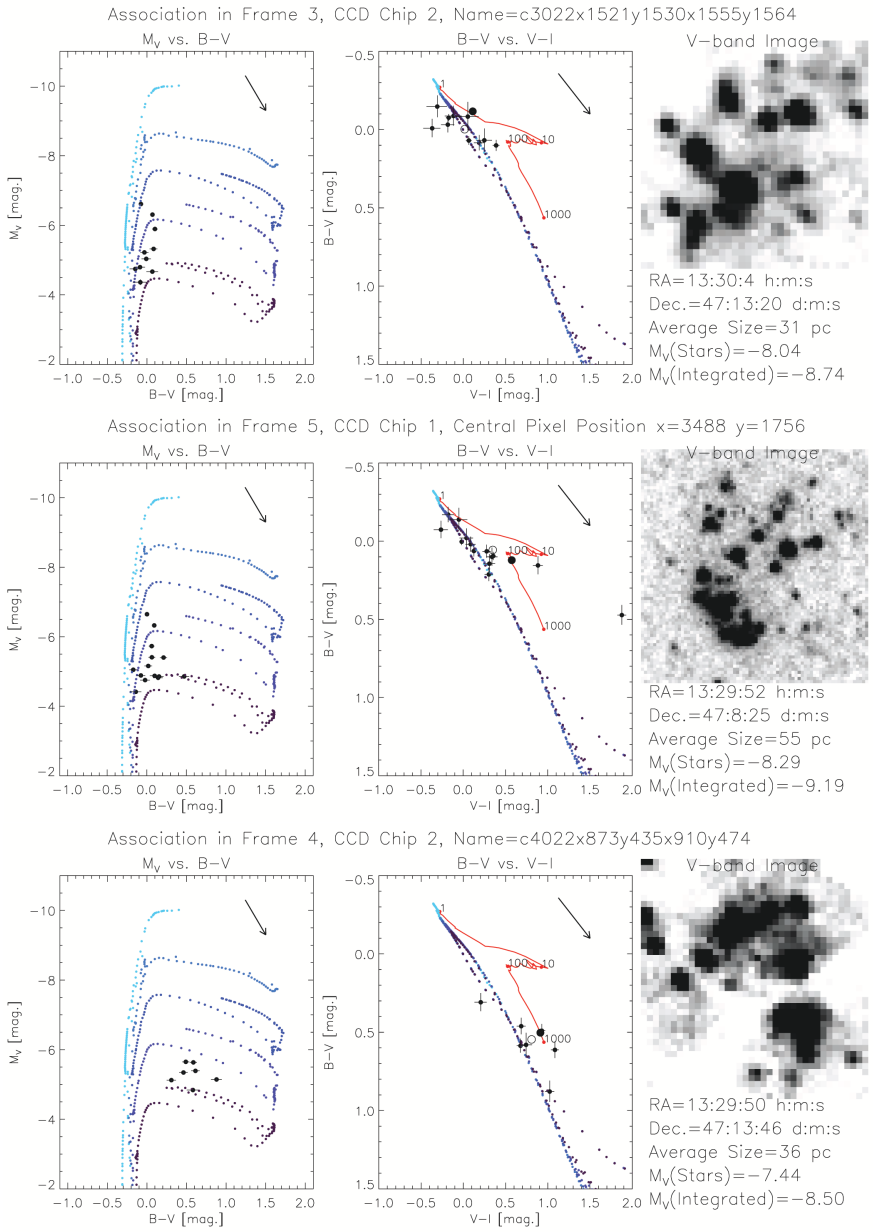


Figure 2.1: CM and CC diagrams, and $V$-band images for three example stellar associations from our set. The blue-purple dotted lines are Padova stellar isochrones for stellar masses from 0.15 to 66.56 $M_{\odot}$ , metallicity Z=0.019, and ages are 1 Myr (lightest blue), 6 Myr, 10 Myr, 20 Myr, and 50 Myr (purple) (Girardi 2002, and 2006, unpublished: http://pleiadi.pd. astro.it/isoc_photsys.02/isoc_acs_wfc/). The red line in the left hand panel is a BC03 model evolutionary track for an instantaneous burst stellar population of metallicity Z=0.02. Datapoints have been corrected for Milky Way dust, and $A_{V_{M51}}$=0.3 mags has been added to all models plotted. The two large dots represent the total association flux from summing the sources (open circle), and the total flux from within a large circular aperture centered on the association(closed circle). Ages for these three associations are, from top to bottom, 4 Myr, 160 Myr, and 610 Myr.

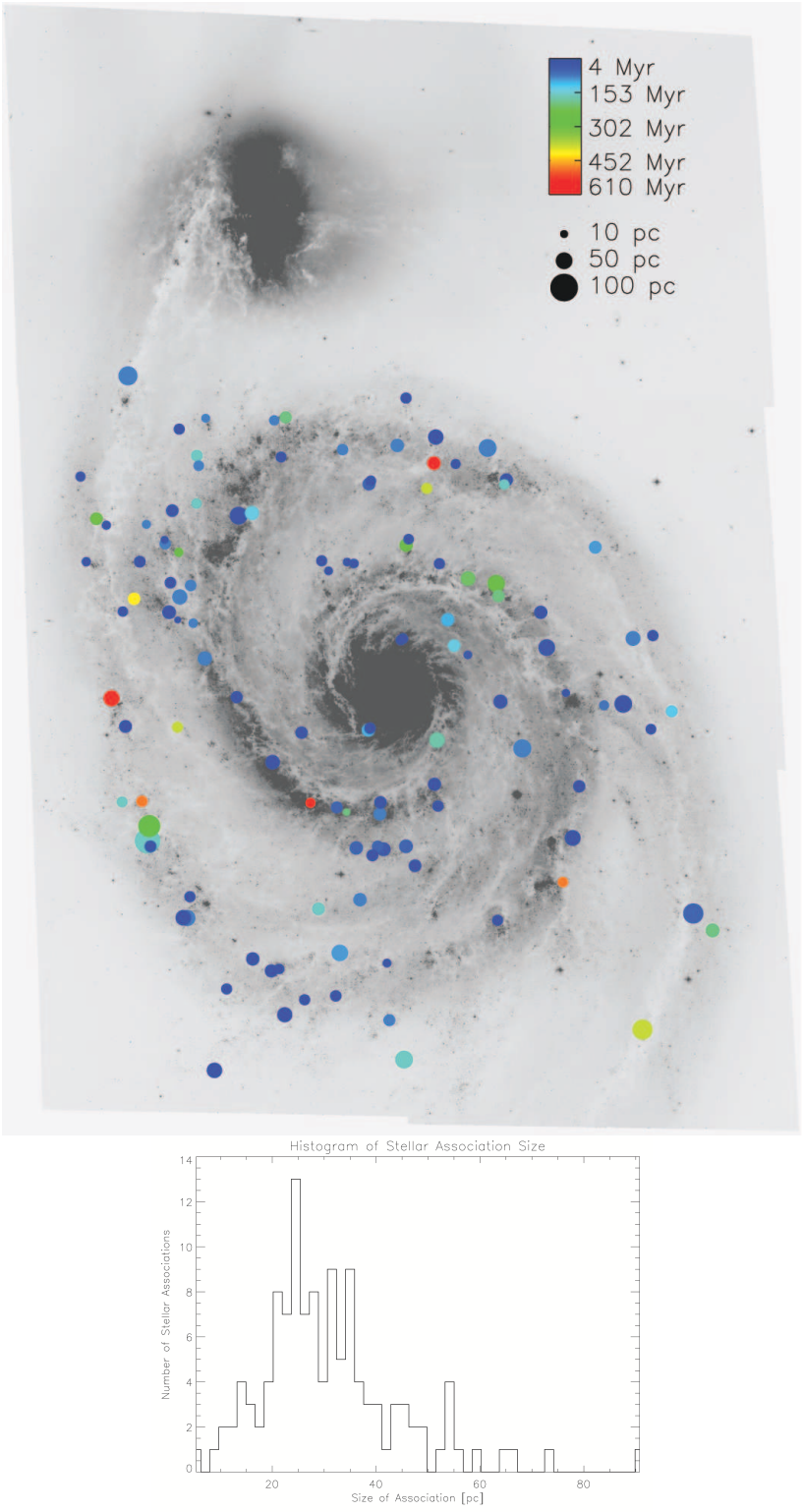


Figure 2.2: Top: A map of M51 indicating the age, size and location of each of the associations in our 120-association sample. For each association the relative size is represented by the size of the circle used, the age is represented by the color of the circle, and the location is presented as an overlay on the full field ACS V-band image itself. Bottom: A histogram of number of associations per size bin.

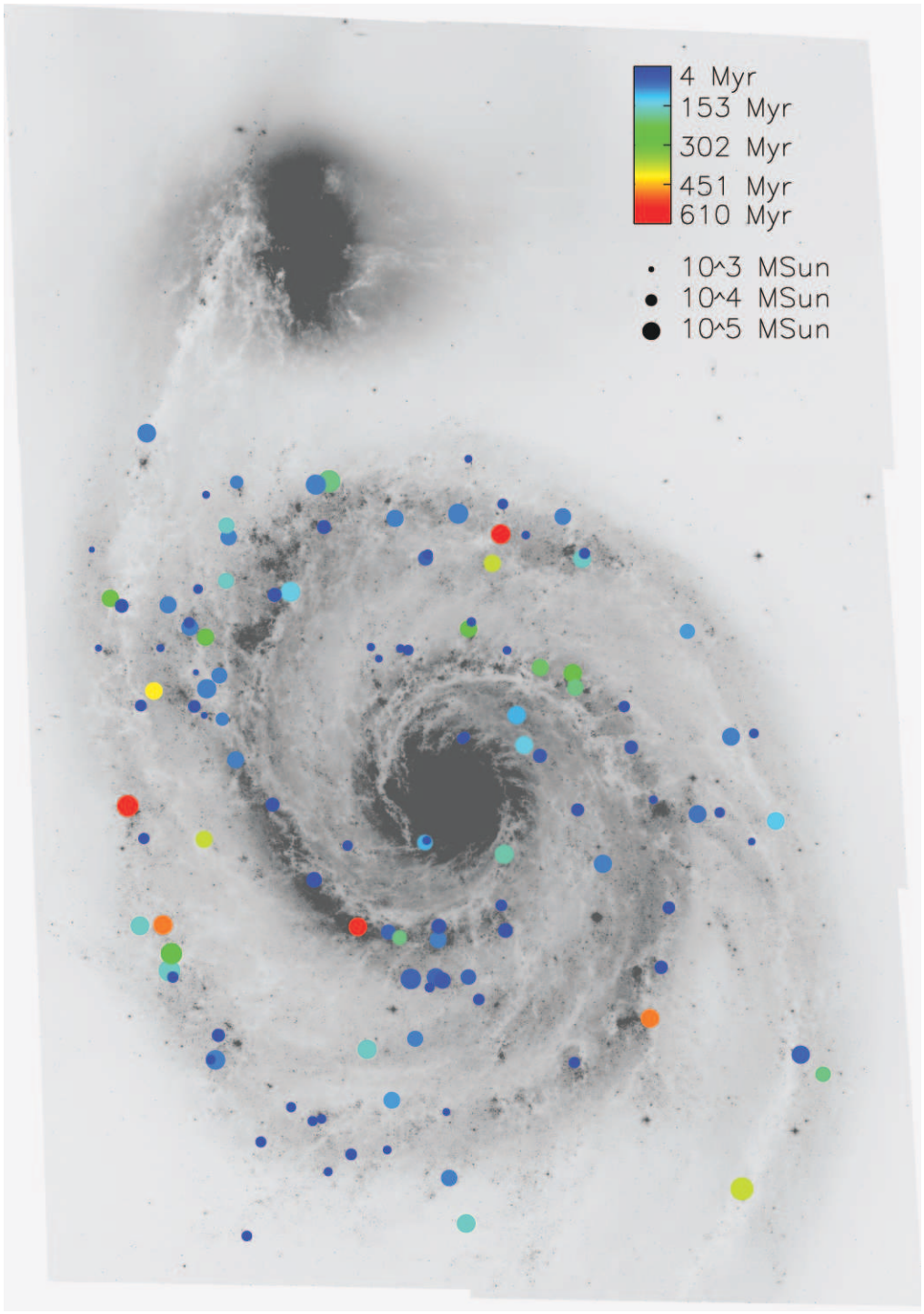


Figure 2.3: A map of M51 indicating the age, mass and location of the 120 associations in our sample. For each association the mass is represented by the size of the circle used, the age is represented by the color of the circle, and the location is presented as an overlay on the ACS V-band image.

Table 2.1: Stellar Association Parameters for 120 Single-Aged Associations in the M51/NGC 5195 System

| Identifier | RA[1] | Dec.[1] | $M_{B_{int}}$[2] | $M_{V_{int}}$[2] | $M_{I_{int}}$[2] | $M_{B_{stars}}$[3] | $M_{V_{stars}}$[3] | $M_{I_{stars}}$[3] | Radius[4] (pc) | Mass ($M_\odot$) | Age (Myrs) |
|---|---|---|---|---|---|---|---|---|---|---|---|
| c1022x3960y1058x4062y1147 | 13:30:6.6247 | 47:14:33.358 | -9.42 | -9.51 | -10.0 | -8.19 | -8.25 | -8.55 | 61.0 | $1.37x10^5$ | 86 |
| c3021x450y731x488y760 | 13:29:58.297 | 47:14:11.042 | -10.2 | -10.3 | -11.0 | -9.64 | -9.82 | -10.4 | 29.4 | $5.05x10^5$ | 200 |
| c3021x489y601x526y630 | 13:29:58.897 | 47:14:9.6002 | -10.0 | -10.1 | -10.5 | -8.91 | -9.05 | -9.23 | 21.4 | $2.41x10^5$ | 86 |
| c3021x708y1939x758y1988 | 13:29:52.393 | 47:13:55.922 | -10.0 | -10.1 | -10.5 | -8.97 | -9.11 | -9.47 | 36.0 | $2.47x10^5$ | 86 |
| c3021x782y1340x816y1376 | 13:29:55.294 | 47:13:53.766 | -8.93 | -9.00 | -9.41 | -7.93 | -8.03 | -8.19 | 26.4 | $8.43x10^4$ | 86 |
| c3021x889y657x923y688 | 13:29:58.535 | 47:13:49.797 | -10.6 | -10.5 | -10.4 | -9.89 | -9.81 | -9.69 | 24.1 | $2.34x10^4$ | 4 |
| c3021x1124y1635x1143y1662 | 13:29:53.785 | 47:13:36.833 | -9.12 | -9.00 | -8.96 | -8.24 | -8.22 | -8.30 | 22.8 | $5.61x10^3$ | 4 |
| c3021x1154y1610x1177y1651 | 13:29:53.902 | 47:13:35.405 | -8.24 | -8.22 | -8.76 | -7.17 | -7.24 | -7.88 | 33.5 | $3.31x10^4$ | 57 |
| c3021x1508y293x1566y332 | 13:30:0.0732 | 47:13:19.557 | -9.72 | -9.80 | -10.3 | -8.69 | -8.94 | -9.56 | 39.7 | $2.40x10^5$ | 140 |
| c3021x1533y136x1596y190 | 13:30:0.7910 | 47:13:18.115 | -10.5 | -10.4 | -10.9 | -9.95 | -9.97 | -10.2 | 55.0 | $2.59x10^4$ | 5 |
| c3021x2008y1044x2042y1071 | 13:29:56.400 | 47:12:54.000 | -8.28 | -8.21 | -8.19 | -7.66 | -7.59 | -7.38 | 25.0 | $2.62x10^3$ | 4 |
| c3021x2016y1329x2042y1352 | 13:29:55.056 | 47:12:53.286 | -8.22 | -8.21 | -8.57 | -7.59 | -7.61 | -7.71 | 13.8 | $3.09x10^3$ | 5 |
| c3021x2031y1397x2057y1430 | 13:29:54.697 | 47:12:52.558 | -9.07 | -9.05 | -9.35 | -8.11 | -8.13 | -8.12 | 18.5 | $6.68x10^3$ | 5 |
| c3021x2122y1118x2145y1141 | 13:29:56.015 | 47:12:48.603 | -8.06 | -8.00 | -8.09 | -7.62 | -7.54 | -7.47 | 14.2 | $2.17x10^3$ | 4 |
| c3021x2847y1871x2878y1907 | 13:29:52.199 | 47:12:11.524 | -9.53 | -9.52 | -9.48 | -8.82 | -8.82 | -8.68 | 23.0 | $8.36x10^3$ | 4 |
| c3021x3532y20x3577y56 | 13:30:0.8642 | 47:11:40.556 | -10.4 | -10.4 | -10.7 | -9.38 | -9.37 | -9.56 | 30.3 | $2.40x10^4$ | 5 |
| c3021x3823y1487x3857y1521 | 13:29:53.833 | 47:11:23.995 | -8.30 | -8.19 | -8.65 | -7.19 | -7.31 | -7.65 | 27.7 | $3.29x10^3$ | 5 |
| c3021x3842y1462x3880y1493 | 13:29:53.928 | 47:11:22.923 | -8.15 | -8.21 | -8.92 | -6.67 | -6.81 | -7.04 | 36.7 | $4.91x10^4$ | 110 |
| c3021x3898y716x3935y757 | 13:29:57.454 | 47:11:21.481 | -8.95 | -9.00 | -9.37 | -8.10 | -8.18 | -8.29 | 31.0 | $6.20x10^3$ | 5 |
| c3022x517y1929x543y1960 | 13:30:2.5195 | 47:14:10.685 | -7.26 | -7.32 | -7.77 | -5.82 | -6.06 | -6.38 | 14.5 | $1.82x10^4$ | 86 |

Continued on Next Page. . .

Table 2.1 – Continued

| Identifier | RA[1] | Dec.[1] | $M_{B_{int}}$[2] | $M_{V_{int}}$[2] | $M_{I_{int}}$[2] | $M_{B_{stars}}$[3] | $M_{V_{stars}}$[3] | $M_{I_{stars}}$[3] | Radius[4] (pc) | Mass ($M_\odot$) | Age (Myrs) |
|---|---|---|---|---|---|---|---|---|---|---|---|
| c3022x628y1633x683y1680 | 13:30:3.9111 | 47:14:4.9172 | -7.89 | -7.85 | -8.13 | -6.51 | -6.53 | -6.54 | 24.7 | $2.24x10^3$ | 5 |
| c3022x904y1815x949y1860 | 13:30:2.9772 | 47:13:50.525 | -8.04 | -8.15 | -8.74 | -6.49 | -6.72 | -6.93 | 28.1 | $5.59x10^4$ | 160 |
| c3022x1022y1829x1058y1866 | 13:30:2.8784 | 47:13:45.114 | -8.55 | -8.61 | -9.15 | -7.58 | -7.64 | -7.98 | 22.5 | $6.08x10^4$ | 86 |
| c3022x1186y571x1205y590 | 13:30:9.1186 | 47:13:39.360 | -7.16 | -7.14 | -7.41 | -6.72 | -6.76 | -6.73 | 20.3 | $1.14x10^3$ | 5 |
| c3022x1435y1792x1470y1826 | 13:30:2.9992 | 47:13:24.597 | -7.93 | -8.09 | -8.59 | -6.88 | -7.00 | -7.25 | 22.6 | $5.05x10^4$ | 160 |
| c3022x1521y1530x1555y1564 | 13:30:4.2736 | 47:13:20.999 | -8.86 | -8.75 | -8.86 | -8.05 | -8.05 | -8.06 | 31.9 | $4.49x10^3$ | 4 |
| c3022x1633y721x1664y746 | 13:30:8.2800 | 47:13:16.673 | -7.87 | -8.18 | -8.86 | -7.25 | -7.52 | -7.80 | 32.3 | $8.80x10^4$ | 310 |
| c3022x1680y1247x1705y1277 | 13:30:5.6396 | 47:13:13.446 | -8.83 | -8.85 | -9.43 | -8.04 | -8.15 | -8.71 | 15.3 | $7.82x10^4$ | 86 |
| c3022x1708y820x1723y844 | 13:30:7.7526 | 47:13:13.075 | -8.28 | -8.29 | -9.20 | -7.88 | -7.85 | -8.42 | 16.2 | $2.15x10^4$ | 22 |
| c3022x1842y1441x1868y1463 | 13:30:4.6801 | 47:13:5.1654 | -9.26 | -9.21 | -9.77 | -8.23 | -8.20 | -8.57 | 11.1 | $8.27x10^3$ | 5 |
| c3022x1875y1444x1915y1469 | 13:30:4.6545 | 47:13:2.9956 | -8.78 | -8.87 | -9.43 | -8.01 | -8.14 | -8.31 | 26.7 | $7.66x10^4$ | 86 |
| c3022x1965y1585x2005y1614 | 13:30:3.9367 | 47:12:58.683 | -8.08 | -8.18 | -9.05 | -6.92 | -7.10 | -7.79 | 17.0 | $8.30x10^4$ | 250 |
| c3022x2085y1165x2106y1188 | 13:30:5.9985 | 47:12:53.643 | -7.90 | -7.93 | -8.37 | -7.42 | -7.42 | -7.65 | 28.0 | $2.37x10^3$ | 5 |
| c3022x2101y588x2126y614 | 13:30:8.8073 | 47:12:53.286 | -7.50 | -7.57 | -7.96 | -6.75 | -6.80 | -6.95 | 16.9 | $1.65x10^3$ | 5 |
| c3022x2309y1481x2332y1505 | 13:30:4.3688 | 47:12:42.121 | -7.13 | -7.12 | -7.30 | -6.45 | -6.53 | -6.72 | 27.4 | $1.11x10^3$ | 5 |
| c3022x2324y1687x2354y1731 | 13:30:3.3105 | 47:12:40.679 | -8.31 | -8.37 | -8.94 | -7.38 | -7.55 | -8.00 | 27.2 | $4.91x10^4$ | 86 |
| c3022x2449y1572x2491y1611 | 13:30:3.8891 | 47:12:34.554 | -9.71 | -9.85 | -10.2 | -9.01 | -9.22 | -9.47 | 43.7 | $1.76x10^5$ | 86 |
| c3022x2480y1085x2514y1112 | 13:30:6.2878 | 47:12:33.483 | -7.65 | -7.90 | -8.83 | -6.54 | -6.84 | -7.65 | 32.1 | $9.92x10^4$ | 430 |
| c3022x2618y1453x2655y1485 | 13:30:4.4384 | 47:12:26.273 | -10.0 | -9.99 | -10.0 | -9.41 | -9.37 | -9.36 | 37.1 | $1.39x10^4$ | 4 |
| c3022x2629y959x2659y986 | 13:30:6.8884 | 47:12:26.644 | -9.72 | -9.63 | -9.63 | -8.99 | -8.89 | -8.71 | 21.8 | $9.92x10^3$ | 4 |
| c3022x2709y1546x2723y1568 | 13:30:3.9843 | 47:12:22.318 | -7.50 | -7.41 | -7.75 | -7.12 | -7.03 | -7.31 | 5.40 | $1.54x10^3$ | 5 |

Continued on Next Page. . .

Table 2.1 – Continued

| Identifier | RA[1] | Dec.[1] | $M_{B_{int}}$[2] | $M_{V_{int}}$[2] | $M_{I_{int}}$[2] | $M_{B_{stars}}$[3] | $M_{V_{stars}}$[3] | $M_{I_{stars}}$[3] | Radius[4] (pc) | Mass ($M_\odot$) | Age (Myrs) |
|---|---|---|---|---|---|---|---|---|---|---|---|
| c3022x2735y1709x2753y1728 | 13:30:3.1677 | 47:12:20.519 | -7.27 | -7.33 | -7.76 | -6.60 | -6.68 | -7.07 | 17.6 | $1.84x10^4$ | 86 |
| c3022x3101y1813x3143y1850 | 13:30:2.5671 | 47:12:1.4447 | -8.82 | -8.92 | -9.35 | -8.08 | -8.22 | -8.52 | 40.0 | $7.75x10^4$ | 86 |
| c3022x3561y786x3605y846 | 13:30:7.4890 | 47:11:39.842 | -8.96 | -9.28 | -10.3 | -8.08 | -8.51 | -9.55 | 47.5 | $4.34x10^5$ | 540 |
| c3022x3861y1479x3894y1527 | 13:30:3.9843 | 47:11:24.365 | -7.62 | -7.78 | -8.72 | -6.58 | -6.67 | -7.51 | 25.2 | $8.43x10^4$ | 390 |
| c3022x3861y936x3908y973 | 13:30:6.7456 | 47:11:24.722 | -9.51 | -9.47 | -9.43 | -8.79 | -8.77 | -8.68 | 33.0 | $8.26x10^3$ | 4 |
| c4021x1738y32x1775y74 | 13:29:41.953 | 47:13:1.1965 | -8.01 | -8.04 | -8.70 | -7.20 | -7.30 | -7.38 | 33.0 | $3.96x10^4$ | 96 |
| c4021x2677y615x2717y650 | 13:29:38.902 | 47:12:13.680 | -8.69 | -8.72 | -8.91 | -8.14 | -8.17 | -8.19 | 25.5 | $4.70x10^3$ | 5 |
| c4021x2711y385x2759y443 | 13:29:39.960 | 47:12:12.238 | -9.14 | -9.27 | -9.67 | -8.60 | -8.73 | -8.99 | 41.8 | $1.04x10^5$ | 86 |
| c4021x3433y239x3487y286 | 13:29:40.462 | 47:11:36.958 | -8.08 | -8.28 | -9.43 | -7.36 | -7.63 | -8.64 | 54.4 | $6.20x10^3$ | 7 |
| c4021x3464y32x3497y67 | 13:29:41.495 | 47:11:36.244 | -9.13 | -9.19 | -9.81 | -8.34 | -8.44 | -8.78 | 20.0 | $9.77x10^4$ | 77 |
| c4021x3501y776x3544y818 | 13:29:37.921 | 47:11:33.003 | -8.80 | -8.90 | -9.59 | -7.45 | -7.64 | -8.15 | 28.6 | $9.79x10^4$ | 130 |
| c4021x3707y534x3744y571 | 13:29:39.023 | 47:11:23.280 | -8.00 | -7.85 | -7.91 | -7.16 | -7.06 | -6.90 | 22.8 | $2.00x10^3$ | 4 |
| c4022x186y169x217y197 | 13:29:51.936 | 47:14:21.479 | -7.90 | -7.94 | -8.30 | -7.17 | -7.19 | -7.16 | 25.5 | $2.34x10^3$ | 5 |
| c4022x587y467x642y497 | 13:29:50.375 | 47:14:0.6051 | -9.06 | -9.13 | -9.28 | -8.26 | -8.31 | -8.23 | 44.4 | $6.65x10^3$ | 5 |
| c4022x692y1002x744y1066 | 13:29:47.640 | 47:13:54.480 | -8.65 | -8.75 | -9.25 | -7.54 | -7.71 | -7.93 | 55.6 | $6.72x10^4$ | 86 |
| c4022x873y435x910y474 | 13:29:50.471 | 47:13:46.556 | -8.00 | -8.50 | -9.42 | -6.90 | -7.45 | -8.26 | 36.3 | $2.07x10^5$ | 610 |
| c4022x880y668x911y698 | 13:29:49.321 | 47:13:46.199 | -8.20 | -8.27 | -8.61 | -7.59 | -7.77 | -7.98 | 19.9 | $3.10x10^3$ | 5 |
| c4022x1032y1210x1081y1238 | 13:29:46.633 | 47:13:37.561 | -9.44 | -9.39 | -9.48 | -8.55 | -8.52 | -8.57 | 33.9 | $7.79x10^3$ | 4 |
| c4022x1093y1186x1115y1208 | 13:29:46.750 | 47:13:35.034 | -8.94 | -9.07 | -9.58 | -8.21 | -8.48 | -8.80 | 22.4 | $1.27x10^5$ | 160 |
| c4022x1158y346x1180y376 | 13:29:50.855 | 47:13:32.878 | -7.71 | -7.88 | -8.79 | -6.73 | -6.88 | -7.44 | 25.7 | $9.14x10^4$ | 390 |
| c4022x1713y118x1738y161 | 13:29:51.793 | 47:13:5.5224 | -8.72 | -8.66 | -8.76 | -8.41 | -8.37 | -8.32 | 22.6 | $3.98x10^3$ | 4 |

Continued on Next Page. . .

Table 2.1 – Continued

| Identifier | RA[1] | Dec.[1] | $M_{B_{int}}$[2] | $M_{V_{int}}$[2] | $M_{I_{int}}$[2] | $M_{B_{stars}}$[3] | $M_{V_{stars}}$[3] | $M_{I_{stars}}$[3] | Radius[4] (pc) | Mass ($M_\odot$) | Age (Myrs) |
|---|---|---|---|---|---|---|---|---|---|---|---|
| c4022x1775y105x1807y139 | 13:29:51.936 | 47:13:2.2814 | -8.08 | -8.15 | -9.04 | -7.32 | -7.44 | -7.68 | 35.4 | $8.22x10^4$ | 250 |
| c4022x1965y456x1995y487 | 13:29:50.185 | 47:12:52.558 | -8.48 | -8.44 | -8.39 | -8.00 | -7.96 | -7.78 | 25.5 | $3.17x10^3$ | 4 |
| c4022x2109y746x2156y785 | 13:29:48.647 | 47:12:44.277 | -8.09 | -8.23 | -9.03 | -7.41 | -7.63 | -8.02 | 41.5 | $7.67x10^4$ | 220 |
| c4022x2149y1043x2199y1084 | 13:29:47.182 | 47:12:41.764 | -8.56 | -8.76 | -9.54 | -7.94 | -8.16 | -8.62 | 53.4 | $1.32x10^5$ | 250 |
| c4022x2289y1064x2329y1103 | 13:29:47.065 | 47:12:35.282 | -8.01 | -8.15 | -8.87 | -7.01 | -7.21 | -7.63 | 31.3 | $6.48x10^4$ | 200 |
| c4022x2457y1512x2491y1553 | 13:29:44.831 | 47:12:26.273 | -9.61 | -9.58 | -9.74 | -8.81 | -8.77 | -8.71 | 35.2 | $9.17x10^3$ | 4 |
| c4022x2554y502x2612y566 | 13:29:49.727 | 47:12:22.318 | -9.34 | -9.39 | -10.0 | -8.59 | -8.63 | -9.00 | 36.4 | $1.46x10^5$ | 110 |
| c4022x2787y25x2821y58 | 13:29:52.104 | 47:12:12.238 | -9.43 | -9.40 | -9.35 | -8.78 | -8.76 | -8.67 | 24.5 | $7.59x10^3$ | 4 |
| c4022x2826y1550x2879y1603 | 13:29:44.520 | 47:12:7.1987 | -7.99 | -8.03 | -8.84 | -6.64 | -6.70 | -7.03 | 50.7 | $1.95x10^4$ | 31 |
| c4022x2840y571x2883y602 | 13:29:49.390 | 47:12:8.2836 | -8.94 | -9.03 | -9.63 | -8.33 | -8.55 | -9.15 | 32.7 | $1.18x10^5$ | 140 |
| c4022x2945y717x2974y749 | 13:29:48.673 | 47:12:3.2437 | -8.12 | -8.04 | -8.74 | -7.48 | -7.49 | -7.79 | 13.8 | $2.39x10^4$ | 40 |
| c4022x3333y1755x3350y1779 | 13:29:43.487 | 47:11:43.083 | -8.26 | -8.29 | -8.57 | -7.40 | -7.50 | -7.76 | 11.7 | $3.21x10^3$ | 5 |
| c4022x3437y1043x3468y1084 | 13:29:46.944 | 47:11:38.400 | -7.96 | -7.82 | -8.59 | -7.48 | -7.37 | -7.53 | 38.6 | $1.57x10^4$ | 24 |
| c4022x3868y340x3912y396 | 13:29:50.302 | 47:11:17.526 | -9.25 | -9.36 | -10.0 | -8.44 | -8.67 | -9.30 | 46.2 | $1.85x10^5$ | 180 |
| c5021x264y445x314y509 | 13:29:58.967 | 47:11:5.6341 | -11.3 | -11.2 | -11.4 | -10.5 | -10.5 | -10.6 | 41.6 | $4.56x10^4$ | 4 |
| c5021x665y1627x700y1662 | 13:29:53.280 | 47:10:44.046 | -10.8 | -10.9 | -11.1 | -10.0 | -10.1 | -10.3 | 24.3 | $3.49x10^4$ | 5 |
| c5021x669y1626x701y1667 | 13:29:53.280 | 47:10:44.046 | -10.8 | -10.9 | -11.1 | -10.2 | -10.2 | -10.4 | 32.0 | $3.61x10^4$ | 5 |
| c5021x703y849x726y885 | 13:29:56.975 | 47:10:43.675 | -7.73 | -8.00 | -9.13 | -6.63 | -7.11 | -8.02 | 21.0 | $1.40x10^5$ | 540 |
| c5021x739y1142x770y1180 | 13:29:55.583 | 47:10:41.519 | -8.33 | -8.32 | -8.86 | -7.76 | -7.80 | -7.94 | 29.1 | $3.61x10^4$ | 57 |
| c5021x791y1253x813y1271 | 13:29:55.081 | 47:10:38.635 | -7.31 | -7.44 | -8.16 | -6.50 | -6.67 | -6.98 | 9.30 | $3.38x10^4$ | 200 |
| c5021x791y1620x828y1644 | 13:29:53.327 | 47:10:37.921 | -8.88 | -8.96 | -9.49 | -7.93 | -8.19 | -8.66 | 34.5 | $8.27x10^4$ | 86 |

Continued on Next Page. . .

Table 2.1 – Continued

| Identifier | RA[1] | Dec.[1] | $M_{B_{int}}$[2] | $M_{V_{int}}$[2] | $M_{I_{int}}$[2] | $M_{B_{stars}}$[3] | $M_{V_{stars}}$[3] | $M_{I_{stars}}$[3] | Radius[4] (pc) | Mass ($M_\odot$) | Age (Myrs) |
|---|---|---|---|---|---|---|---|---|---|---|---|
| c5021x1141y1883x1167y1934 | 13:29:51.936 | 47:10:20.274 | -8.49 | -8.49 | -9.10 | -7.40 | -7.43 | -7.80 | 37.2 | $4.25x10^4$ | 57 |
| c5021x1149y1574x1182y1604 | 13:29:53.422 | 47:10:20.274 | -9.58 | -9.58 | -10.1 | -8.72 | -8.75 | -9.06 | 29.0 | $1.14x10^5$ | 57 |
| c5021x1169y1324x1217y1377 | 13:29:54.576 | 47:10:19.560 | -10.5 | -10.5 | -11.1 | -9.68 | -9.77 | -10.2 | 35.8 | $2.83x10^5$ | 57 |
| c5021x1178y1641x1213y1673 | 13:29:53.111 | 47:10:18.846 | -9.10 | -9.07 | -9.77 | -8.32 | -8.34 | -8.78 | 37.8 | $5.79x10^4$ | 38 |
| c5021x1253y1509x1284y1540 | 13:29:53.712 | 47:10:15.605 | -9.06 | -8.90 | -8.73 | -8.44 | -8.33 | -8.03 | 28.8 | $5.20x10^3$ | 4 |
| c5021x1735y1344x1775y1378 | 13:29:54.360 | 47:9:51.833 | -8.35 | -8.41 | -8.87 | -7.42 | -7.47 | -7.66 | 35.6 | $4.97x10^4$ | 86 |
| c5021x1852y874x1899y907 | 13:29:56.568 | 47:9:46.793 | -9.22 | -9.33 | -9.86 | -8.60 | -8.67 | -8.98 | 32.3 | $1.63x10^5$ | 160 |
| c5021x2324y1077x2369y1134 | 13:29:55.440 | 47:9:23.035 | -8.62 | -8.69 | -9.32 | -7.75 | -7.78 | -8.01 | 50.0 | $7.00x10^4$ | 96 |
| c5021x2429y1611x2449y1636 | 13:29:52.943 | 47:9:17.638 | -8.15 | -8.02 | -7.95 | -7.66 | -7.57 | -7.36 | 14.3 | $2.28x10^3$ | 4 |
| c5021x2430y121x2470y157 | 13:30:0.0256 | 47:9:19.794 | -8.83 | -8.83 | -9.07 | -8.04 | -8.10 | -8.19 | 35.3 | $5.33x10^3$ | 5 |
| c5021x2537y414x2560y438 | 13:29:58.630 | 47:9:14.397 | -8.61 | -8.60 | -8.79 | -8.02 | -8.05 | -8.23 | 22.6 | $4.27x10^3$ | 5 |
| c5021x2552y318x2590y354 | 13:29:59.040 | 47:9:13.326 | -8.90 | -8.90 | -9.14 | -8.03 | -8.04 | -8.11 | 34.4 | $5.66x10^3$ | 5 |
| c5021x2806y1020x2840y1051 | 13:29:55.631 | 47:9:0.0054 | -8.51 | -8.36 | -8.31 | -7.80 | -7.67 | -7.41 | 26.5 | $3.18x10^3$ | 4 |
| c5021x2854y667x2890y702 | 13:29:57.286 | 47:8:57.835 | -9.73 | -9.66 | -9.61 | -9.28 | -9.24 | -9.13 | 25.0 | $1.00x10^4$ | 4 |
| c5021x3033y439x3063y481 | 13:29:58.344 | 47:8:49.925 | -8.38 | -8.39 | -8.64 | -7.72 | -7.78 | -7.99 | 43.4 | $3.53x10^3$ | 5 |
| c5021x3054y1592x3074y1629 | 13:29:52.822 | 47:8:47.041 | -8.54 | -8.57 | -9.09 | -7.74 | -7.86 | -8.68 | 28.9 | $5.91x10^4$ | 86 |
| c5021x3454y1722x3527y1797 | 13:29:52.031 | 47:8:25.796 | -9.07 | -9.19 | -9.77 | -8.24 | -8.29 | -8.64 | 55.8 | $1.45x10^5$ | 160 |
| c5022x754y1102x784y1132 | 13:30:5.8813 | 47:10:44.760 | -8.16 | -8.50 | -9.43 | -7.39 | -7.78 | -8.45 | 26.0 | $1.82x10^5$ | 490 |
| c5022x770y887x805y922 | 13:30:6.9104 | 47:10:44.403 | -9.10 | -9.24 | -9.72 | -8.33 | -8.51 | -8.99 | 23.8 | $1.46x10^5$ | 160 |
| c5022x997y1153x1075y1223 | 13:30:5.4711 | 47:10:31.439 | -9.61 | -9.79 | -10.6 | -8.72 | -8.97 | -9.47 | 74.7 | $3.86x10^5$ | 280 |
| c5022x1158y1106x1236y1208 | 13:30:5.5664 | 47:10:23.158 | -10.3 | -10.4 | -10.9 | -9.60 | -9.78 | -10.1 | 90.7 | $4.53x10^5$ | 160 |

Continued on Next Page. . .

Table 2.1 – Continued

| Identifier | RA[1] | Dec.[1] | $M_{B_{int}}$[2] | $M_{V_{int}}$[2] | $M_{I_{int}}$[2] | $M_{B_{stars}}$[3] | $M_{V_{stars}}$[3] | $M_{I_{stars}}$[3] | Radius[4] (pc) | Mass ($M_\odot$) | Age (Myrs) |
|---|---|---|---|---|---|---|---|---|---|---|---|
| c5022x1240y1176x1269y1207 | 13:30:5.4235 | 47:10:20.274 | -9.55 | -9.50 | -9.66 | -8.95 | -8.94 | -9.06 | 28.9 | $8.73x10^3$ | 4 |
| c5022x1771y1568x1806y1607 | 13:30:3.3361 | 47:9:53.275 | -10.3 | -10.2 | -10.2 | -9.86 | -9.77 | -9.73 | 25.5 | $1.75x10^4$ | 4 |
| c5022x1994y1499x2037y1542 | 13:30:3.6950 | 47:9:42.124 | -8.90 | -8.89 | -8.96 | -7.78 | -7.88 | -8.04 | 45.6 | $4.76x10^3$ | 4 |
| c5022x1997y1528x2043y1581 | 13:30:3.4790 | 47:9:41.753 | -9.80 | -9.91 | -10.4 | -8.99 | -9.15 | -9.53 | 47.7 | $1.95x10^5$ | 86 |
| c5022x2754y1933x2787y1967 | 13:30:1.3916 | 47:9:3.6035 | -9.20 | -9.19 | -9.56 | -8.53 | -8.56 | -8.84 | 24.8 | $7.64x10^3$ | 5 |
| c5022x3634y1749x3685y1816 | 13:30:2.0397 | 47:8:20.042 | -9.27 | -9.19 | -9.16 | -8.55 | -8.48 | -8.38 | 44.6 | $6.52x10^3$ | 4 |
| c6021x1727y965x1790y1024 | 13:29:36.793 | 47:9:44.280 | -9.60 | -9.61 | -10.2 | -8.95 | -9.02 | -9.58 | 66.5 | $1.19x10^5$ | 57 |
| c6021x1921y1183x1954y1216 | 13:29:35.760 | 47:9:35.285 | -7.54 | -7.66 | -8.40 | -6.76 | -6.85 | -7.19 | 37.7 | $4.21x10^4$ | 200 |
| c6021x3007y329x3096y394 | 13:29:39.481 | 47:8:42.001 | -9.95 | -10.1 | -11.0 | -9.01 | -9.24 | -9.81 | 66.1 | $7.40x10^5$ | 390 |
| c6022x10y1270x53y1333 | 13:29:45.816 | 47:11:13.200 | -9.31 | -9.34 | -9.91 | -8.59 | -8.72 | -9.07 | 57.3 | $1.22x10^5$ | 86 |
| c6022x402y1882x442y1909 | 13:29:42.791 | 47:10:52.684 | -10.1 | -10.0 | -9.95 | -9.43 | -9.45 | -9.30 | 30.8 | $1.40x10^4$ | 4 |
| c6022x433y325x461y367 | 13:29:50.423 | 47:10:53.755 | -9.49 | -9.52 | -9.90 | -8.70 | -8.77 | -9.07 | 34.3 | $1.01x10^4$ | 5 |
| c6022x669y359x695y390 | 13:29:50.255 | 47:10:42.233 | -10.9 | -10.9 | -10.9 | -10.1 | -10.1 | -10.0 | 26.1 | $3.18x10^4$ | 4 |
| c6022x957y1773x1014y1824 | 13:29:43.150 | 47:10:24.957 | -10.2 | -10.2 | -10.5 | -9.27 | -9.40 | -9.66 | 46.6 | $1.93x10^4$ | 5 |
| c6022x1313y77x1352y130 | 13:29:51.456 | 47:10:9.8373 | -9.40 | -9.36 | -9.85 | -8.55 | -8.61 | -8.94 | 32.4 | $9.30x10^3$ | 5 |
| c6022x1450y1665x1480y1688 | 13:29:43.656 | 47:10:1.1993 | -7.90 | -8.15 | -9.20 | -7.27 | -7.55 | -8.26 | 22.2 | $1.42x10^5$ | 490 |

Continued on Next Page. . .

Table 2.1 – Continued

| Identifier | RA[1] | Dec.[1] | $M_{B_{int}}$[2] | $M_{V_{int}}$[2] | $M_{I_{int}}$[2] | $M_{B_{stars}}$[3] | $M_{V_{stars}}$[3] | $M_{I_{stars}}$[3] | Radius[4] (pc) | Mass ($M_\odot$) | Age (Myrs) |
|---|---|---|---|---|---|---|---|---|---|---|---|
| c6022x1887y953x1912y972 | 13:29:47.113 | 47:9:40.682 | -9.59 | -9.51 | -9.64 | -9.13 | -9.06 | -9.14 | 25.2 | 8.96x10$^3$ | 4 |



[1]Epoch J2000

[2]Total integrated magnitude from a circular aperture of radius and central position listed in Table 1. All magnitudes in the Vega magnitude system.

[3]Total magnitude from summing all sources in the association. This value will not include diffuse light from unresolved stars, and is thus a lower limit of the magnitude of the association. All magnitudes in the Vega magnitude system.

[4]The average radius of the association as determined by the average FWHM of the flux density distribution.

# Chapter 3

# AUTOMATED STAR CLUSTER/ASSOCIATION SELECTION IN NGC 4214

## 3.1 Overview

In this chapter I explore a uniform treatment to identify stellar conglomerations of all size scales by using a combination of DAOPHOT, for the most compact clusters, and Source Extractor (SExtractor, Bertin & Arnouts, 1996), to select more diffuse clusters from Gaussian-blurred images. After selection, the sizes are measured in a uniform way by using annular surface brightness profiles. In a subsequent publication, I will use MASSCLEAN (Popescu & Hanson, 2009) to simulate clusters and associations to more fully quantify the selection effects and results.

NGC 4214 is an irregular type IAB(s)m galaxy (de Vaucouleurs et al., 1991). Its relative proximity to the Milky Way ($2.98$ Mpc, $(m-M)=27.37$, Dopita et al., 2010) and active star-formation make it ideal for the study of stellar associations and compact star clusters in an external galaxy. Previous studies of the sizes of stellar groups in nearby galaxies have produced conflicting results. Maíz-Apellániz (2001) found evidence for two main modes of stellar clustering in $27$ massive young star clusters from seven nearby galaxies and the Milky Way: centrally compact super-star clusters (SSCs) with half-light radii on the $\sim 2-30$ pc scale, and more diffuse scaled O and B associations (SOBAs) with half-light radii $\sim 15-100$ pc. This ground-breaking work also found tentative evidence that younger clusters were more centrally concentrated, a result that has been recently confirmed by several studies (TBD). However, this study used subjective cluster selection criteria and included only a small number of clusters in the sample (27). More recently, Elmegreen et al. (2006) found a power law relationship with an index of $\alpha \approx -1.5$ between the Gaussian-blur radius and the number of regions with radii larger than the blur radius in NGC 628, indicating a fractal-like nature in the size-scale of stellar clustering

resulting from hierarchical star-formation. In the current work, I explore the size distribution of star clusters and associations in NGC 4214 using a new objective method of selecting stellar groups.

Another set of relevant papers are by Bastian et al. on M51, M33, and the LMC (i.e., Bastian et al., 2005b, 2007, 2009). Using a variety of different techniques (i.e., point-like objects found by DAOFIND in M51, subjective selection of cluster "complexes" for M51 with R $> 85$ pc, a minimum spanning tree approach for M33 for and the LMC for associations $> 20$ pc). They conclude that there is a "continuum of star-forming group sizes" rather than a "characteristic scale for OB associations" (Bastian et al., 2007). They also find power law mass versus radius relationships ($N\,dM \propto M^{\alpha}\,dM$) with indices that range from $\alpha \approx -1.8 \pm 0.2$ (M33) to $-2.3 \pm 0.2$ (M51), which are similar to the results for giant molecular clouds (i.e., $\alpha \approx -2$ and $-2.2$, respectively, for Solomon et al., 1987; Bastian et al., 2005b), and a much shallower relationship (consistent with zero at the $2\sigma$ level) for compact clusters in M51. I will revisit several of these results in the current chapter, but note here that a primary difference in the two studies is the development of a uniform technique designed to identify stellar groupings of all sizes, rather than only compact or diffuse clustering separately.

Many of the historically used names for stellar groupings spawn the populations seen in a particular galaxy or sample of galaxies. These divisions may not be apparent when when applied to another population of stellar groupings. Classical names such as globular clusters, open clusters and associations, as well as more recent terms such as populous clusters (van den Bergh & Lafontaine, 1984), and the aforementioned SSCs and SOBAs are descriptive of the stellar groupings investigated in the studies that coined them. In this dissertation I do not attempt to map the objects onto specific historical categories of stellar groupings (this will be included in a future publication), but simply refer to the compact, centrally concen-

trated groupings as “clusters”, and the more diffuse groupings where the individual stars are well separated as “associations”.

Once I have identified the stellar groupings and measured their sizes, the next step is to obtain a variety of measurements using techniques developed in recent publications, e.g., ages (Chandar et al., 2010), morphological categories, and surface brightness fluctuations (Whitmore et al., 2011). The primary science goals of this chapter are: 1) to establish whether the size distributions of stellar groupings are continuous or bimodal; 2) determine the formation history of stellar groupings of physically different scales; and 3) use the size and age distributions to assess the dissolution of stellar groupings of different physical length scales.

This chapter is organized as follows. Section 3.2 presents the observations and basic data reduction. Section 3.3 presents both a manual and automated catalog, and describes the selection methods in detail. In Section 3.4 I estimate the sizes of the stellar groupings, and in Section 3.5 I estimate their ages from three independent techniques. Section 3.6 discusses the physical implications of the size and age distributions of stellar groupings in NGC 4214, and Section 3.7 summarizes the main results.

## 3.2 Observations and Data Processing

NGC 4214 was observed with the WFC3 onboard the *Hubble Space Telescope* ($HST$) on December 22-23, 2009, with a single pointing covering the galaxy nucleus and most of the active star-forming regions in this dwarf starburst galaxy. In this work, I will use the following broad-band optical filters, $F336W$ (“$U$”; $1683$ sec. image exposure time), $F438W$ (“$B$”; $1530$ sec), $F547M$ (“$V$”; $1050$ sec), and $F814W$ (“$I$”; $1339$ sec), as well as the narrow-band $F657N$ (“$H\alpha$”; $1592$ sec) filter.

The flat-fielded WFC3/UVIS images in each filter were co-added using the PyRAF task MULTIDRIZZLE (Koekemoer et al. 2002), and have a final pixel scale

of $0.0396''$/pixel (corresponding to $0.563$ pc/pixel at a distance of $2.98$ Mpc, Dopita et al., 2010). This resolution is high enough that most star clusters are partially resolved, and can be distinguished from individual bright stars at the distance of NGC 4214. A color image of the field is shown in Figure 3.1.

Circular aperture photometry was performed on the stellar groupings detected in NGC 4214 (Section 3.3), in the drizzled images for each filter using the IRAF task PHOT. For the narrow-band $H\alpha$ image photometry was done on the original image without subtracting the stellar continuum flux. The total $H\alpha$ emission (from stellar photospheres and from surrounding gas in the ISM) is used to disentangle reddening effects of age and dust: if no $H\alpha$ is present the stellar grouping must be older than $6$ Myr. I convert the instrumental magnitudes to the VEGAMAG system by applying the following zeropoints: $F336W$=$23.46$ mags, $F438W$=$24.98$ mags, $F547M$=$24.72$ mags, $F657N$=$22.35$ mags, and $F814W$=$24.67$mags, which are provided by The Space Telescope Institute (STScI)[2], except for the $F657N$ zeropoint which was calculated using the STSDAS SYNPHOT package[3]. I refer to these as "$U$","$B$", "$V$", "$H\alpha$", and "$I$" band magnitudes, although I do not actually transform to the Johnson-Cousins photometric system.

## 3.3 Selection and Catalogs of Stellar Groupings

I have developed an automated method to select the full physical range of stellar groupings, from compact clusters to diffuse stellar complexes. The selection and measurement techniques are described in detail below. However, I first manually select a catalog of stellar groupings. The manual catalog provides a consistency check on the automated catalog, and more importantly, is used as a "training set" to

[2]http://www.stsci.edu/hst/wfc3/phot_zp_lbn

[3]STSDAS SYNPHOT is a product of the Space Telescope Science Institute, which is operated by AURA for NASA.

guide the development of the automated method, particularly in terms of removing artifacts and contamination. In later sections I use the results from both catalogs to assess how robust the results are to selection effects.

In the following, I select stellar groupings from the $U$-band image. The $U$-band was used for this purpose since it is most sensitive to recent star formation. The biggest disadvantages of using the $U$-band is that it is more affected by extinction than longer wavelengths, and that the stellar flux falls more rapidly with age at these wavelengths. I will explore the impact of selecting stellar groupings from images taken with other filters in future work.

### 3.3.1 Manual Catalog

I selected a manual catalog of $132$ stellar groupings as a "training set" for the automated catalog. These range from compact star clusters, which are broader than the point spread function but where no individual stars are discernible, to more resolved clusters where individual stars can be identified near the cluster outskirts, and to associations which appear as over-densities of individual stars.

At the small end of the size distribution, the primary difficulty is distinguishing the compact clusters from individual stars. The primary tool for this purpose was the *imexamine* task in the IRAF software package, where compact clusters typically have FWHM of $\sim 3$ versus $\sim 2$ pixels for individual stars in the $U$-band image.

By visually inspecting the image, I was able to assess the performance of the tool in more difficult cases, such as the case where background galaxies are present, or in the case where there are only a few stars which may simply represent a chance superposition of stars. Such an approach is not possible with a fully automatic selection procedure. The primary shortcoming to this manual approach is that it is not possible to automatically reproduce the cluster selection, and hence

to quantitatively assess the completeness of the sample. The sources in the final manual catalog are shown in Figures 3.2 and 3.3 and their locations and other basic properties are compiled in Table 3.2.

### 3.3.2 Automatic Catalog

For the automated catalog, I first select the most compact star clusters using techniques that I have developed previously (i.e., Chandar et al., 2010), and then move on to more diffuse groupings, which require different techniques. The two catalogs are then merged together, with care being taken not to duplicate the same stellar groupings.

#### 3.3.2.1 Construction of Compact Cluster Catalog using DAOphot

Even in relatively nearby galaxies, compact clusters of stars are not resolved into their individual stars in their central regions. Hence compact clusters can be identified as single point-like objects that are slightly resolved when compared to stars (i.e. broader than the PSF). It is generally relatively straightforward to distinguish stars from clusters based on their size in these cases. I employ the DAOPHOT (Stetson, 1987) software for this purpose, using a technique discussed in several recent papers (Chandar et al., 2010; Whitmore et al., 2010, 2011). I briefly summarize this selection method here, and refer the interested reader to Chandar et al. (2010) for more details. I select point-like sources on a median-divided $U$-band image, and select sources to have a concentration index $C > 2.3$, where $C$ is the magnitude difference measured using $0.5$ and $3.0$-pixel apertures (corresponding to $0.28$ and $1.7$ pc, respectively, using the pixel scale of $0.563$ pc/pix). Because star clusters are more extended than a point source, they have larger values of $C$. I also apply a magnitude cutoff of $m_{F547M} = 21.41$ ($M_{F547M} = -6.0$) mags in a $20$-pixel radius aperture, since $C$ values become more uncertain for fainter sources and it

becomes difficult to distinguish between stars and compact clusters.

#### 3.3.2.2 Construction of Diffuse Association Catalog using Source Extractor

The basic technique for identifying diffuse stellar associations containing separate, resolved stars is to blur the image so that the groupings can be selected as a single object, a technique used by several previous studies (e.g., Elmegreen et al., 2006). Each image is convolved, or "Gaussian-blurred", with a series of Gaussians in order to make it possible to identify stellar groupings of different size scales, as in Elmegreen et al. (2006). Gaussians of $\sigma = 10$, $20$, $40$, and $80$ pc (corresponding to $\sim$17, $35$, and $70$ and $139$ pixels, respectively), were created (Figure 3.4), using the IDL function *psf_gaussian.pro*, and convolution with the image was completed using the IDL routine *convolve.pro*, both part of the GSFC ASTROLIB. I find that the specific values of $\sigma$ used for the Gaussian blurring has little effect on the selected objects and on the overall size distribution of the stellar groupings in NGC 4214. Gaussian-blurred images with $\sigma = 1-5$ pc tend to blur bright stars and compact clusters to a similar scale, making these objects indistinguishable. Thus, it is more effective to separate stars and compact clusters on the un-blurred original image, as described in the previous section. At the upper end of the size distribution, I find that a Gaussian blur with $\sigma = 80$ pc does not result in additional identifications of "real" clusters, as defined by the manual catalog. I select candidate stellar groupings on the Gaussian-blurred images to have a minimum contiguous area (using the parameter DETECT_MINAREA) at a certain level above the background (DETECT_THRESH), using the SExtractor software (Bertin & Arnouts, 1996). The specific values of these parameters used for each Gaussian-blurred image are listed in Table 3.1.

Figure 3.5 shows sources detected by SExtractor in the $\sigma = 10$, $20$, $40$, and $80$ pc Gaussian blurred images, using the parameter setting listed in Table 3.1.

It is evident in Figure 3.5 that many of the SExtractor selected candidate objects are not desired stellar groupings. The initial SExtractor selection contains many extraneous objects, including bright single stars, close pairs or triplets of stars which are likely to be chance superpositions and not physically associated with one another, and artifacts associated with the blurring effects on the background and edges of the image. I employ the following series of 'cleaning' steps to remove unwanted sources from the detection list.

I first remove highly elongated detections ($a/b < 1.9$, marked by black ellipses in Figure 3.5), which are almost always edge effects or other spurious detections. I also discard any detections that are within $15$ pixels of a manually selected background galaxy or an image edge. I use three additional criteria to eliminate spurious or multiple detections: a unique position condition, a magnitude cutoff, and a concentration index cutoff using both upper and lower limits. The unique position condition is necessary to account for the fact that a single stellar grouping can be detected at slightly different size scales in multiple blurred images. To remedy this "double-counting", I require that the central position of each stellar grouping must be $20$ pixels away from any other grouping. When more than one objects's central position is found within $20$ pixels of another, I choose the brightest detected object within a $10$-pixel radius aperture in the $F547M$ image. The cutoff values and photometry aperture sizes used in these steps were selected to roughly reproduce the stellar groupings in the manual catalog, and are defined in Table 3.1.

At this point I add the compact star cluster list to the cleaned list of potential stellar groupings from SExtractor, and apply the unique position condition to the combined list, retaining the brightest source in a $20$-pixel radius aperture in the $F547M$ image in any instance where a potential stellar grouping's central position is within $30$ pixels of another grouping. The final automated catalog has $100$ candidate stellar groupings.

### 3.3.3 Comparison Between Manual and Automated Catalogs

The automated catalog contains $100$ of the $116$ sources in the manual catalog. The vast majority of the discrepancies in these two lists are compact star clusters which are only partially resolved, and thus are sometimes erroneously removed in the process of rejecting single stars. Also, some compact clusters which I would like to retain are rejected when I impose the "unique position" condition, demanding that two potential sources be at least $20$ pixels away from one another. The remaining sources that are missed in the automated selection process are diffuse associations in areas of low background. The lack of central concentration fo these stellar groupings make them difficult to differentiate from the field star population.

## 3.4 Size Measurements and Stellar Groupings

Following the selection process, I uniformly measure the sizes of the clusters based on their radial surface brightness profiles. For each grouping, I perform circular photometry centered at radii of $r = 2.5$, $5$, $7.5$, $10$, $12.5$,...$215$, $217.5$, $220$ pixels with a width of $5$ pixels. I divide the flux in each annulus by the area in that annulus to get flux/pixel, and take the "background" level as the mean of the flux/pixel of the $10$ largest annulus. I then find the annulus at which the flux/pixel is closest to $1.5$ times the background value, and take that radius to be $r_{tot}$, the radius which encloses the "total" flux.

Figure 3.6 shows the resulting sizes using three different values of the $r_{tot}$ threshold, namely $1.9$ (smallest), $1.5$, and $1.1$ (largest). The $r_{tot}$ threshold value of $1.5$ times above the background value was chosen to roughly match the estimates of the cluster sizes made by eye during the development of the manual catalog. The size histograms from each of these thresholds are shown in Figure 3.7. In Section 3.6 I will examine how different values of $r_{tot}$ threshold affect the resulting

size histograms.

I note that the selection of a value for the $r_{tot}$ threshold is largely an arbitrary choice; another person might subjectively choose the sizes of clusters and associations to be systematically larger or smaller. In Figures 3.2 and 3.3 I compare the stellar groupings with those of Maíz-Apellániz (2001). While it is reassuring that I find the same basic stellar groupings (plus $\approx 100$ more since I go deeper and include more compact clusters) I note that the Maíz-Apellániz sizes tend to be larger.

A key point is that the goal is to define an objective, repeatable method for defining clusters and associations that *roughly mimics what the eye selects as physically related stellar groupings*. There is no "right" answer to the size of a cluster. Selection effects can then be quantified by adding artificial clusters with different densities and running the images through the same objective software to see which are recovered and which are not (something that is not possible with subjective methods). In addition, I can choose a different value for $r_{tot}$ threshold (and other parameters) and rerun the analysis to see how it affects the final results.

Completeness checks indicate better than $80$% completeness for stellar groupings with total magnitudes brighter than $M_V \gtrsim 22$, out and $r_{tot}$ values in the range $1-100$ pc.

Once $r_{tot}$ is determined, I perform circular aperture photometry and determine the radii that contain $1/4$, $1/2$, $3/4$, and the total light, i.e., $r_{1/4}$, $r_{1/2}$, $r_{3/4}$, and $r_{tot}$. A background correction is performed using a $10$ pixel wide annulus with inner radius $5$ pixels larger than $r_{tot}$, and an outer radius $15$ pixels larger than $r_{tot}$.

While assessing the characteristic size of the stellar groupings at a given x,y position, I invoke two further conditions in order to minimize false detections. The first stipulation requires that the magnitude difference between the highest flux/pixel in a $25$-pixel radius and the determined background level be greater than

$0.85$ mags. The second condition demands that $r_{tot}$ must be chosen on a negative gradient slope of the annular flux plot, i.e. that the radius interior to $r_{tot}$ have a higher flux/pixel than $r_{tot}$, and that the radius exterior to $r_{tot}$ have a lower flux/pixel than $r_{tot}$. This ensures that the correct total radius is chosen for stellar groupings that are not centrally-concentrated.

The method is illustrated for the stellar groupings with very different physical scales in Figure 3.8. While the determination of $r_{tot}$ is relatively straightforward for two of the three examples, the middle one shows that sub-groupings can make the determination sensitive to the value of the $r_{tot}$ threshold. However, as explained in the philosophy above, as long as I have a well-defined, objective, repeatable procedure, I can test the robustness of the results by changing the various parameters and seeing the effect.

Maíz-Apellániz (2001) measured sizes ($r_{1/4}$, $r_{1/2}$, $r_{3/4}$) for seven stellar groupings, selected by hand, in NGC 4214 from archival $HST$/WFPC2 $U$-band images. The illustrative examples in Figure 3.3 include all of the Maíz-Apellániz regions, which are shown by the red circles. I find that the values for $r_{tot}$ are smaller than those of the Maíz-Apellániz (2001) sizes for $5/7$ of the groupings.

In Figure 3.2 the green circles (manual catalog) show the manually estimated size determinations while the right panel shows the automatically determined values of $r_{tot}$, obtained using the procedure described above and illustrated in Figure 3.8. I note that in the central regions the manual and automatic sizes are comparable but in the outer regions the manual estimates are often smaller. If I adjust the value of the $r_{tot}$ threshold to match the outer regions better, the inner clusters tend to be too large.

## 3.5 Photometry and Age Estimates of Stellar Groupings

In this section, I estimate the ages of stellar groupings in the manual and automated catalogs using three independent methods developed in previous publications (Chandar et al., 2010; Whitmore et al., 2011).

The first method compares measured magnitudes of each grouping in different filters with the predictions from stellar evolutionary models to estimate their ages. I perform circular aperture photometry for each stellar grouping, as described in Section 3.2. The $U-B$ vs. $V-I$ two-color diagram of the stellar groupings in the manual and automated catalogs are shown in Figure 3.9. These are compared with new Simple Stellar Population (SSP) models from Bruzual & Charlot (2010; private communication; see also 2003) which use the WFC3 filter transmission curves. The colors and luminosities have been corrected for foreground reddening and extinction in the Milky Way ($A_V = 0.07$, Schlegel et al., 1998); but not for internal extinction in NGC 4214. However, I note that internal extinction is relatively small in most of NGC 4214 (i.e., typical values $A_V \approx 0.2$ compared to $A_V \approx 0.5$ in M83). This will be addressed in more detail in Kim et al. (2011, in preparation).

Padova models appropriate for individual stars are also included in the diagram (to the left of the Bruzual-Charlot models). Overall, there is an excellent match between the measured colors of the stellar groupings and the model predictions, with stellar groupings matching the models at the youngest ages and hugging the model curves. The diagram looks similar to those I have obtained in the past for compact clusters (e.g., Figures 6 and 7 from Chandar et al., 2010). Roughly half the regions have colors in the top part of the diagram with $U-B$ colors $<-1$, consistent with ages less than $10$ Myr. The rest of the groupings follow along the models relatively well with an enhancement at an age around $100$ Myr. Other points fall farther toward the red in $V-I$ (possibly more extincted clusters), or blue-ward at

the models (some of these may be stars rather than clusters since they fall almost on the Padova stellar isochrones).

The age, extinction, and mass of each stellar grouping were estimated by R. Chandar as in previous works (e.g., Fall et al., 2005; Chandar et al., 2010), by performing a least $\chi^2$ fit comparing measurements in five filters ($UBVI$,$H\alpha$) with new Charlot & Bruzual models (BC09) using the WFC3 filter transmission curves with $1/2$ solar metallicity. I refer to this as the spectral energy distribution, or 'SED' method. I assume a Chabrier (2003) initial stellar mass function (IMF), and a Galactic extinction law (Fitzpatrick, 1999). The mass of each cluster is estimated from the observed, extinction corrected $V$-band magnitude and the mass-to-light ratio predicted by the models, assuming a distance modulus $\Delta(m-M)$=27.41 to NGC 4214. If I had adopted the Salpeter (1955) rather than the Chabrier IMF, the $M/L_V$ and hence the masses would increase by a near constant (age-independent) $\approx 40$%. The best fit age and mass for each stellar grouping is compiled in Table 3.2. I show the resulting age histogram from the $1/2$ solar metallicity model in Figure 3.10. This will be discussed in more detail in Section 3.6.

Figure 3.10 shows an apparent lack of stellar groupings with ages in the range $7 < \log \tau < 7.6$. While some of this may be due to the well known artifact in this age range (for a discussion see Chandar et al., 2010), I note that the color-color diagram in Figure 3.9 also shows an enhancement around $100$ Myr. A similar enhancement is NOT seen in the M83 data, which lends credibility to the idea that the apparent increase in the cluster/association (and hence star) formation in NGC 4214 around $100$ Myr ago is real. Number statistics are not sufficient to say whether there is a similar gap in the range $8.4 < \log \tau < 8.8$. The reality of the apparent gap in star formation in the range $7 < \log \tau < 7.6$ will be further examined in a future publication (Kim et al. - in preparation).

The second method uses the visual appearance of the cluster, in both nar-

row and broad optical filters, to assign it to a "morphological category", which is essentially an age sequence. The method relies on the simple premise that the ionized gas, as traced by $H\alpha$ emission, in very young ($\tau \leq$ few Myr) is largely coincident with the cluster stars (category 3), in somewhat older ($\tau \approx$ Myr) clusters the gas is in a small, ring-like structure surrounding the stars (category 4a), and in still older ($\tau \approx 5-10$ Myr) clusters the gas is in an even larger bubble (category 4b). Ionized gas is not observed in clusters older than $\tau \geq 10$ Myr (categories 5 and 6). For older ages, the pixel-to-pixel flux variations, as discussed in the next paragraph, are used to help distinguish ages. This new classification scheme was developed and tested on compact star clusters in M83, and is described in detail in Whitmore et al. (2011). Here, I apply this classification scheme to compact clusters in NGC 4214 to test whether it also works in this lower mass galaxy, while also extending the classification to more diffuse stellar groupings. Based on the classification scheme described above, I assigned a morphological category to each stellar grouping.

Figure 3.11 shows the resulting correlations between morphological category and age (top panel). As found for the compact clusters in M83 (Whitmore et al., 2011), there is a strong correlation, although perhaps not as well defined as for M83. This is probably because of the inclusion of the more diffuse associations in the current study, since they include a larger percentage of light from the field than is the case for the compact clusters in M83.

The third age-dating method is based on an observed relationship between the pixel-to-pixel variations within clusters and their ages. The peak pixel-to-pixel flux variations, or RMS, occurs at ages around $10$ Myr when the brightest evolved stars appear, and has lower values at both older and younger ages (Whitmore et al., 2011). Figure 10 in Whitmore et al. (2011) shows that the highest RMS occurs for groupings in category 4, and has lower values for both lower and higher categories, similar to trends observed for compact star clusters in M83.

In the middle panel of Figure 3.11 I compare the SED ages and the RMS pixel-to-pixel flux variations determined for stellar groupings in NGC 4214. The same trends found for the compact clusters in M83 (Whitmore et al., 2011) are found for the stellar groupings in NGC 4214, with the highest values for groupings around $10$ Myr, and lower values at both younger and older ages. However, as is true above for the morphological categories, the correlations are not as well defined as in M83, probably because of the inclusion of diffuse associations with larger fractions of light from the field stars.

In the rest of this chapter I use the SED ages as the primary method for assigning ages to the stellar groupings and examining the size distributions as a function of age. The bottom panel in Figure 3.11 shows the size vs. age diagram. At young ages I find a wide variety of sizes while at older ages nearly all of the diffuse associations are gone. This will be discussed in more detail in § 3.6.

## 3.6 Results and Discussion

With both objectively determined stellar groupings and age estimates in hand I are now ready to address some of the questions outlined in the Introduction.

### 3.6.1 The Size Distribution of Stellar Groupings

I present the size histograms, $r_{tot}$, $r_{3/4}$, $r_{1/2}$, $r_{1/4}$, etc for the stellar groupings in the automatic and manual catalogs. Figure 3.7 shows the size histograms resulting from automated selections of sources with different thresholds for $r_{tot}$. The left panels of Figure 3.12 and of Figure 3.13 show the size histograms from the automatic catalog, whereas the right panels of these figures show sources from the manual catalog. The only difference in the two panels is the use of linear or logarithmic binning.

In Figure 3.7, I see the same general trends in the automated list regardless

of the threshold above the background chosen for $r_{tot}$: the peak of $r_{1/4}$ distribution is located towards the small scales, while the $r_{tot}$ distribution is peaked closer to the midpoint of the histogram. While the overall shape of the size distribution is consistent between different thresholds, the exact position of the peak of the histograms does shift depending on the threshold used. In Figure 3.12 and Figure 3.13, I note good agreement in the general appearance of the distributions obtained by using the manual and the automated catalogs. This is reassuring and suggests that the results are not dominated by selection effects.

Focusing primarily on Figure 3.13 with logarithmic binning, the size distributions can be described, to first order, by a peaked, Gaussian-like, roughly symmetric distribution (when plotting vs. log R) for $r_{tot}$. However, for $r_{1/4}$ the story is different, with an asymmetric, roughly power-law type distribution. The distributions for the $r_{3/4}$ and $r_{1/2}$ histograms appear to be a combination of the two. The median values are $r_{tot}$/$r_{3/4}$/$r_{1/2}$/$r_{1/4}$=7.2/4.8/3.4/2.0 pc for the manual catalog and $r_{tot}$/$r_{3/4}$/$r_{1/2}$/$r_{1/4}$=5.5/4.4/3.4/2.5 pc for the automatic catalog, with percent differences of $27\%$, $9\%$, $1\%$, and $23\%$, respectively. The $20-30\%$ differences between the average $r_{1/4}$ and $r_{tot}$ values for the automated and manual lists highlight the difficulty of automatically reproducing the groups of stars detected by the human eye on the smallest and largest scales. The $r_{3/4}$ and $r_{1/2}$ both show less than $10\%$ difference when comparing the automated and manual lists, and thus these measurements of characteristic size are least subject to selection effects in the automated code or observer bias in the manual code. The $1\%$ difference in the average $r_{1/2}$ between the automated and manual lists shows that this is the least biased measure of size scale to use for analysis of the size distribution of stellar clustering in a larger sample of galaxies.

Before attempting to interpret the data in more detail I now factor in the age distributions, which may help to clarify the situation.

### 3.6.2 The Age Distribution of Stellar Groupings in NGC 4214

In a future publication I will perform an analysis of the age, luminosity, and mass distributions for the stellar groupings discussed in this chapter in more detail (i.e., similar to Chandar et al., 2010, for M83). In particular, by having the new information about the sizes, I will be able to examine a new dimension, dependencies on the densities of the clusters. In the present chapter I only briefly examine the age distribution, and then use it to break the size sample into three subsamples in order to provide new insight into the evolution of star clusters. Figure 3.10 presents the age distribution observed for the stellar groupings in NGC 4214. I note that like the actively star forming galaxies in past studies (i.e., the Antennae galaxies, M51, M83) the majority of the ages are less than $10$ Myr. This supports the interpretation that the dissolution of clusters (and associations in this case) is the dominant influence in determining the demographics of stellar groupings, rather than the unlikely coincidence that all of these galaxies happen to have had a burst of star formation in the past $10$ Myr.

The size analysis from the previous section was then repeated, this time breaking the sample into three subsamples as follows:

- very young: log T $< 6.8$ (i.e., $\sim 6$ Myr)
- young: $6.8 <$ log T $< 7.8$ (i.e., $\sim 6-60$ Myr)
- intermediate: log T $> 7.8$ (i.e., $> \sim 60$ Myr)

Figure 3.14 shows the resulting distributions. There are two interesting results that come out of this exercise. The first is that while $60\%$ of the very young sample have values of $r_{tot} > 20$ pc, and only $5\%$ of the intermediate age sample have this large a radius. The second result is that unlike the full sample, the age-selected

subsamples appear to show some degree of size bimodality, with an apparent gap between the compact clusters and diffuse associations.

A possible working hypothesis that appears to be consistent with the data is the following. The original size distribution of stellar groups is bimodal, with approximately $1/4$ of the groupings being compact clusters (with a mean $r_{tot} \approx 3$ pc), and $3/4$ being diffuse associations (with a mean $r_{tot}$ around $30$ pc). With time, two things happen. First, both the compact clusters and the diffuse associations continue to dissolve, the compact clusters becoming associations for a certain period of time and the most diffuse associations diffusing into the field (or at least below the detection threshold). As time progresses, nearly all the associations are removed from the sample, and only the compact clusters remain, hence the large spike ($70$ % of the sample) with ages $>30$ Myr are compact clusters.

## 3.7 Conclusions

I have used the WFC3 Early Release observations of NGC 4214, and a new objective, uniform method of identifying and measuring the sizes of stellar groupings in order to obtain the following results.

1. Both the automated and manual catalogs have fairly continuous size distributions (for $r_{tot}$, $r_{1/2}$, etc) between a few parsecs to several tens of parsecs. These distributions are not strongly bimodal, in contradiction to the suggestion from Maíz-Apellániz (2001).

2. The automated method I have developed detects the majority of the stellar grouping selected in the manual list, and determines sizes with a $80\%$??? percent discrepancy from the sizes estimated by eye for sources in the manual list.

3. The size distribution of stellar clustering is peaked (i.e., roughly Gaussian) and has a fairly systemic shape for $r_{tot}$, but transitions to an asymmetric distribution when using $r_{1/4}$, with many more compact rather than diffuse nuclei.

4. Most stellar groupings are younger than $10$ Myr. This support the idea that most clusters and associations are disrupted on short time scales (i.e., infant mortality - see Whitmore et al., 2007).

5. If the size distribution is divided into three age ranges ($<3$ Myr, $3-10$ Myr, $>30$ Myr), some degree of bimodality is seen in each age range, with an original populations of about $1/4$ of the sample being compact and $3/4$ being diffuse associations.

6. The size distributions evolve with age, with the clearest result being that while $60$% of the very young sample have values of $r_{tot}>20$ pc, only $40$% of the young sample, and only $5\%$ of the intermediate age sample does.

7. A simple working scenario is developed for the dissolution of both compact clusters and diffuse associations. In this scenario, most of the compact clusters and diffuse associations disperse with time, but ultimately, only a small percentage ($1/20$th) of the compact clusters survive to have ages $>200$ Myr stars diffuse into the field population of the galaxy.

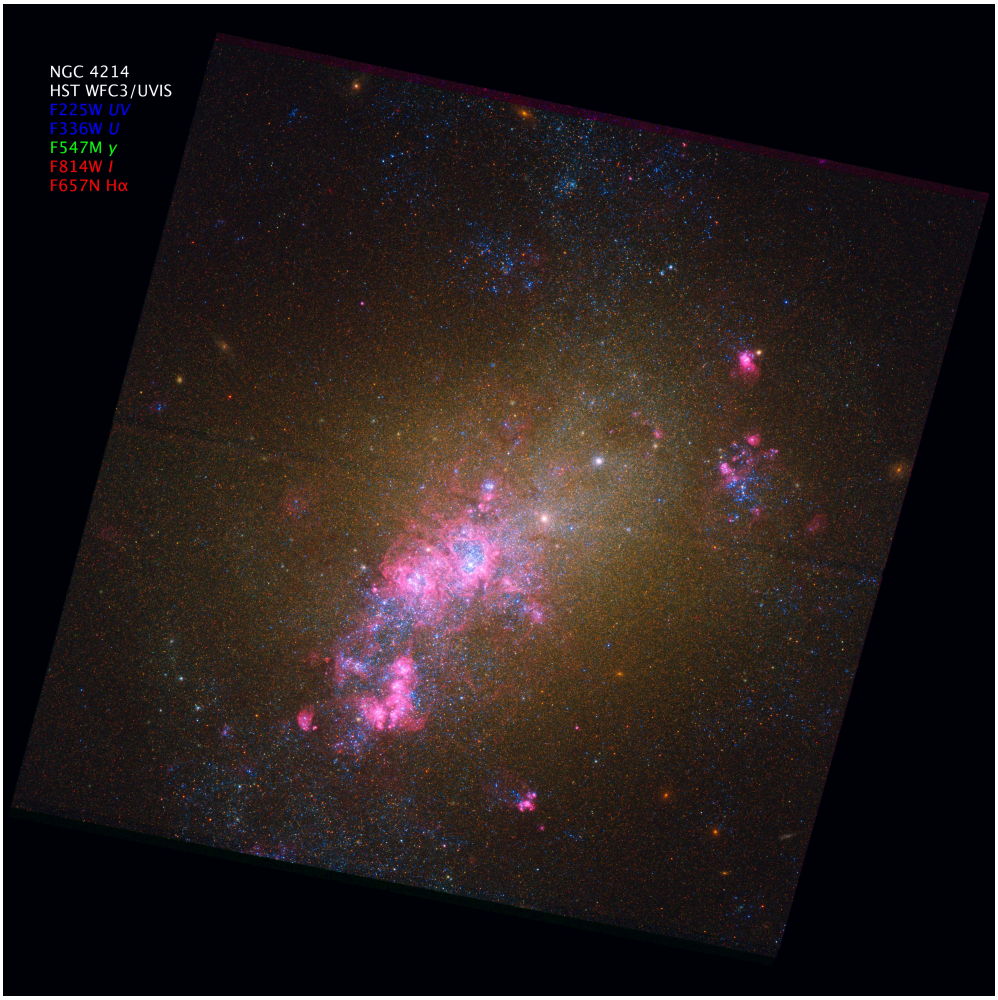


Figure 3.1: *HST* WFC3/UVIS image of NGC 4214. The $F225W$ and $F336W$ filters are shown in blue, $F547M$ in green, and $F814W$ and $F657N$ in red. North is up and East is right. *Image Credit: Z. Levay, NASA, R. O'Connell (University of Virginia), the WFC3 Science Oversight Committee.*

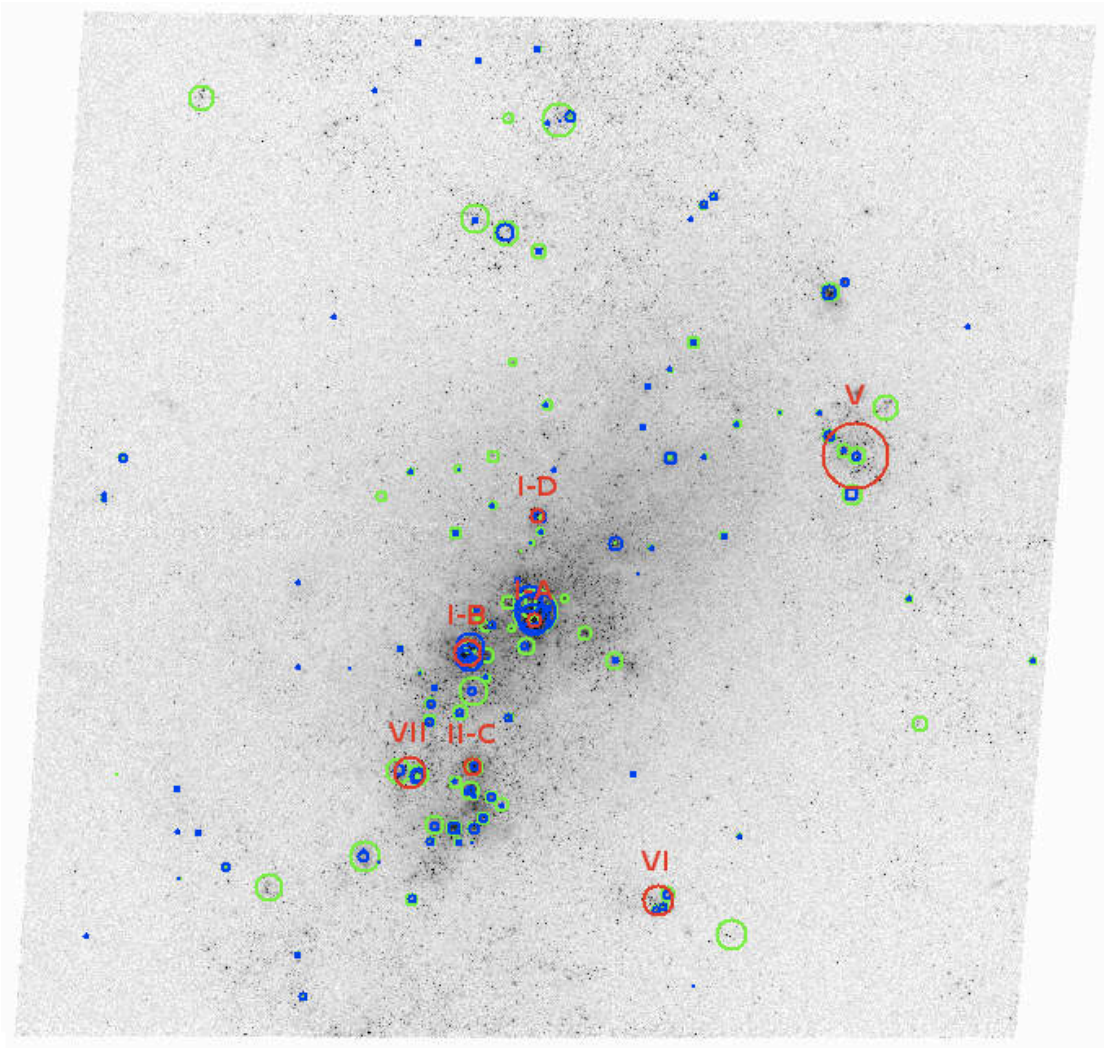


Figure 3.2: Manual (green) and automatically selected (blue) stellar groupings from this study, and seven massive young clusters (MYCs) from Maíz-Apellániz (2001) (red), overlaid on the $F336W$ *HST* WFC3/UVIS image of NGC 4214. Of the seven MYCs from the Maíz-Apellániz (2001) study, six are scaled OB associations (SOBAs), and only one (cluster I-A) is a compact super star cluster (SSC).

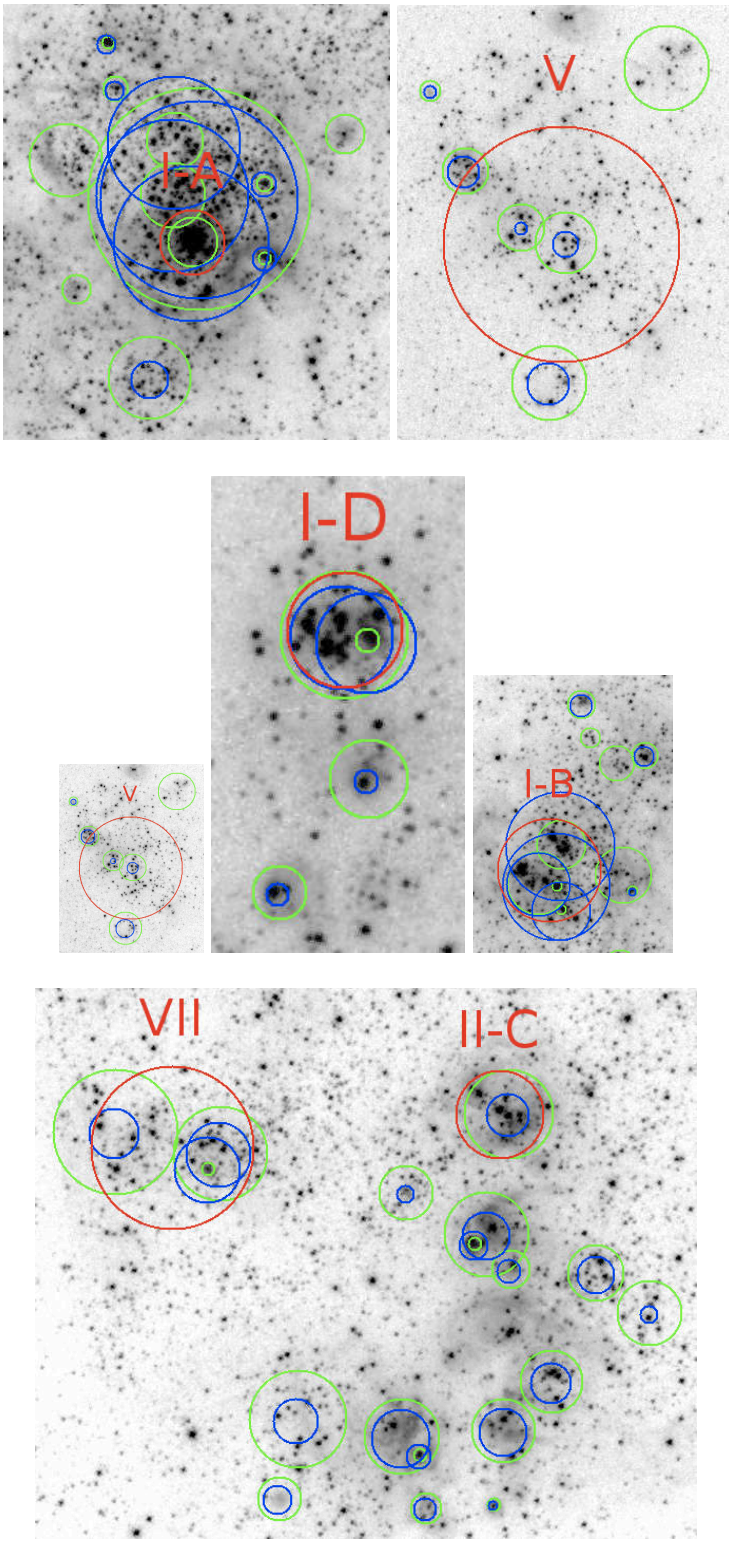


Figure 3.3: Zoom-ins of previous figure: Manual (green) and automatically selected (blue) stellar groupings from this study, and seven massive young clusters (MYCs) from Maíz-Apellániz (2001) (red), overlaid on the $F336W$ *HST* WFC3/UVIS image of NGC 4214.

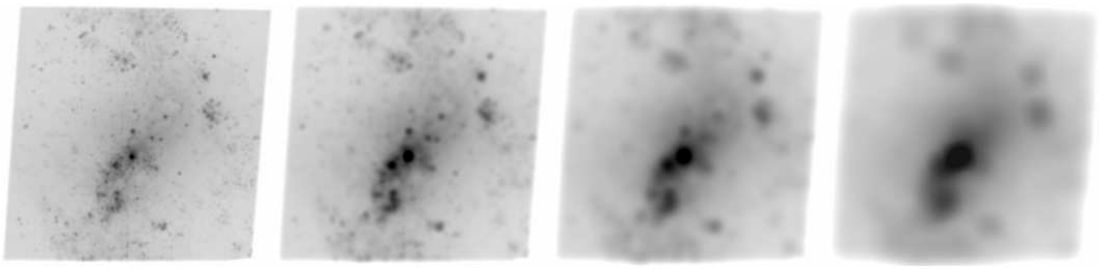

Figure 3.4: *HST* WFC3/UVIS $F336W$ image of NGC 4214 convolved with Gaussians of $\sigma = 10, 20, 40$ and $80$ pc (from left to right). North has been rotated $11$ degrees counter-clockwise from vertical on these images and all subsequent images of NGC 4214, unless otherwise noted.

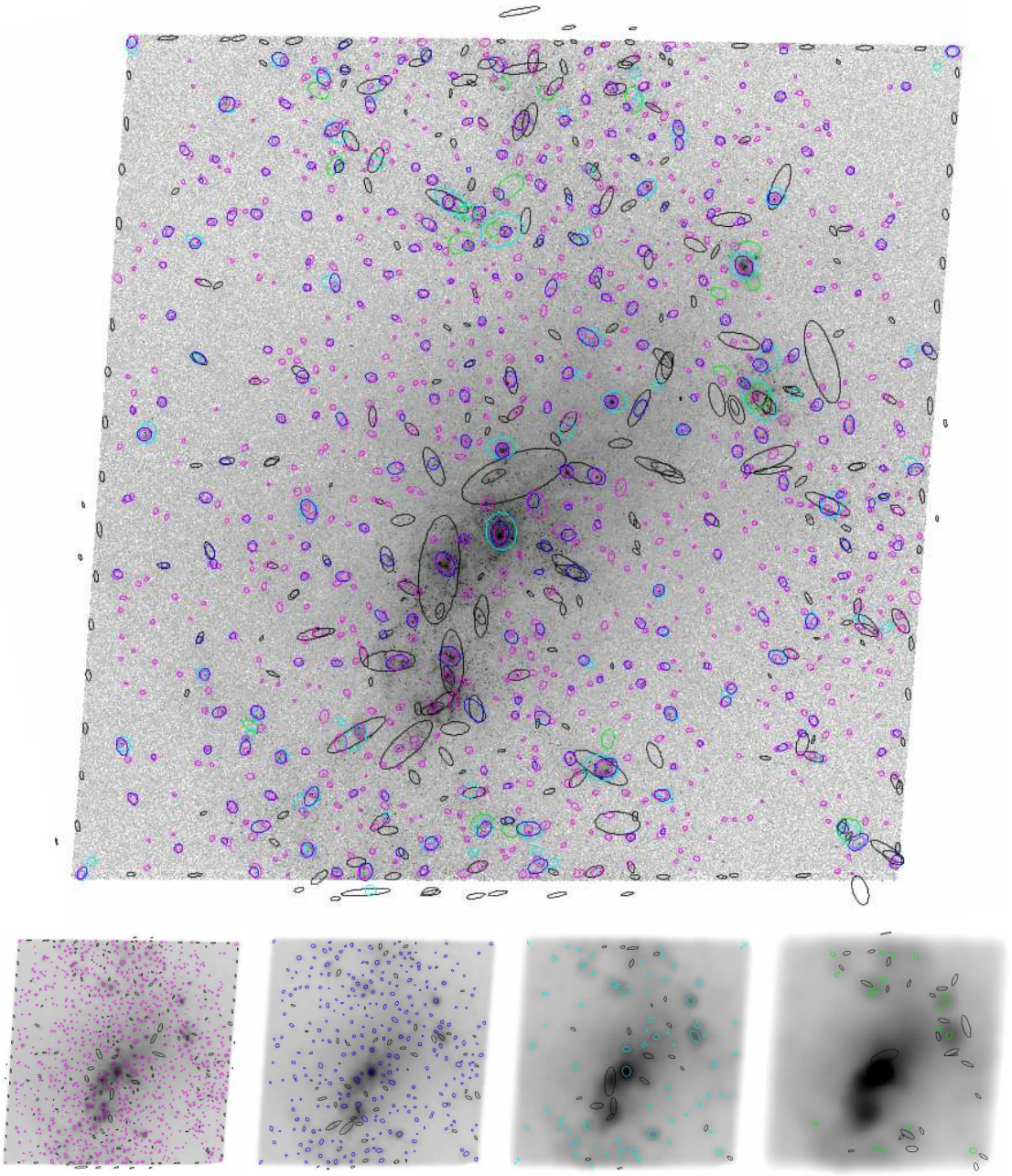

Figure 3.5: Sources detected using SExtractor on Gaussian-blurred *HST* WFC3/UVIS $F336W$ images of NGC 4214. The top image shows all detections overlaid on the original $F336W$ image, while the four images below show the detections found for individually blurred images with Gaussians of $\sigma = 10, 20, 40,$ and $80$ pc, from left to right. Detections are color-coded according to the standard deviation of the blurring Gaussian used on the image in which they were found: $\sigma = 10$ pc (magenta), $20$ pc (blue), $40$ pc (cyan), $80$ pc (green). Black ellipses demark highly elongated detections ($a/b < 1.9$), which are usually spurious and are rejected from the potential source list.

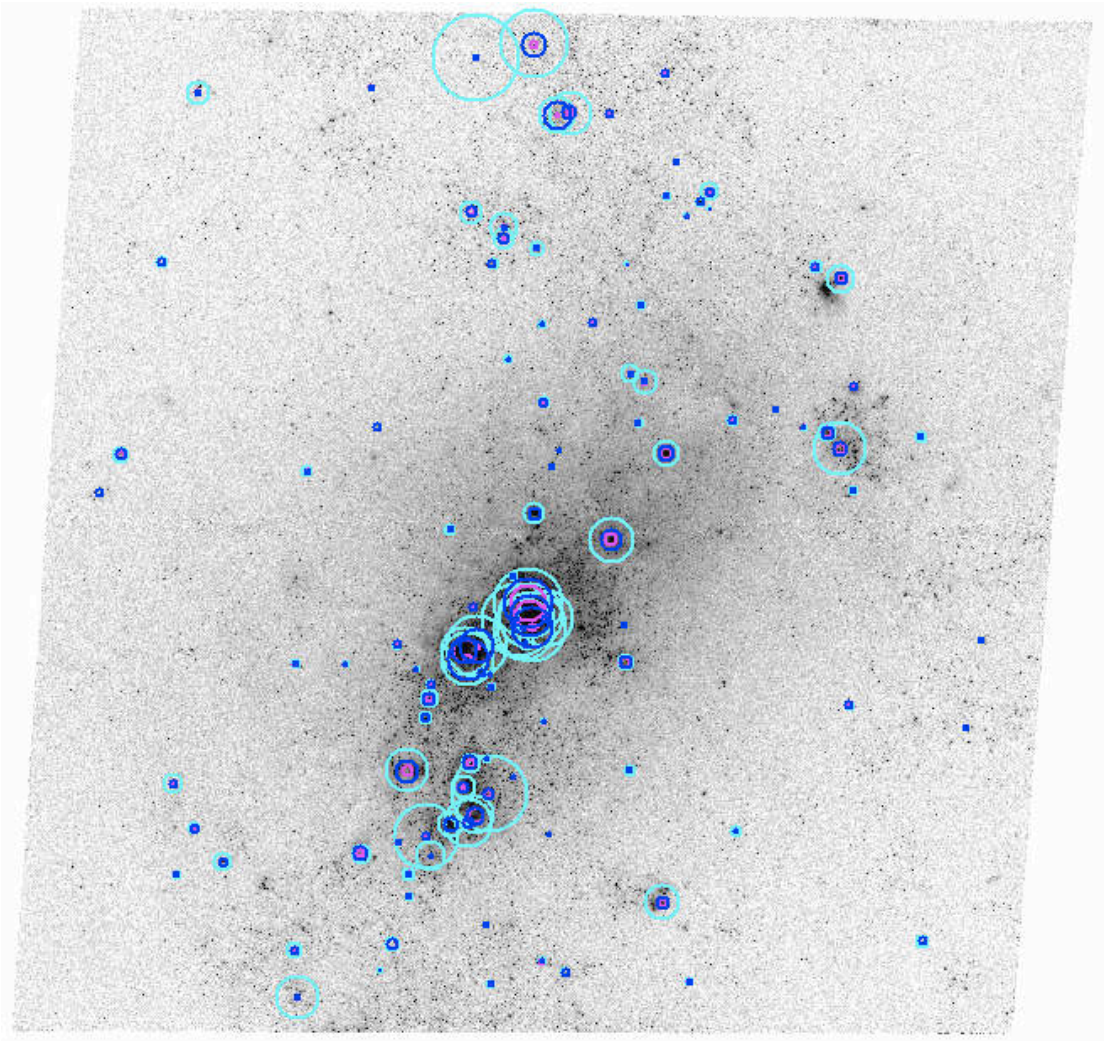

Figure 3.6: Automatically selected stellar groupings with the radius which encloses the total flux ($r_{tot}$) shown for three different thresholds above the background value: 1.9 (magenta), 1.5 (blue), 1.1 (cyan). The threshold of 1.5 (blue) provides the best $r_{tot}$ for the majority of objects in NGC 4214.

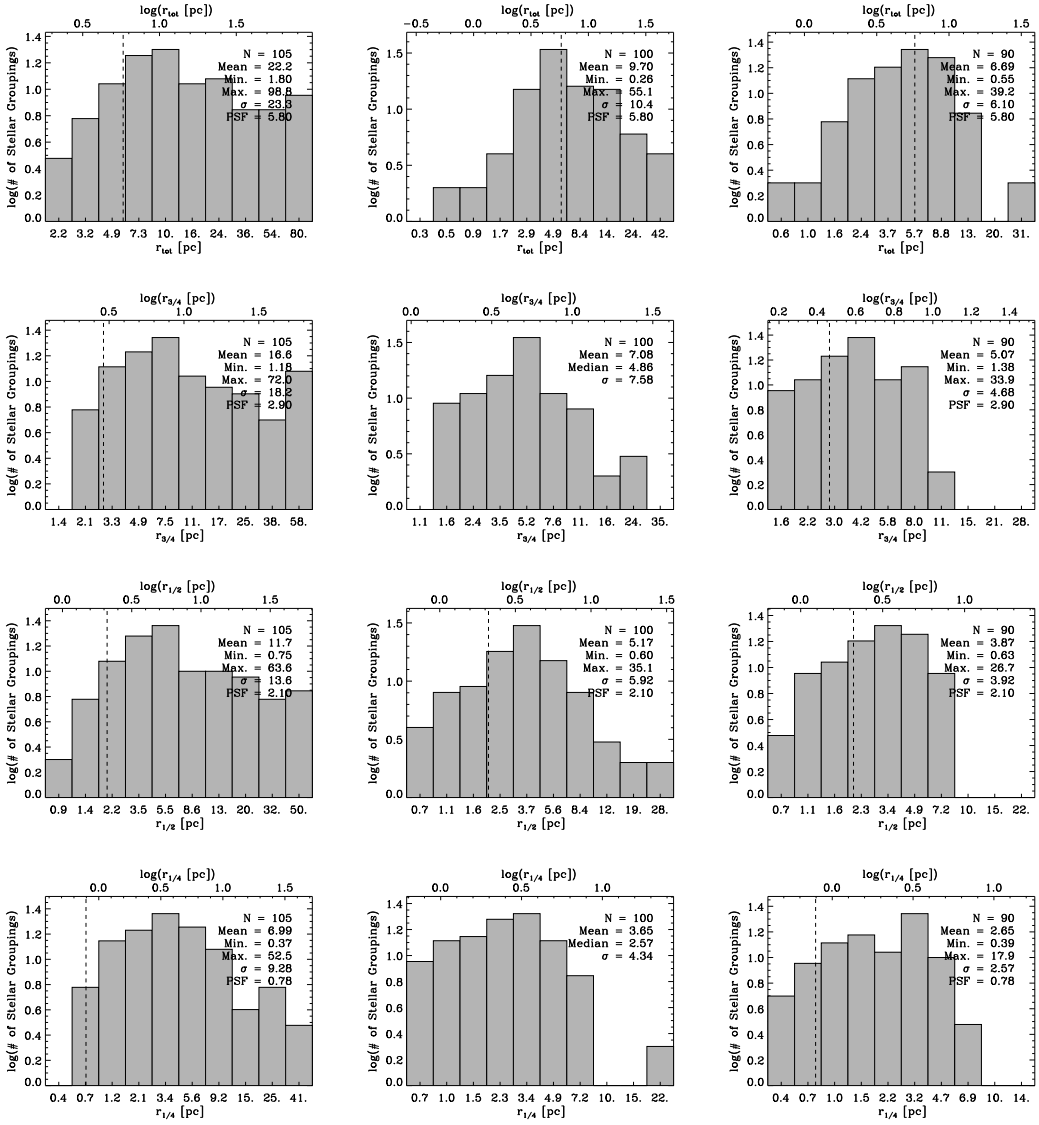


Figure 3.7: Size histograms for three different thresholds above the background for determining $r_{tot}$: 1.1 times the background (left), 1.5 (middle), and 1.9 (right). The dashed vertical lines represent the respective radii of a star as determined by the automated method for this data.

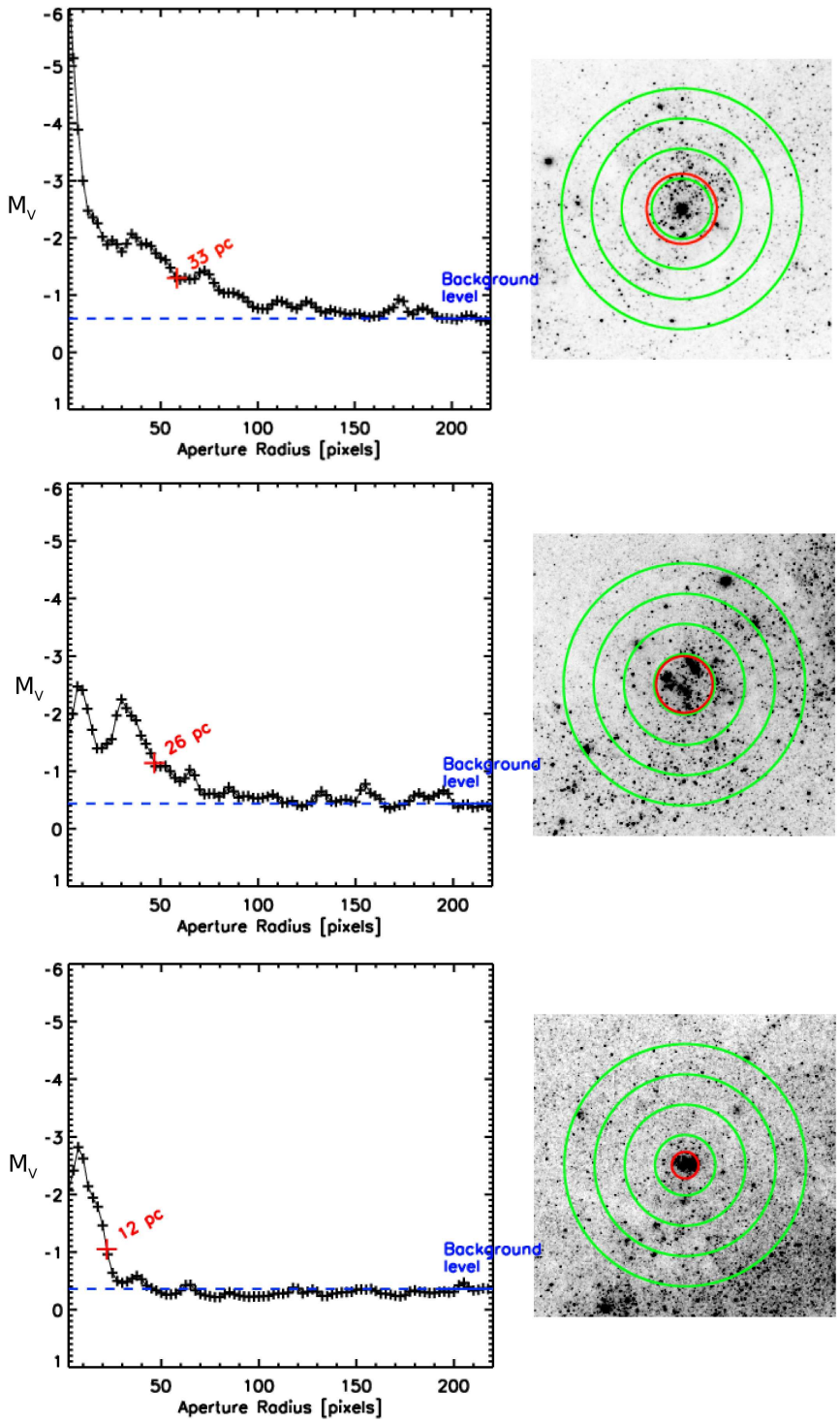


Figure 3.8: LEFT: Annular flux per until area versus the central radii of the annulus. The labeled "background" level is determined by taking the mean of the flux/pixel of the $10$ largest annuli. The radius which encloses the total flux, $r_{tot}$, is indicated in red. See § 3.4 for more details. RIGHT: A $250 \times 250$ pixel cutout of the *HST* WFC3/UVIS $F547M$ image of NGC 4214, centered at the candidate stellar grouping position. North is up and East is right on the thumbnail images.

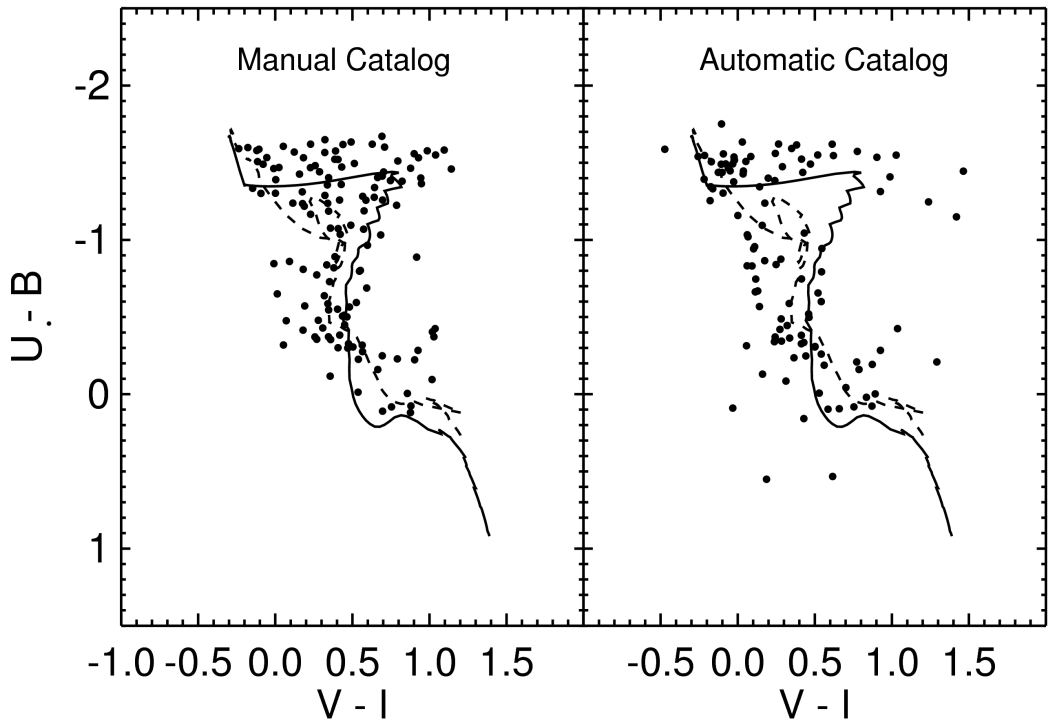


Figure 3.9: Color-color diagrams for manually selected stellar groupings in NGC 4214 (LEFT), and automatically selected stellar groupings (RIGHT). The y-axis color is $F336W-F438W$, whereas the x-axis color is $F336W-F438W$. The overlaid models are GALAXEV (Bruzual & Charlot, 2003, unpublished updated 2010 models, personal correspondance) evolutionary tracks for star clusters of twice-solar metallicity (solid line) and half-solar metallicity (dashed line). *Figure credit: R. Chandar.*

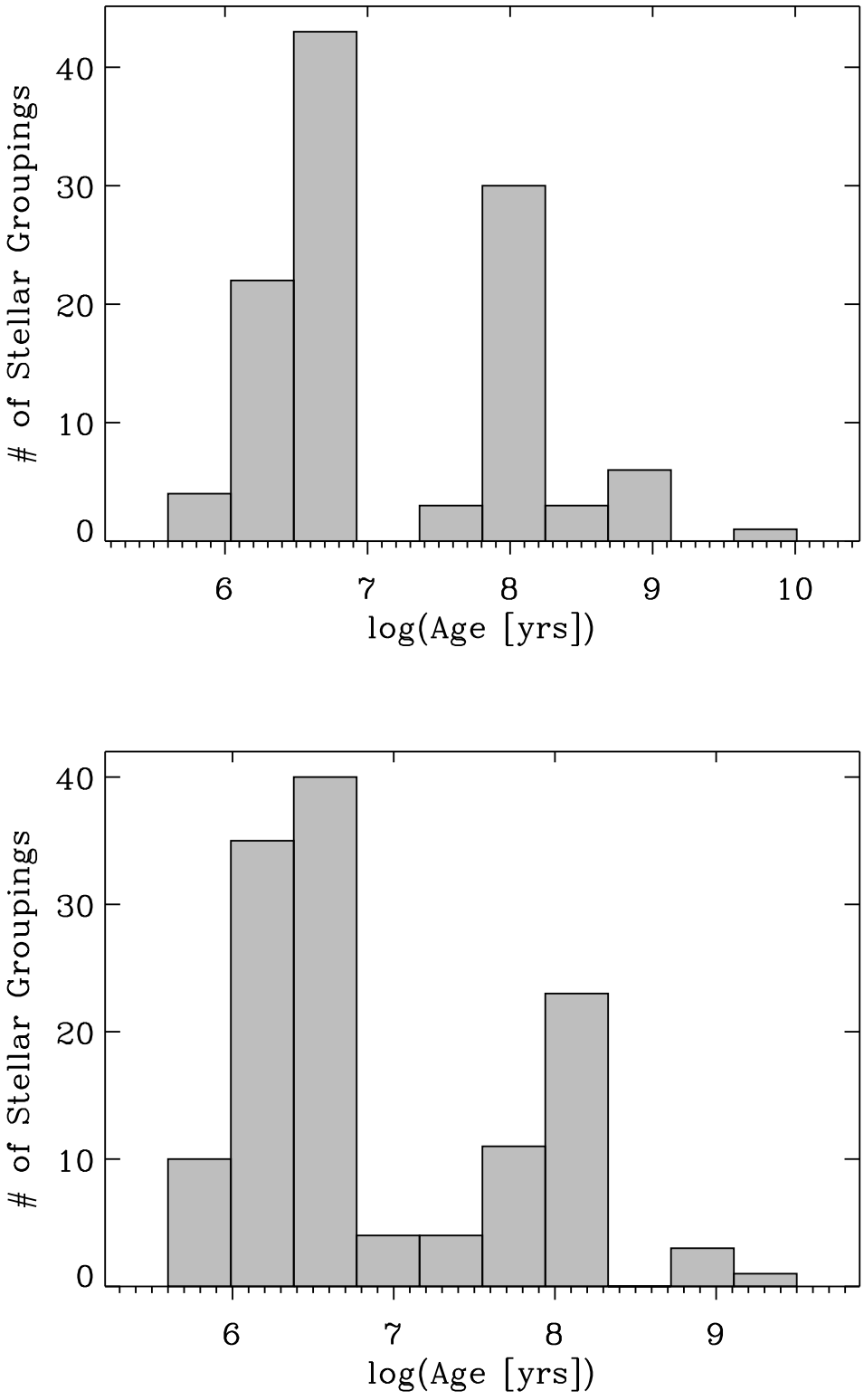


Figure 3.10: Age histograms for all automatically selected regions (TOP) and manually selected regions (BOTTOM) in NGC 4214. The dashed vertical lines represent the respective radii of a star as determined by the automated method for this data.

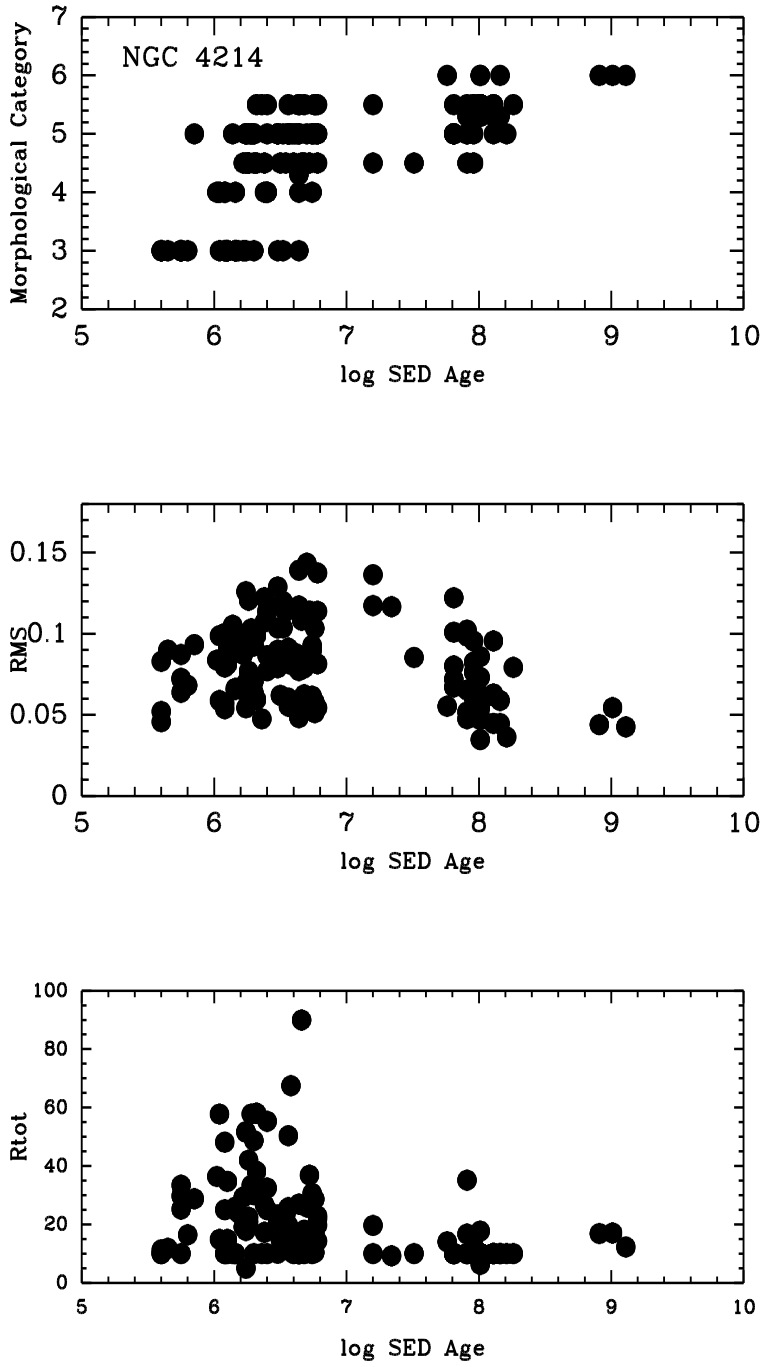


Figure 3.11: Three alternative age classification schemes versus SED-fitted age for the manually selected stellar groupings in NGC 4214: Morphological classification (TOP), RMS (MIDDLE) and total radius from the automated size determination method (BOTTOM). *Figure credit: B. Whitmore.*

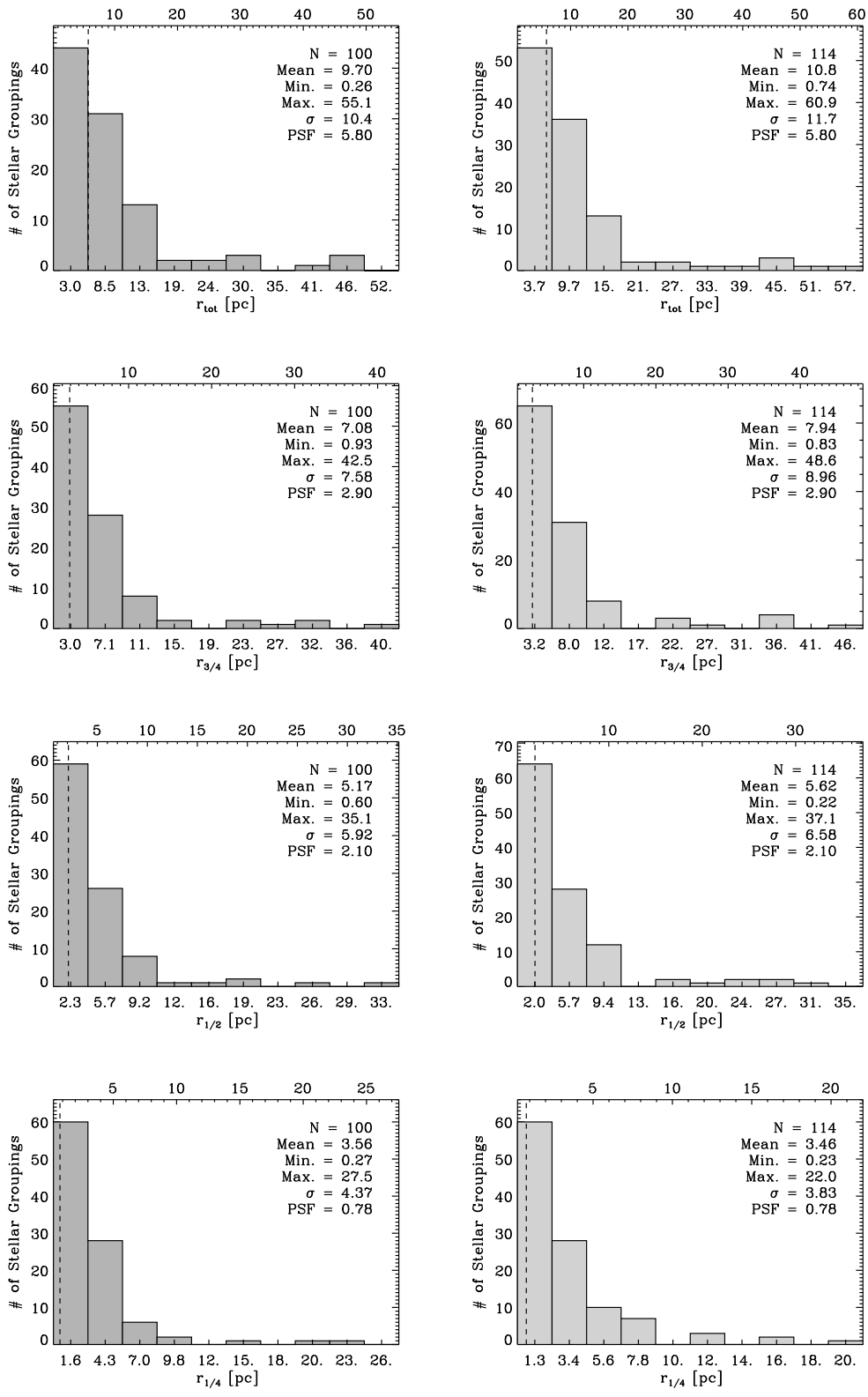


Figure 3.12: Linear-linear size histograms for $r_{tot}, r_{3/4}, r_{1/2}$, and $r_{1/4}$ (top to bottom) for stellar groupings selected by the automated method (left column) and the manual method (right column). The dashed vertical lines represent the respective radii of a star as determined by the automated method for this data.

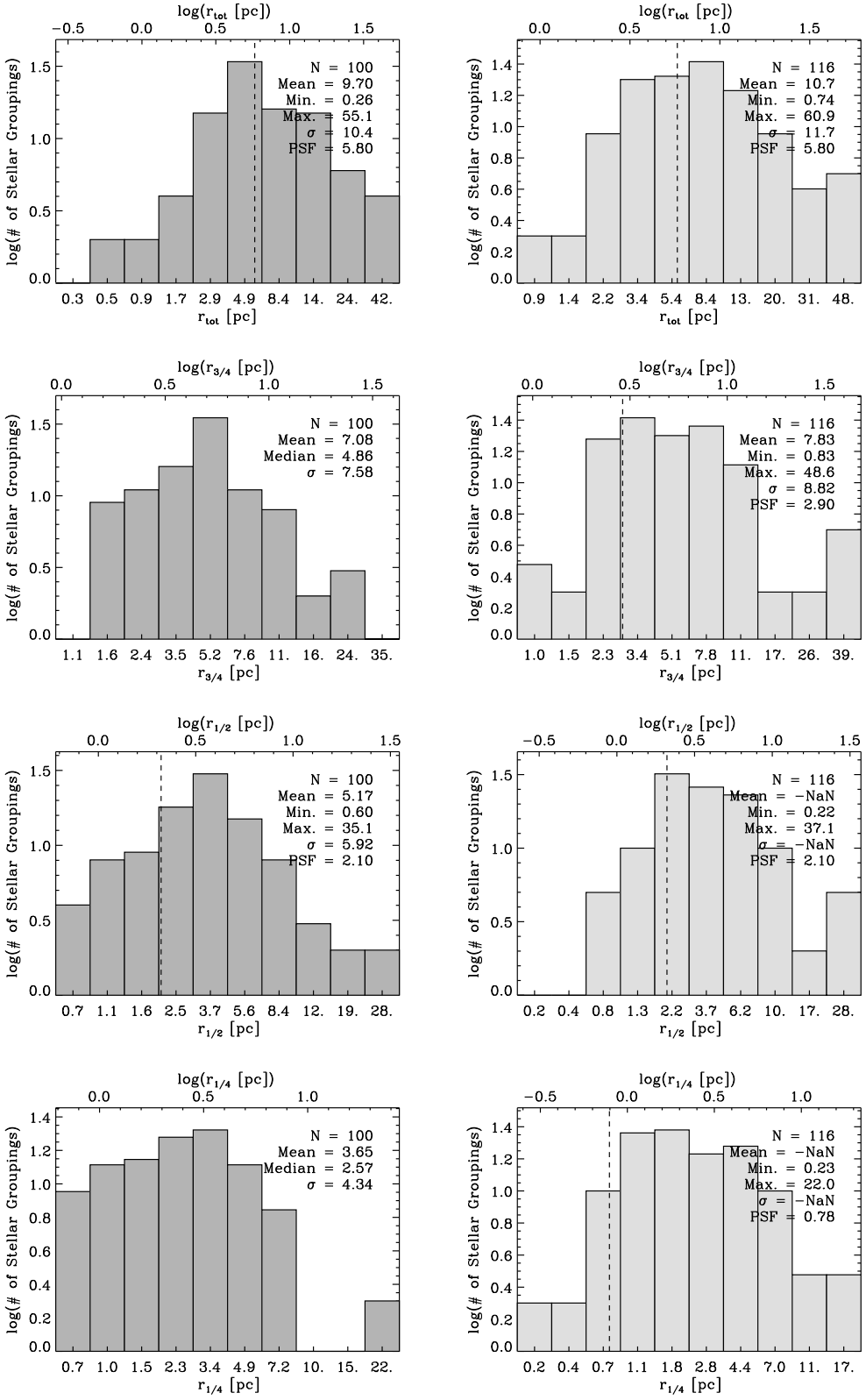


Figure 3.13: Log-log size histograms for $r_{tot}, r_{3/4}, r_{1/2},$ and $r_{1/4}$ (top to bottom) for stellar groupings selected by the automated method (left column) and the manual method (right column). The dashed vertical lines represent the respective radii of a star as determined by the automated method for this data.

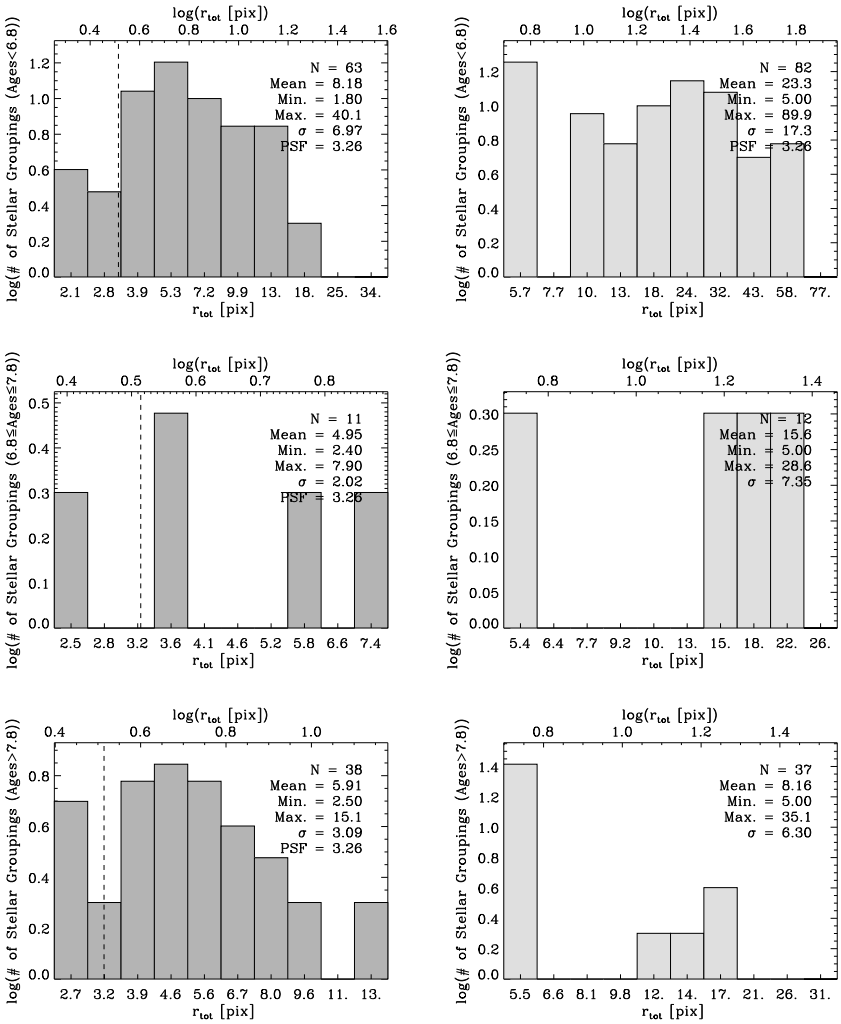


Figure 3.14: Lograrithmic size histograms of $r_{tot}$ for stellar groupings binned by age: $< 6.8$ Myr (top), $6.8-7.8$ Myr (middle), and $> 7.8$ Myr (bottom) for stellar groupings selected by the automated method (left), the manual method (right). The dashed vertical lines represent the respective radii of a star as determined by the automated method for this data.

Table 3.1: SExtractor Parameter Values Used for each Gaussian Blur Size

| $\sigma$ of Blurring Gaussian (pc) [4] | DETECT_MINAREA [1] ((pixels)) | DETECT_THRESH [2] ((pixels)) | PHOT_AUTOAPERS [3] (pixels) |
|---|---|---|---|
| 10 | 238 | 2.75 | 17.3975 |
| 20 | 951 | 2.25 | 34.7950 |
| 40 | 3804 | 1.40 | 69.5901 |
| 80 | 15214 | 0.446 | 130.180 |

[1] Minumum number of pixels above threshold = $\pi \times$(aperture radius in pixels)$^2$

[2] Required sigma above background

[3] MAG_AUTO minimum circular aperture diameter

[4] Root-Mean-Squared of the stellar grouping, as in Whitmore et al. (2011).

Table 3.2: Master Table of Stellar Groupings in NGC 4214[1]

| ID | x (pix) | y (pix) | $M_V$[2] | $U-B$ | $V-I$ | E($B-V$) | $log$(Age) (years) | Mass ($M_\odot$) | $r_{tot,Manual}$[4] (pix) | Morph. Cat.[3] | RMS[5] |
|---|---|---|---|---|---|---|---|---|---|---|---|
| 1 | 1883.43 | 3630.26 | -5.90 | -1.53 | 0.18 | 0.14 | 6.30 | $3.50\times10^2$ | 3.9 | 3 | 0.071 |
| 2 | 2224.26 | 4505.34 | -6.33 | -1.30 | -0.09 | 0.04 | 6.64 | $3.87\times10^2$ | 6.2 | 5.5 | 0.077 |
| 3 | 821.95 | 3097.29 | -5.54 | -1.59 | -0.24 | 0.00 | 6.60 | $1.53\times10^2$ | 3.3 | 4.5 | 0.081 |
| 4 | 1536.47 | 2592.12 | -5.75 | -1.22 | 0.19 | 0.18 | 6.68 | $3.81\times10^2$ | 2.4 | 4.5 | 0.079 |
| 5 | 884.98 | 1860.15 | -6.08 | -0.23 | 0.54 | 0.24 | 8.01 | $6.70\times10^3$ | 12.4 | 5.3 | 0.062 |
| 6 | 652.87 | 1964.82 | -3.92 | -1.36 | 0.34 | 0.36 | 6.36 | $9.91\times10^1$ | 3.2 | 5.5 | 0.048 |
| 7 | 855.40 | 1684.93 | -5.63 | -0.55 | 0.35 | 0.06 | 7.91 | $2.32\times10^3$ | 6.1 | 5.3 | 0.052 |
| 8 | 1467.52 | 2251.54 | -5.85 | -0.35 | 0.36 | 0.14 | 8.01 | $4.03\times10^3$ | 3.7 | 5.3 | 0.049 |
| 9 | 1672.32 | 2206.03 | -6.04 | -0.36 | 0.27 | 0.10 | 8.01 | $4.27\times10^3$ | 3.0 | 5.5 | 0.055 |
| 10 | 935.04 | 1664.45 | -7.16 | -0.30 | 0.41 | 0.02 | 8.16 | $1.13\times10^4$ | 9.5 | 5.3 | 0.059 |
| 11 | 825.81 | 1496.06 | -6.32 | -0.33 | 0.48 | 0.18 | 8.01 | $7.00\times10^3$ | 6.6 | 5.5 | 0.062 |
| 12 | 1021.51 | 1509.71 | -6.99 | -0.55 | 0.40 | 0.06 | 7.96 | $8.56\times10^3$ | 11.8 | 4.5 | 0.082 |
| 13 | 407.11 | 1339.04 | -4.64 | -1.58 | -0.12 | 0.08 | 6.40 | $7.54\times10^1$ | 3.2 | 5.5 | 0.077 |
| 14 | 1239.11 | 1098.97 | -7.04 | -0.37 | 0.26 | 0.00 | 8.11 | $8.97\times10^3$ | 8.5 | 5.5 | 0.063 |
| 15 | 1230.86 | 924.89 | -6.19 | -0.12 | 0.36 | 0.06 | 8.26 | $5.85\times10^3$ | 6.7 | 5.5 | 0.079 |
| 16 | 2803.81 | 662.93 | -6.66 | -0.48 | 0.28 | 0.02 | 8.01 | $5.98\times10^3$ | 6.6 | 5.5 | 0.073 |
| 17 | 1638.72 | 1407.04 | -5.65 | -1.36 | 0.95 | 0.50 | 6.08 | $1.05\times10^3$ | 8.2 | 3 | 0.054 |
| 18 | 2027.84 | 1413.87 | -5.83 | -1.58 | 1.10 | 0.48 | 5.75 | $1.41\times10^3$ | 7.2 | 3 | 0.064 |
| 19 | 1893.05 | 2246.99 | -7.52 | -0.28 | 0.57 | 0.14 | 8.11 | $2.11\times10^4$ | 4.6 | 5.3 | 0.062 |
| 20 | 1952.21 | 2133.21 | -6.70 | -1.50 | 0.51 | 0.28 | 6.10 | $1.49\times10^3$ | 4.8 | 3 | 0.081 |

Continued on Next Page. . .

Table 3.2 – Continued

| ID | x (pix) | y (pix) | $M_V$[1] | $U-B$ | $V-I$ | E($B-V$) | $log$(Age) (years) | Mass ($M_\odot$) | $r_{tot}$[2] (pix) | Morph. Cat.[3] | RMS[4] |
|---|---|---|---|---|---|---|---|---|---|---|---|
| 21 | 2052.34 | 1618.94 | -7.71 | -1.46 | 1.14 | 0.48 | 5.60 | $8.60\times10^3$ | 9.8 | 3 | 0.046 |
| 22 | 1977.78 | 1463.93 | -7.16 | -1.38 | 0.75 | 0.44 | 6.16 | $3.46\times10^3$ | 7.7 | 3 | 0.066 |
| 23 | 1998.26 | 2062.40 | -8.71 | -1.33 | -0.15 | 0.00 | 7.20 | $1.51\times10^4$ | 7.3 | 5.5 | 0.136 |
| 24 | 1856.89 | 1717.37 | -7.24 | -0.86 | 0.09 | 0.26 | 6.64 | $1.72\times10^3$ | 4.8 | 5.5 | 0.117 |
| 25 | 2240.32 | 2137.21 | -6.44 | -1.58 | 0.99 | 0.40 | 5.60 | $2.12\times10^3$ | 5.1 | 3 | 0.052 |
| 26 | 2729.57 | 1559.22 | -6.23 | -0.51 | 0.45 | 0.14 | 7.91 | $5.11\times10^3$ | 9.0 | 5.5 | 0.065 |
| 27 | 2904.79 | 2360.21 | -6.54 | -0.16 | 0.67 | 0.30 | 7.96 | $1.15\times10^4$ | 7.3 | 5.5 | 0.060 |
| 28 | 2165.23 | 2132.66 | -8.22 | -1.59 | -0.11 | 0.00 | 6.64 | $1.97\times10^3$ | 6.8 | 4 | 0.139 |
| 29 | 2165.23 | 2157.69 | -8.49 | -1.39 | 0.00 | 0.06 | 6.64 | $3.00\times10^3$ | 5.0 | 3 | 0.117 |
| 30 | 2506.56 | 2235.06 | -8.08 | -1.52 | 0.41 | 0.22 | 6.16 | $4.25\times10^3$ | 7.7 | 3 | 0.066 |
| 31 | 3124.38 | 2803.38 | -9.71 | -0.30 | 0.47 | 0.04 | 8.21 | $1.32\times10^5$ | 13.7 | 5 | 0.036 |
| 32 | 2837.66 | 2503.00 | -10.58 | -0.23 | 0.79 | 0.26 | 8.16 | $5.35\times10^5$ | 10.2 | 6 | 0.045 |
| 33 | 2414.40 | 2430.19 | -8.21 | -1.04 | 0.42 | 0.02 | 7.51 | $1.42\times10^4$ | 6.5 | 4.5 | 0.085 |
| 34 | 2651.06 | 2844.34 | -8.02 | -0.31 | 0.50 | 0.10 | 8.11 | $2.96\times10^4$ | 4.7 | 5 | 0.096 |
| 35 | 3040.18 | 2951.29 | -6.48 | -0.01 | 0.54 | 0.32 | 8.01 | $1.22\times10^4$ | 3.9 | 6 | 0.035 |
| 36 | 3090.24 | 3110.58 | -6.45 | -0.43 | 0.31 | 0.06 | 8.01 | $5.56\times10^3$ | 4.3 | 5.5 | 0.057 |
| 37 | 2440.00 | 4664.78 | -6.00 | -0.65 | 0.01 | 0.00 | 7.81 | $2.48\times10^3$ | 2.6 | 5.5 | 0.072 |
| 38 | 2667.56 | 4544.18 | -6.31 | -0.32 | 0.05 | 0.00 | 8.01 | $4.09\times10^3$ | 2.7 | 5.5 | 0.086 |
| 39 | 2897.57 | 4240.68 | -6.44 | -0.81 | 0.18 | 0.00 | 7.81 | $3.72\times10^3$ | 3.6 | 5 | 0.122 |
| 40 | 3500.98 | 3819.70 | -7.74 | -0.69 | 0.59 | 0.16 | 7.81 | $1.97\times10^4$ | 9.5 | 5 | 0.101 |
| 41 | 3394.03 | 3742.33 | -6.22 | -0.59 | 0.53 | 0.14 | 7.81 | $4.58\times10^3$ | 2.9 | 5 | 0.080 |

Continued on Next Page. . .

Table 3.2 – Continued

| ID | x (pix) | y (pix) | $M_V$[1] | $U-B$ | $V-I$ | E($B-V$) | $log$(Age) (years) | Mass ($M_\odot$) | $r_{tot}$[2] (pix) | Morph. Cat.[3] | RMS[4] |
|---|---|---|---|---|---|---|---|---|---|---|---|
| 42 | 4423.72 | 3095.50 | -5.74 | -0.51 | 0.44 | 0.10 | 7.91 | $2.90\times10^3$ | 6.3 | 5 | 0.048 |
| 43 | 3109.23 | 1229.40 | -6.78 | -0.37 | 0.35 | 0.04 | 8.11 | $7.91\times10^3$ | 8.3 | 5.5 | 0.045 |
| 44 | 2558.54 | 2665.48 | -8.47 | -0.50 | 0.47 | 0.08 | 7.96 | $3.54\times10^4$ | 5.5 | 5.5 | 0.095 |
| 45 | 1582.58 | 1457.84 | -6.99 | -1.61 | 0.05 | 0.00 | 6.74 | $8.76\times10^2$ | 9.0 | 4 | 0.093 |
| 46 | 2771.99 | 1052.01 | -7.73 | -1.62 | 0.23 | 0.18 | 6.16 | $2.74\times10^3$ | 25.3 | 3 | 0.091 |
| 47 | 2714.54 | 993.93 | -7.00 | -1.57 | 0.32 | 0.18 | 6.22 | $1.27\times10^3$ | 19.1 | 3 | 0.087 |
| 48 | 2451.03 | 2258.84 | -11.86 | -1.51 | -0.12 | 0.00 | 7.20 | $2.74\times10^5$ | 19.6 | 4.5 | 0.117 |
| 49 | 2548.44 | 2669.98 | -10.11 | -1.24 | 0.18 | 0.18 | 6.64 | $1.91\times10^4$ | 27.0 | 4.3 | 0.114 |
| 50 | 2177.05 | 2198.00 | -10.22 | -1.24 | 0.34 | 0.32 | 6.40 | $2.61\times10^4$ | 25.0 | 4 | 0.113 |
| 51 | 2098.23 | 1714.60 | -9.46 | -1.65 | 0.32 | 0.12 | 6.10 | $1.18\times10^4$ | 34.7 | 3 | 0.091 |
| 52 | 2063.40 | 1624.48 | -9.35 | -1.56 | 0.90 | 0.34 | 5.75 | $2.40\times10^4$ | 33.4 | 3 | 0.073 |
| 53 | 3894.61 | 3342.69 | -8.95 | -1.63 | 0.49 | 0.20 | 6.02 | $9.43\times10^3$ | 45.6 | 4 | 0.084 |
| 54 | 1952.75 | 1933.47 | -9.31 | -1.24 | 0.11 | 0.16 | 6.54 | $6.50\times10^3$ | 23.3 | 4.5 | 0.114 |
| 55 | 2278.66 | 2272.46 | -9.17 | -1.17 | 0.23 | 0.26 | 6.52 | $7.44\times10^3$ | 13.2 | 3 | 0.120 |
| 56 | 3830.34 | 2691.47 | -8.72 | -1.46 | -0.01 | 0.16 | 6.38 | $4.59\times10^3$ | 26.7 | 4.5 | 0.107 |
| 57 | 1867.91 | 1727.55 | -9.52 | -1.07 | 0.41 | 0.26 | 6.72 | $1.78\times10^4$ | 36.9 | 4.5 | 0.114 |
| 58 | 1967.00 | 1480.28 | -9.09 | -1.55 | 1.04 | 0.48 | 5.75 | $2.85\times10^4$ | 35.2 | 3 | 0.072 |
| 59 | 2142.23 | 1577.96 | -8.46 | -1.60 | -0.18 | 0.06 | 6.26 | $3.29\times10^3$ | 22.4 | 4.5 | 0.121 |
| 60 | 2091.37 | 1500.43 | -8.67 | -1.57 | 0.12 | 0.08 | 6.08 | $4.92\times10^3$ | 25.0 | 4 | 0.100 |
| 61 | 2647.21 | 2161.70 | -8.54 | -1.46 | 0.88 | 0.42 | 6.18 | $1.07\times10^4$ | 24.0 | 3 | 0.094 |
| 62 | 2413.84 | 2392.22 | -7.99 | -0.84 | 0.33 | 0.38 | 6.48 | $4.08\times10^3$ | 10.1 | 3 | 0.129 |

Continued on Next Page. . .

Table 3.2 – Continued

| ID | x (pix) | y (pix) | $M_V$[1] | $U-B$ | $V-I$ | E($B-V$) | $log$(Age) (years) | Mass ($M_\odot$) | $r_{tot}$[2] (pix) | Morph. Cat.[3] | RMS[4] |
|---|---|---|---|---|---|---|---|---|---|---|---|
| 63 | 2212.78 | 2063.38 | -8.05 | -1.40 | 0.66 | 0.40 | 6.38 | $5.02\times10^3$ | 17.3 | 4 | 0.122 |
| 64 | 3779.57 | 2767.34 | -8.35 | -1.58 | 0.39 | 0.20 | 6.16 | $5.12\times10^3$ | 25.9 | 4 | 0.102 |
| 65 | 3877.46 | 2664.65 | -9.66 | -0.64 | 0.32 | 0.08 | 7.91 | $1.00\times10^5$ | 35.1 | 4.5 | 0.102 |
| 66 | 2452.49 | 2341.77 | -9.72 | -1.44 | 0.29 | 0.02 | 6.78 | $1.39\times10^4$ | 22.9 | 4.5 | 0.137 |
| 67 | 1790.42 | 1760.20 | -9.52 | -1.36 | 0.43 | 0.38 | 6.30 | $2.00\times10^4$ | 48.7 | 4.5 | 0.092 |
| 68 | 2758.41 | 3730.59 | -8.05 | -1.43 | 0.16 | 0.08 | 6.74 | $2.94\times10^3$ | 30.6 | 5 | 0.090 |
| 69 | 2638.23 | 3834.68 | -9.25 | -1.19 | 0.35 | 0.30 | 6.56 | $1.02\times10^4$ | 50.4 | 5 | 0.091 |
| 70 | 2517.35 | 2294.45 | -8.49 | -0.48 | 0.07 | 0.00 | 8.01 | $3.03\times10^4$ | 6.3 | 5.5 | 0.190 |
| 71 | 2147.44 | 2164.03 | -10.52 | -1.47 | 0.23 | 0.22 | 6.40 | $2.56\times10^4$ | 32.4 | 4 | 0.114 |
| 72 | 1969.15 | 1998.92 | -8.63 | -0.89 | 0.92 | 0.50 | 6.52 | $9.12\times10^3$ | 22.0 | 5 | 0.104 |
| 73 | 2224.92 | 2335.87 | -8.89 | -0.43 | 1.04 | 0.50 | 7.76 | $1.45\times10^5$ | 9.5 | 6 | 0.055 |
| 74 | 2449.14 | 2542.37 | -6.40 | -1.52 | 0.39 | 0.24 | 6.24 | $8.07\times10^2$ | 3.9 | 3 | 0.126 |
| 75 | 1862.13 | 1451.39 | -7.71 | 0.08 | 0.75 | 0.00 | 9.01 | $7.04\times10^4$ | 12.6 | 6 | 0.054 |
| 76 | 3421.53 | 2882.69 | -7.73 | 0.11 | 0.70 | 0.00 | 8.91 | $5.83\times10^4$ | 10.8 | 6 | 0.044 |
| 77 | 3598.99 | 2899.75 | -6.51 | -0.38 | 0.42 | 0.12 | 8.01 | $7.00\times10^3$ | 6.4 | 5.5 | 0.054 |
| 78 | 1520.81 | 4616.31 | -7.37 | -1.29 | 0.32 | 0.36 | 6.24 | $2.80\times10^3$ | 51.8 | 5 | 0.054 |
| 79 | 2942.95 | 4243.19 | -9.09 | -0.80 | 0.55 | 0.50 | 6.58 | $1.71\times10^4$ | 67.5 | 5 | 0.081 |
| 80 | 2525.39 | 3912.06 | -8.67 | -1.38 | 0.82 | 0.46 | 6.40 | $9.47\times10^3$ | 55.3 | 5 | 0.086 |
| 81 | 3455.61 | 3790.72 | -7.67 | -0.59 | 0.34 | 0.04 | 7.91 | $1.43\times10^4$ | 16.7 | 5 | 0.099 |
| 82 | 2987.61 | 4252.94 | -7.31 | -0.57 | 0.19 | 0.00 | 7.96 | $9.64\times10^3$ | 14.1 | 5 | 0.076 |
| 83 | 2568.72 | 3308.28 | -6.68 | -0.82 | 0.38 | 0.40 | 6.60 | $1.42\times10^3$ | 16.8 | 5 | 0.082 |

Continued on Next Page. . .

Table 3.2 – Continued

| ID | x (pix) | y (pix) | $M_V$[1] | $U-B$ | $V-I$ | E($B-V$) | $log$(Age) (years) | Mass ($M_\odot$) | $r_{tot}$[2] (pix) | Morph. Cat.[3] | RMS[4] |
|---|---|---|---|---|---|---|---|---|---|---|---|
| 84 | 820.94 | 3079.58 | -6.82 | -1.47 | 0.02 | 0.14 | 6.26 | $9.17\times10^2$ | 11.4 | 4.5 | 0.077 |
| 85 | 2201.83 | 2669.83 | -7.89 | -1.10 | 0.49 | 0.36 | 6.48 | $3.48\times10^3$ | 20.7 | 5 | 0.104 |
| 86 | 2265.39 | 2921.17 | -6.58 | 0.12 | 0.88 | 0.50 | 6.76 | $2.85\times10^3$ | 16.9 | 5.5 | 0.051 |
| 87 | 1930.28 | 2872.06 | -6.39 | -0.37 | 1.03 | 0.50 | 6.78 | $2.66\times10^3$ | 19.7 | 5.5 | 0.054 |
| 88 | 2669.83 | 3108.94 | -7.16 | -0.25 | 0.69 | 0.50 | 6.68 | $3.59\times10^3$ | 18.0 | 5.5 | 0.062 |
| 89 | 3758.94 | 2863.39 | -6.72 | -0.22 | 0.90 | 0.50 | 6.74 | $2.96\times10^3$ | 10.2 | 5 | 0.061 |
| 90 | 3279.39 | 2444.50 | -7.35 | -0.57 | 0.48 | 0.50 | 6.64 | $3.84\times10^3$ | 14.4 | 5 | 0.053 |
| 91 | 1743.05 | 1230.62 | -6.98 | -0.80 | 0.55 | 0.48 | 6.48 | $2.16\times10^3$ | 20.4 | 5 | 0.079 |
| 92 | 2047.28 | 1469.50 | -8.55 | -1.62 | 0.63 | 0.30 | 5.75 | $1.02\times10^4$ | 28.9 | 3 | 0.087 |
| 93 | 2177.28 | 1538.83 | -8.56 | -0.77 | 0.27 | 0.42 | 6.56 | $7.70\times10^3$ | 25.7 | 5 | 0.116 |
| 94 | 2006.83 | 1668.83 | -8.11 | -1.07 | 0.57 | 0.40 | 6.48 | $4.80\times10^3$ | 21.2 | 5 | 0.090 |
| 95 | 2076.17 | 1593.72 | -7.62 | -1.48 | 0.26 | 0.20 | 6.10 | $2.75\times10^3$ | 6.3 | 3 | 0.089 |
| 96 | 1584.86 | 1439.20 | -8.68 | -1.51 | 0.80 | 0.48 | 6.04 | $1.72\times10^4$ | 53.7 | 4 | 0.059 |
| 97 | 1174.83 | 1391.50 | -8.06 | -1.26 | 0.70 | 0.44 | 6.24 | $6.67\times10^3$ | 51.5 | 4.5 | 0.064 |
| 98 | 1888.39 | 1509.94 | -8.74 | -0.89 | 0.39 | 0.46 | 6.32 | $1.18\times10^4$ | 42.5 | 4.5 | 0.099 |
| 99 | 2743.50 | 2032.83 | -8.26 | -1.47 | 0.43 | 0.28 | 6.30 | $4.65\times10^3$ | 33.4 | 5 | 0.093 |
| 100 | 2079.06 | 1943.28 | -8.71 | -1.03 | 0.68 | 0.36 | 6.76 | $1.34\times10^4$ | 28.6 | 5 | 0.103 |
| 101 | 2148.39 | 2018.39 | -9.68 | -1.28 | 0.64 | 0.44 | 6.28 | $2.86\times10^4$ | 57.8 | 5 | 0.103 |
| 102 | 2396.52 | 2157.12 | -8.96 | -1.44 | 0.70 | 0.38 | 6.28 | $1.24\times10^4$ | 33.4 | 5 | 0.096 |
| 103 | 2742.86 | 4289.09 | -5.81 | -0.32 | 0.56 | 0.50 | 6.56 | $7.76\times10^2$ | 19.7 | 5 | 0.055 |
| 104 | 4027.33 | 2838.30 | -7.88 | -1.40 | 0.94 | 0.42 | 6.08 | $6.49\times10^3$ | 48.1 | 4 | 0.057 |

Continued on Next Page. . .

Table 3.2 – Continued

| ID | x (pix) | y (pix) | $M_V$[1] | $U-B$ | $V-I$ | E($B-V$) | $log$(Age) (years) | Mass ($M_\odot$) | $r_{tot}$[2] (pix) | Morph. Cat.[3] | RMS[4] |
|---|---|---|---|---|---|---|---|---|---|---|---|
| 105 | 3305.99 | 3250.22 | -7.84 | -0.40 | 1.02 | 0.50 | 6.78 | $1.00\times10^4$ | 15.8 | 5 | 0.081 |
| 106 | 2073.37 | 2945.32 | -6.81 | 0.08 | 0.88 | 0.00 | 9.11 | $3.37\times10^4$ | 12.2 | 6 | 0.043 |
| 107 | 2373.05 | 2751.50 | -6.85 | -1.08 | 0.36 | 0.28 | 6.50 | $9.63\times10^2$ | 14.7 | 4.5 | 0.062 |
| 108 | 2411.27 | 2948.37 | -6.88 | -0.97 | 0.60 | 0.50 | 6.24 | $2.68\times10^3$ | 20.5 | 5 | 0.070 |
| 109 | 3261.83 | 2780.17 | -6.82 | -0.10 | 1.02 | 0.50 | 6.76 | $3.54\times10^3$ | 8.4 | 5.5 | 0.058 |
| 110 | 2546.98 | 2608.15 | -6.88 | -1.60 | 0.71 | 0.30 | 5.80 | $2.20\times10^3$ | 16.4 | 3 | 0.068 |
| 112 | 2233.52 | 2155.15 | -8.83 | -1.53 | 0.93 | 0.38 | 5.85 | $1.55\times10^4$ | 28.8 | 5 | 0.093 |
| 113 | 2352.02 | 2239.25 | -6.60 | -1.31 | 0.18 | 0.32 | 5.65 | $1.98\times10^3$ | 11.8 | 3 | 0.090 |
| 114 | 2248.81 | 2269.83 | -7.61 | -1.26 | 0.42 | 0.38 | 6.24 | $3.71\times10^3$ | 17.9 | 5 | 0.091 |
| 115 | 2442.81 | 2299.46 | -10.20 | -1.53 | -0.06 | 0.00 | 6.70 | $1.45\times10^4$ | 26.0 | 5 | 0.143 |
| 116 | 2979.23 | 2453.23 | -8.76 | -1.30 | 0.00 | 0.00 | 7.34 | $1.83\times10^4$ | 7.2 | 5 | 0.117 |
| 117 | 2501.19 | 2568.08 | -6.76 | -1.67 | 0.69 | 0.18 | 5.60 | $1.49\times10^3$ | 11.3 | 3 | 0.083 |
| 118 | 3194.86 | 3154.80 | -6.55 | -0.45 | 0.45 | 0.50 | 6.56 | $1.53\times10^3$ | 6.8 | 5.5 | 0.060 |
| 119 | 2912.00 | 4544.52 | -5.97 | -0.73 | 0.35 | 0.10 | 7.81 | $3.24\times10^3$ | 11.1 | 5 | 0.067 |
| 120 | 3972.00 | 2047.00 | -6.63 | -0.42 | 0.18 | 0.42 | 6.62 | $1.49\times10^3$ | 12.0 | 5 | 0.088 |
| 121 | 4422.48 | 1704.57 | -5.11 | -0.85 | -0.01 | 0.26 | 6.64 | $2.41\times10^2$ | 9.7 | 5 | 0.048 |
| 122 | 1974.39 | 1421.56 | -6.19 | -1.41 | 0.69 | 0.42 | 6.08 | $1.36\times10^3$ | 19.1 | 3 | 0.079 |
| 123 | 3915.00 | 1538.01 | -6.37 | -1.40 | 0.35 | 0.28 | 6.30 | $8.19\times10^2$ | 30.2 | 5 | 0.064 |
| 124 | 2750.00 | 1006.07 | -7.50 | -1.62 | 0.44 | 0.18 | 6.04 | $2.41\times10^3$ | 14.9 | 3 | 0.099 |
| 125 | 2996.04 | 838.00 | -7.82 | -1.22 | 0.79 | 0.50 | 6.32 | $5.72\times10^3$ | 58.1 | 5.5 | 0.059 |
| 126 | 2362.80 | 2343.73 | -8.66 | -1.28 | 0.57 | 0.40 | 6.22 | $1.11\times10^4$ | 29.3 | 4.5 | 0.095 |

Continued on Next Page. . .

Table 3.2 – Continued

| ID | x (pix) | y (pix) | $M_V$[1] | $U-B$ | $V-I$ | E($B-V$) | $log$(Age) (years) | Mass ($M_\odot$) | $r_{tot}$[2] (pix) | Morph. Cat.[3] | RMS[4] |
|---|---|---|---|---|---|---|---|---|---|---|---|
| 127 | 3827.14 | 2512.46 | -8.29 | -1.19 | 0.58 | 0.50 | 6.26 | $1.03\times10^4$ | 42.0 | 5 | 0.072 |
| 128 | 2463.12 | 2292.49 | -12.31 | -1.49 | -0.08 | 0.00 | 6.66 | $8.94\times10^4$ | 90.0 | 4.5 | 0.108 |
| 129 | 2272.79 | 1887.21 | -7.78 | -1.26 | 0.59 | 0.20 | 6.78 | $3.96\times10^3$ | 14.3 | 5 | 0.114 |
| 130 | 2227.68 | 2300.75 | -6.63 | -1.34 | 0.64 | 0.40 | 6.14 | $1.81\times10^3$ | 10.1 | 5 | 0.105 |
| 131 | 3960.88 | 3373.11 | -8.77 | -0.28 | 0.93 | 0.46 | 8.01 | $1.52\times10^5$ | 5.8 | 6 | 0.047 |



[1]Please see Kaleida et al. 2012 (in progress), for the newest, most updated version of this table.
[2]Vega mags.
[3]Total radius as defined in Section 3.4.
[4]Morphological Category, as per the system in Whitmore et al. (2011).
[5]Root-Mean-Squared of the stellar grouping, as in Whitmore et al. (2011).

# Chapter 4

# FINAL CONCLUSIONS

## 4.1 Summary

To summarize, the aim of this research is to answer some fundamental questions about the structure of galaxies and how they evolve over time. The first chapter of this dissertation provides background on the field of stellar clustering and its importance within the scope of galaxy structure and evolution. Chapters 2 and 3 outline the methods we have developed in order to select stellar grouping in galaxies in a uniform matter, so that we may compare results for various galaxies on equal footing. Chapter 4 compares and contrasts the basic properties of stellar groupings selected using the automatic selection method in four different galaxies. The galaxies chosen, M51, NGC 4214, M83, and NGC 2841, represent four of the main morphological categories actively star-forming galaxies tend to belong to: interacting galaxies, dwarf irregular galaxies, spiral, and flocculent spiral. The basic tends we see in the properties of stellar groupings with respect to the characteristics of the host galaxy elucidate the role these groupings play in the evolution of galaxies. The main conclusions we make are enumerated below.

From the selection, photometry and SED fitting of $120$ single-aged stellar associations in the M51/NGC 5195 system, we conclude the following main points:

1. Visual inspection of the CM and CC diagrams for each potential stellar association is an effective way to weed out groups of star that are not coeval. We find that the vast majority of the single-aged stellar associations selected in this manner lie along one of the spiral arms on M51, or on spurs coming off the spiral arms.

2. Very few single-aged associations are found in the interarm regions, suggest-

ing that either the conditions in these inter-arm regions are not ripe for the formation of stellar associations, or that stellar associations formed here disperse quickly after their birth.

3. There is an enhancement in the number of single-aged stellar associations in the northern arm spiral arm closest to the companion, most likely triggered by the interaction of M51 and NGC 5195.

4. No correlation between position within the galaxy and age of the association was found. There is also not an apparent relationship between the physical size of the association and position.

5. We see few instances of sequential formation of stellar associations, which suggests that this type of triggering may only occur on scales smaller than investigated in this study (i.e. smaller $\sim 5$ pc, on the scale of compact clusters).

6. Single-aged associations in this system range in size from $5$ to $90$ parsecs, with the peak in the size-number density histogram occurring at an average radius of $\sim 25$ parsecs, hinting that this may be the dominant size of the scale length for collapse within the molecular clouds that stellar associations form from.

7. There is a slight trend for more massive associations to to exist preferentially in the region of M51 closest to NGC 5195. This indicates that the galaxy interaction facilitates the collapse of larger segments of molecular hydrogen clouds than would occur without this interaction, resulting in higher-mass stellar associations.

8. Even with the resolution of Hubble ACS/WFC, main sequence turnoffs are not evident for the vast majority of stellar associations in M51, due to the limiting

magnitude of our images, and the vertical nature of the turnoff at the bright end of the main sequence.

From the selection and photometry of stellar groupings (clusters and associations) in the galaxy NGC 4214, we find the following:

1. Both the automated and manual catalogs have fairly continuous size distributions (for $r_{tot}$, $r_{1/2}$, etc) between a few parsecs to several tens of parsecs. These distributions are not strongly bimodal, in contradiction to the suggestion from Maíz-Apellániz (2001).

2. The automated method we have developed detects the majority of the stellar grouping selected in the manual list, and determines sizes with a 80 $\%$ discrepancy from the sizes estimated by eye for sources in the manual list.

3. The size distribution of stellar clustering is peaked (i.e., roughly gaussian) and has a fairly systemic shape for $r_{tot}$, but transitions to an asymmetric distribution when using $r_{1/4}$, with many more compact rather than diffuse nuclei.

4. Most stellar groupings are younger than $10$ Myr. This support the idea that most clusters and associations are disrupted on short time scales (i.e., infant mortality - see Whitmore et al., 2007).

5. If the size distribution is divided into three age ranges ($<3$ Myr, $3$–$10$ Myr, $>30$ Myr), some degree of bimodality is seen in each age range, with an original populations of about $1/4$ of the sample being compact and $3/4$ being diffuse associations.

6. The size distributions evolve with age, with the clearest result being that while $60\%$ of the very young sample have values of $r_{tot}>20$ pc, only $40\%$ of the young sample, and only $5\%$ of the intermediate age sample does.

7. A simple working scenario is developed for the dissolution of both compact clusters and diffuse associations. In this scenario, most of the compact clusters and diffuse associations disperse with time, but ultimately, only a small percentage ($1/20$th) of the compact clusters survive to have ages $>200$ Myr stars diffuse into the field population of the galaxy.

## 4.2 Future Work

In future work, I will use the methods outlined herein to uniformly study the size distribution of stellar groupings in a sample of approximately $50$ nearby galaxies, determine cluster/association disruption times, and examine general trends in the characteristics of stellar groupings in relation to the host galaxy properties. A first step into this more extended study has been made, using *HST* WFC3 images of the flocculent spiral galaxy NGC 2841 (Figures 4.1 and 4.2), in order to illustrate the automated code's ability to select compact clusters and stellar associations in any galaxy image with pixel scale of $\sim$2pc/pixel or better. The results of this analysis will elucidate the connections between large-scale galaxy morphology and smaller scale clustering of stars within these galaxies. I will use the results of this study to test models of galaxy evolution and inform higher redshift studies which cannot resolve smaller-scale clustering within individual galaxies.

We also plan to extend the work on M51 (Chapter 2) and NGC 4214 (Chapter 3) using data from a wider range of wavelengths (infrared and ultraviolet images, as well various narrowband filters to reveal emission lines), in order to reveal more of overall state of the interstellar medium in these galaxies. Specifically, in M51 we intend to investigate in detail the various star-forming complexes in this galaxy using multiwavelength datasets including additional data from GALEX and Spitzer. In NGC 4214 we will be applying for observing time using an Integral Field Unit Spectragraph to get metallicity information for this galaxy on the scale of a star cluster

or association, in order to investigate the effects of metallicity on the properties of stellar grouping size and disruption time.

Figure 4.1: *HST* WFC3/UVIS image of NGC 2841. $F336W$ is shown in blue, $F547M$ in green, $F814W$ in red, and $F657N$ (H$\alpha$) in red-orange. *Image Credit: Credit: NASA, ESA, and the Hubble Heritage (STScI/AURA)-ESA/Hubble Collaboration, M. Crockett and S. Kaviraj (Oxford University, UK), R. O'Connell (University of Virginia), B. Whitmore (STScI), and the WFC3 Scientific Oversight Committee.*

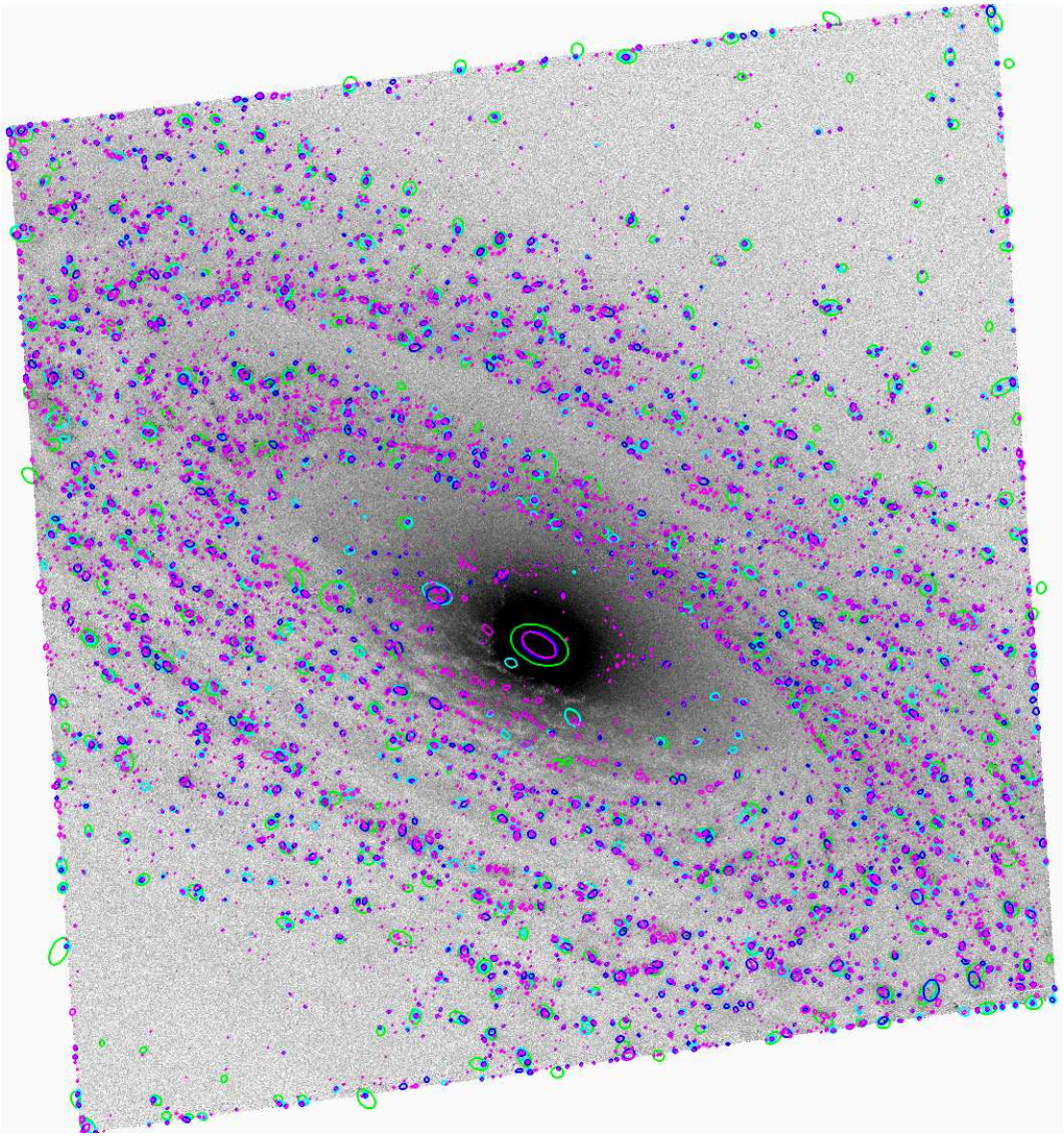

Figure 4.2: *HST* WFC3/UVIS $F336W$ image of NGC 2841, with initial SExtractor-selected sources overlaid, as in Figure 3.5. This is the first step in the automated stellar grouping selection method. The next steps in the automated method clean the initial source list of spurious detections, edge effects, and double-counting, and determines the characteristic size of each grouping.

Anders, P., Bissantz, N., Fritze-v. Alvensleben, U., & de Grijs, R. 2004, MNRAS, 347, 196

Bastian, N., Gieles, M., Ercolano, B., & Gutermuth, R. 2009, MNRAS, 392, 868

Bastian, N., Ercolano, B., Gieles, M., Rosolowsky, E., Scheepmaker, R. A., Gutermuth, R., & Efremov, Y. 2007, MNRAS, 379, 1302

Bastian, N., Gieles, M., Lamers, H. J. G. L. M., Scheepmaker, R. A., & de Grijs, R. 2005a, A&A, 431, 905

Bastian, N., Gieles, M., Efremov, Y. N., & Lamers, H. J. G. L. M. 2005b, A&A, 443, 79

Bertin, E., & Arnouts, S. 1996, A&ApS,117, 393

Bik, A., Lamers, H. J. G. L. M., Bastian, N., Panagia, N., & Romaniello, M. 2003, A&A, 397, 473

Bresolin, F., et al. 1998, AJ, 116, 119

Brown, A. G. A., Blaauw, A., Hoogerwerf, R., de Bruijne, J. H. J., & de Zeeuw, P. T. 1999, NATO ASIC Proc. 540: The Origin of Stars and Planetary Systems, 411

Bruzual, G., & Charlot, S. 2003, MNRAS, 344, 1000

Cardelli, J. A., Clayton, G. C., & Mathis, J. S. 1989, ApJ, 345, 245

Cartwright, A., & Whitworth, A. P. 2004, MNRAS, 348,589

Cerviño, M., & Luridiana, V. 2006, A&A, 451, 475

Chabrier, G. 2003, PASP, 115, 763

Chandar, R., et al. 2010, ApJ, 719, 966

de Vaucouleurs, G., de Vaucouleurs, A., Corwin, H. G., Jr., Buta, R. J., Paturel, G., & Fouque, P. 1991, Volume 1-3, XII, 2069 pp. 7 figs.. Springer-Verlag Berlin Heidelberg New York,

de Vaucouleurs, G., de Vaucouleurs, A., & Corwin, J. R. 1976, Second reference catalogue of bright galaxies, 1976, Austin: University of Texas Press.

Dopita, M. A., et al. 2010, Ap&SS, 330, 123

Elmegreen, B. G., Elmegreen, D. M., & Montenegro, L. 1992, ApJS, 79, 37

Elmegreen, B. G., Elmegreen, D. M., Chandar, R., Whitmore, B., & Regan, M. 2006, ApJ, 644, 879

Fall, S. M., Chandar, R., & Whitmore, B. C. 2005, ApJL, 631, L133

Feldmeier, J. J., Ciardullo, R., & Jacoby, G. H. 1997, ApJ, 479, 231

Fitzpatrick, E. L. 1999, PASP, 111, 63

Ford, H. C., Crane, P. C., Jacoby, G. H., Lawrie, D. G., & van der Hulst, J. M. 1985, ApJ, 293, 132

Fukugita, M., Ichikawa, T., Gunn, J. E., Doi, M., Shimasaku, K., & Schneider, D. P. 1996, AJ, 111, 1748

Garcia, M., Herrero, A., Vicente, B., Castro,N., Corral, L. J., Rosenberg, A., & Monelli, M. 2009, A&A, 502,1015

Girardi, L., Bertelli, G., Bressan, A., Chiosi, C., Groenewegen, M. A. T., Marigo, P., Salasnich, B., & Weiss, A. 2002, A&A, 391, 195 (also most recent isochrones from 2006, unpublished: http://pleiadi.pd.astro.it/isoc_photsys.02 /isoc_acs_wfc/).

Harris, J., Calzetti, D., Gallagher, J. S., III, Conselice, C. J., & Smith, D. A. 2001, AJ, 122, 3046

Harris, W. E. 1996, AJ, 112, 1487

Hernquist, L. 1990, Dynamics and Interactions of Galaxies, ed. R. Wielen (New York: Springer-Verlag), 108

Hwang, N., & Lee, M. G. 2008, AJ, 135, 1567

Joye, W. A., & Mandel, E. 2003, Astronomical Data Analysis Software and Systems XII, 295, 489

Kaleida, C., & Scowen, P. A. 2010, AJ, 140, 379

Koekemoer, A. M., Fruchter, A. S., Hook, R. N., & Hack, W. 2002, The 2002 HST Calibration Workshop : Hubble after the Installation of the ACS and the NICMOS Cooling System, 337

Lada, C. J., & Lada, E. A. 2003, ARA&A, 41, 57

Lamers, H. J. G. L. M., Panagia, N., Scuderi, S., Romaniello, M., Spaans, M., de Wit, W. J., & Kirshner, R. 2002, ApJ, 566, 818

Larsen, S. S. 2004, A&A, 416, 537

Lee, M. G., Chandar, R., & Whitmore, B. C. 2005, AJ, 130, 2128

Lightman, A. P., & Shapiro, S. L. 1978, Reviews of Modern Physics, 50, 437

Maíz-Apellániz, J. 2001, ApJ, 563, 151

Mink, D. J. 1997, Astronomical Data Analysis Software and Systems VI, 125, 249

Mink, D. J. 1999, Astronomical Data Analysis Software and Systems VIII, 172, 498

Mora, M. D., Larsen, S. S., Kissler-Patig, M., Brodie, J. P., & Richtler, T. 2009, A&A, 501, 949

Mutchler, M., et al. 2005, Bulletin of the American Astronomical Society, 37, 452

Papovich, C., Dickinson, M., & Ferguson, H. C. 2001, ApJ, 559, 620

Piskunov, A. E., Kharchenko, N. V., Schilbach, E., Röser, S. Scholz, R.-D., & Zinnecker, H. 2009, A&A, 507, L5

Popescu, B., & Hanson, M. M. 2009, AJ, 138, 1724

Preibisch, T., & Mamajek, E. 2008, Handbook of Star Forming Regions, Volume II, 235

Regan, M. W., & Wilson, C. D. 1993, AJ, 105, 499

Rey, S.-C., et al. 2007, ApJS, 173, 643

Rots, A. H., Bosma, A., van der Hulst, J. M., Athanassoula, E., & Crane, P. C. 1990, AJ, 100, 387

Saha, A., Thim, F., Tammann, G. A., Reindl, B., & Sandage, A. 2006, ApJS, 165, 108

Salpeter, E. E. 1955, ApJ, 121, 161

Salo, H., & Laurikainen, E. 2000, MNRAS, 319, 377

Sandage, A. 1957, ApJ, 125, 435

Sandage, A., & Tammann, G. A. 1987, A Revised Shapley-Ames Catalog of Bright Galaxies (2nd ed., Washington, DC: Carnegie Institute)

Sánchez, N., & Alfaro, E. J. 2009, ApJ, 696, 2086

Schlegel, D. J., Finkbeiner, D. P., & Davis, M. 1998, ApJ, 500, 525

Scoville, N. Z., Polletta, M., Ewald, S., Stolovy, S. R., Thompson, R., & Rieke, M. 2001, AJ, 122, 3017

Shu, F. H., Milione, V., Gebel, W., Yuan, C., Goldsmith, D. W., & Roberts, W. W. 1972, ApJ, 173, 557

Simon, M. 1997, ApJL, 482, L81

Sirianni, M., et al. 2005, PASP, 117, 1049

Solomon, P. M., Rivolo, A. R., Barrett, J., & Yahil, A. 1987, ApJ, 319, 730

Stetson, P. B. 1987, PASP, 99, 191

Theis, C., & Spinneker, C. 2003, Ap&SS, 284, 495

Toomre, A., & Toomre, J. 1972, ApJ, 178, 623

Tully, R. B. 1974, ApJS, 27, 437

Úbeda, L., Maíz-Apellániz, J., & MacKenty, J. W. 2007, AJ, 133, 932

van den Bergh, S., & Lafontaine, A. 1984, AJ, 89, 1822

Wahde, M., & Donner, K. J. 2001, A&A, 379, 115

Whitmore, B. C., et al. 2011, ApJ, 729, 78

Whitmore, B. C., et al. 2010, AJ, 140, 75

Whitmore, B. C., Chandar, R., & Fall, S. M. 2007, AJ, 133, 1067

Whitmore, B. C. 1999, Galaxy Interactions at Low and High Redshift, 186, 251

Zaritsky, D., Kennicutt, R. C., Jr., & Huchra, J. P. 1994, ApJ, 420, 87

Zwicky, F. 1955, PASP, 67, 232